THE DEVELOPMENT OF NOVEL FLUORESCENT PROBES FOR THE INVESTIGATION OF MELANOSOME TRAFFICKING

Ianthe Amy Doumas-Calder

This thesis is submitted for the degree of Master of Science

Department of Biosciences

Durham University

November 2021

Abstract

Melanosomes are pigment cell-specific organelles in which melanin is produced and trafficked within the cell, before being transferred to neighbouring keratinocytes. Their production is essential for the protection of skin cells from UV radiation. Melanosomes are an ideal model for the study of vesicular transport, due to the ease with which they can be detected in darkly pigmented cells. Extensive research has identified the key proteins involved in melanogenesis, including Pmel17, TRP2 and Rab27A. However, melanosomal research thus far has been mostly static, using techniques such as electron microscopy. As a result, the dynamic movement of melanosomes both within melanocytes and during transfer to keratinocytes has not been observed.

Here, the three melanosome-related proteins Rab27A, TRP2 and Pmel17 are fluorescently tagged and examined in SKMEL28 cells for their use in the observation of melanosome dynamics. Rab27A is implicated in the transport of mature pigmented melanosomes to the cell periphery. TRP2 is associated with early stage melanosomes and mediates pigmentation, while Pmel17 initiates melanosome maturation, forming fibrils onto which melanin is deposited. Novel fluorescent probes tdTomato-TRP2 and mNG-Pmel17 were designed, and the latter was determined to be the most effective for the visualisation of melanosomes. The mNG-Pmel17 fluorescent probe produced punctate structures in live cells, of a size consistent with melansomes. The probe co-localised with the actin cytoskeleton and was shown to be distinct from lysosomal compartments. Finally, mNG-Pmel17 is reported as a valuable tool for the evaluation of the effects of bioactive compounds of interest.

The novel mNG-Pmel17 probe was shown to be a useful tool for dynamic melanosome observation, and may be used in further studies for the elucidation of the mechanism(s) of melanosome transfer to keratinocytes.

Table of Contents

List of abbreviations

α-MSH	α-melanocyte-stimulating hormone
ACTH	adrenocorticotropic hormone
ANOVA	analysis of variance
BSA	bovine serum albumin
CAF	core amyloid fragment
cAMP	cyclic-adenosine monophosphate
CREB	cAMP response element binding protein
DCT	dopachrome tautomerase
DTT	dithiothreitol
KLD	kringle-like domain
LAMP-2	lysosomal associated membrane protein 2
MART-1	melanoma-associated antigen recognised by T cells
MC1R	melanocortin-1 receptor
MITF	microphthalmia-associated transcription factor
PAGE	polyacrylamide gel electrophoresis
PAR-2	protease-activated receptor 2
PBS	phosphate buffered saline
PDI	protein disulphide isomerase
PKD	polycystic kidney domain
POMC	pro-opiomelanocortin
RPT	repeat
SDS	sodium dodecyl sulfate
SCF	stem cell factor
Tyr	Tyrosinase
TRP1	tyrosinase-related protein 1
TRP2	tyrosinase-related protein 2
UV	ultraviolet

Declaration

I confirm that this thesis is my own work and includes no material submitted for a higher education degree at this or any other institution. All data are my own except for those contained in Figures 1.4, 1.6 and 1.7.

Statement of copyright

Ianthe Amy Doumas-Calder

Acknowledgements

I would like to firstly thank my excellent supervisors Adam Benham and Tim Hawkins for all of their support throughout my research and write-up. I would also like to thank Max Brown for all of his help and advice in the lab, and Joanne Robson for her advice on microscopy. I would like to thank everyone in lab 8 for their support and great company, including Ellie, Charlotte, Jamie, Patrick, Kleo, Max, Liv, Steven, Dan and Josh.

Finally, I would like to thank Procter & Gamble for their financial contributions to the project and their continued support.

1 Introduction

Melanosomes are a type of specialised organelle, which contains the pigment melanin, produced in melanocytes in the basal layer of the epidermis (Figure 1.1). Melanocytes are also found in hair follicles, the retinal pigment epithelium in the eyes, the inner ear, bones, the heart and the brain. These vesicles allow the transport of melanin from melanocytes to keratinocytes, where the pigment forms the supranuclear cap. This cap is positioned above the nucleus, and absorbs ultraviolet (UV) and visible light, thereby protecting the DNA from damage caused by UV radiation (Bultema *et al*., 2014). This prevents the generation of potentially cancer-causing mutations in basal skin cells (Premi *et al*., 2015). Melanosomes have previously been studied as a model for endosomal maturation (Berson *et al*., 2001; Berson *et al*., 2003), however the precise mechanism of their transfer to keratinocytes has not yet been elucidated. Several of the proteins involved in the maturation of melanosomes have been identified, and their functions described to a great extent. These known proteins can be exploited in order to gain an enriched understanding of melanosome movement within melanocytes, thus far not observed, as well as the moment of transfer of melanosomes to keratinocytes, which would provide a valuable addition to current knowledge.

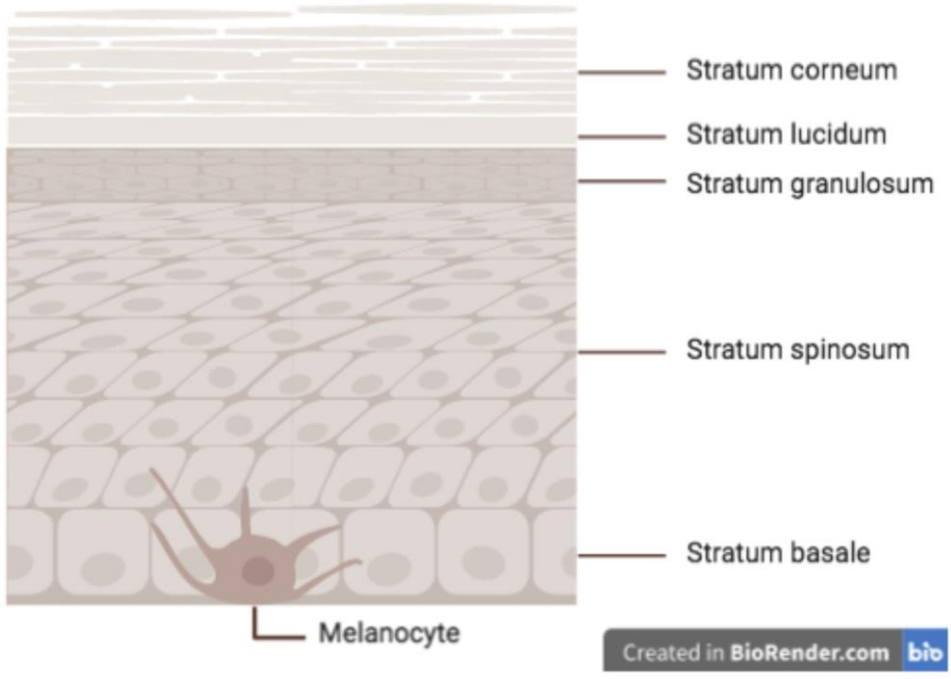

Figure 1.1. Layers of the epidermis

The five layers of the epidermis, with a melanocyte present in the stratum basale.

To begin with, the melanogenesis pathway in the skin is initiated by the induction of p53 as part of the stress response following mild DNA damage to neighbouring keratinocytes due to UV radiation or inflammation (Lim, Jin and Yun, 2016). One of the early targets of p53 is Pro-opiomelanocortin (POMC), for which it acts as a transcription factor. POMC is broken down into α-melanocyte-stimulating hormone (α-MSH), adrenocorticotropic hormone (ACTH) and β-endorphin. ACTH and α-MSH bind to the melanocortin-1 receptor (MC1R), a G-protein-coupled receptor on the surface of melanocytes, triggering various signalling pathways which regulate the activity of the transcription factor microphthalmia-associated transcription factor (MITF). These involve the upregulated production of cAMP and downstream activation of CREB, a MITF transcription factor, as well as the phosphorylation of MITF by MAPK-ERK signalling. Activation of CREB and downstream production of MITF is also achieved by the binding of Stem Cell Factor (SCF) to the receptor tyrosine kinase KIT. This in turn regulates the production of proteins and enzymes responsible for pigmentation (D'Mello *et al*., 2016). There are two distinct types of melanin: the darker brown/black eumelanin and the lighter red/yellow pheomelanin. The type of pigment produced depends on a number of factors, including activation of the MC1R. ACTH and α-MSH are MC1R agonists, which stimulate eumelanin synthesis. On the other hand, the *Asip* (agouti) gene produces a MC1R antagonist (Lin and Fisher, 2007). Activation of MC1R is also dependent on the subunits from which it is formed. Certain alleles produce MC1R which cannot be activated by ACTH or α-MSH, and individuals with these alleles have light coloured skin from pheomelanin alone. The Fitzpatrick scale describes different skin types and their sensitivity to UV radiation, ranging between type I, skin which easily burns and does not tan, to type VI, skin which does not burn and easily tans (Falcon *et al*., 2019). Individuals with very fair skin, usually accompanied by red hair, are the most susceptible to burning (Lin and Fisher, 2007), and most at risk of developing skin cancer due to the lack of protective pigment.

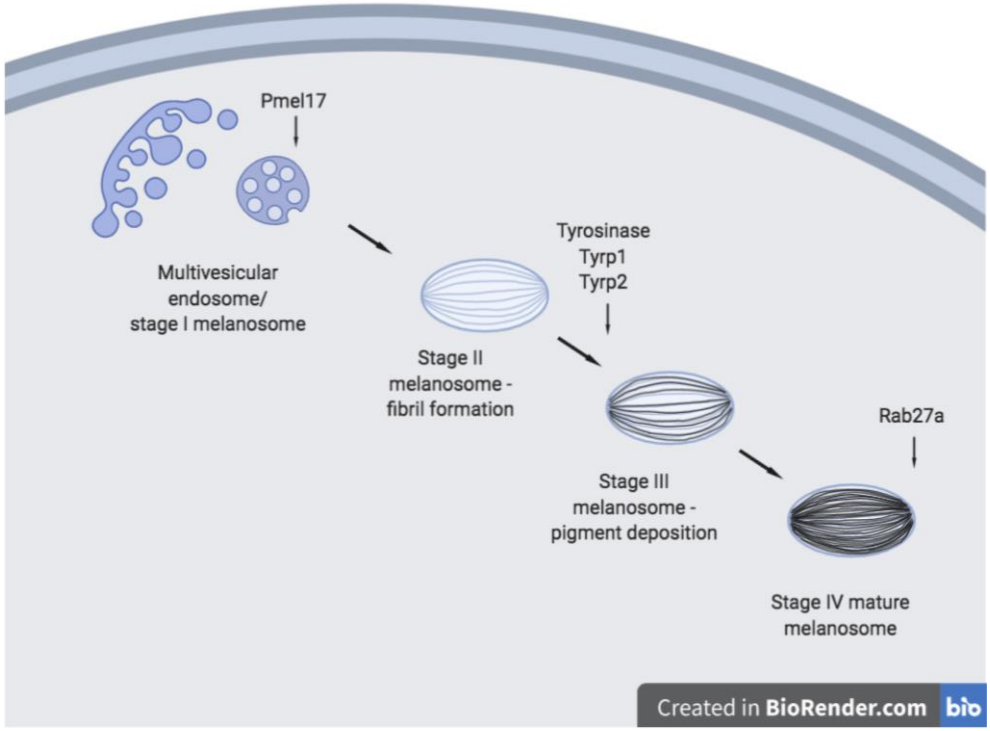

Figure 1.2. The four stages of melanosome maturation

Recruitment of Pmel17 commences maturation to stages I and II, before recruitment of melanogenic enzymes Tyrosinase, Tyrp1 and Tyrp2 leads to the deposition of melanin and progression to stages III and IV.

Following its production and activation, MITF promotes the transcription of several melanogenesis-specific proteins and enzymes, including Tyrosinase (Tyr), Tyrosine-related protein-1 (Tyrp1 or TRP1), Tyrosine-related protein-2 (Tyrp2 or TRP2), Pmel17, Rab27a and MART-1 (Serre, Busuttil and Botto, 2018; Kushimoto *et al.*, 2001). Each of these proteins contributes to a different part of the melanogenesis pathway, which is comprised of four stages (Figure 1.2). The first protein to initiate melanosome maturation is Pmel17. Pmel17 is delivered to early sorting endosomes, where it organises into intraluminal fibrils, mediating the maturation of late multivesicular endosomes into stage I and II melanosomes. Stage II melanosomes are characterised by a striated and elongated appearance, due to the fibrillar nature of the Pmel17 sheets (Hellström *et al.*, 2011). Subsequently, the enzymes Tyr, TRP1 and TRP2 are recruited to melanosomes, where they are responsible for melanin synthesis. Synthesized melanin is deposited onto Pmel17 fibrils, at which point melanosomes reach stage III of their maturation. In mature stage IV melanosomes, melanin covers all the available surface area of Pmel17 fibrils. In addition to providing a scaffold onto which melanin can be deposited, Pmel17 fibrils are thought to sequester toxic products

of melanin synthesis, thus avoiding cell damage (Hellström *et al*., 2011; Fowler *et al*., 2005). Finally, once melanosomes have fully matured, Rab27a is recruited and attaches to their cytoplasmic surface. This protein mediates melanosome attachment to and movement along the actin cytoskeleton towards the periphery of the cell, for transfer to neighbouring keratinocytes

1.1 Pmel17

Each of these proteins and their involvement in melanogenesis has been studied extensively, although questions still remain regarding certain aspects of their biogenesis and activity. Firstly, Pmel17, also known as gp100 or SILV, is transcribed as a 70kDa type I transmembrane protein, with a short N-terminal signal sequence, a large lumenal domain, a single transmembrane domain and a short cytoplasmic domain. Immediate addition of 4 N-linked glycans in the ER produces a 100kDa protein, referred to as P1. The lumenal domain can be separated into four distinct sub-domains based on sequence homology, which include an N-terminal region, a Polycystic kidney disease (PKD)-like region, a repeat (RPT) domain consisting of ten imperfect repeats of a 13-residue sequence, and a Kringle-like domain (KLD). A disulphide bond links cysteine residues in the RPT domain to cysteine residues in the KLD. Following transcription in the ER, Pmel17 is transported to the Golgi network and undergoes further O-glycosylation in the late Golgi, resulting in a 120kDa protein, referred to as P2. The essential nature of the KLD in the correct processing and trafficking of Pmel17 was demonstrated by Ho *et al.* (2015). The researchers showed that Pmel17 forms a dimer linked by a disulphide bond in the ER or early Golgi, the resolution of which is necessary for the correct assembly of Pmel17 monomers into amyloid fibrils. The introduction of mutations within the KLD by the replacement of cysteine residues with serine resulted in stabilisation of the Pmel17 dimer, eliminating detection of the monomer form by non-reducing SDS-PAGE and immunoblotting with anti-HMB45 antibody. Anti-HMB45 recognises a region in the O-glycosylated RPT domain of Pmel17 (Hoashi *et al*., 2006). Furthermore, HeLa cells transiently transfected with Pmel17 encoding a cysteine to serine replacement within the KLD at residue 566 showed greatly reduced visible fibril formation in their multivesicular bodies compared to HeLa cells transfected with wild type Pmel17. They also introduced mutations at cysteine residues in the RPT domain of Pmel17, where cysteine residues form a disulphide bond with the KLD in the same protein. After mutating

several cysteine residues individually, they found that cysteine 301 is the only essential cysteine residue for both RPT-KLD and dimerising disulphide bonds, shown by vastly reduced detection of the Pmel17 dimer, as well as the disulphide bond-tethered Mα and Mβ fragments, by non-reducing SDS-PAGE immunoblotted with anti-HMB45.

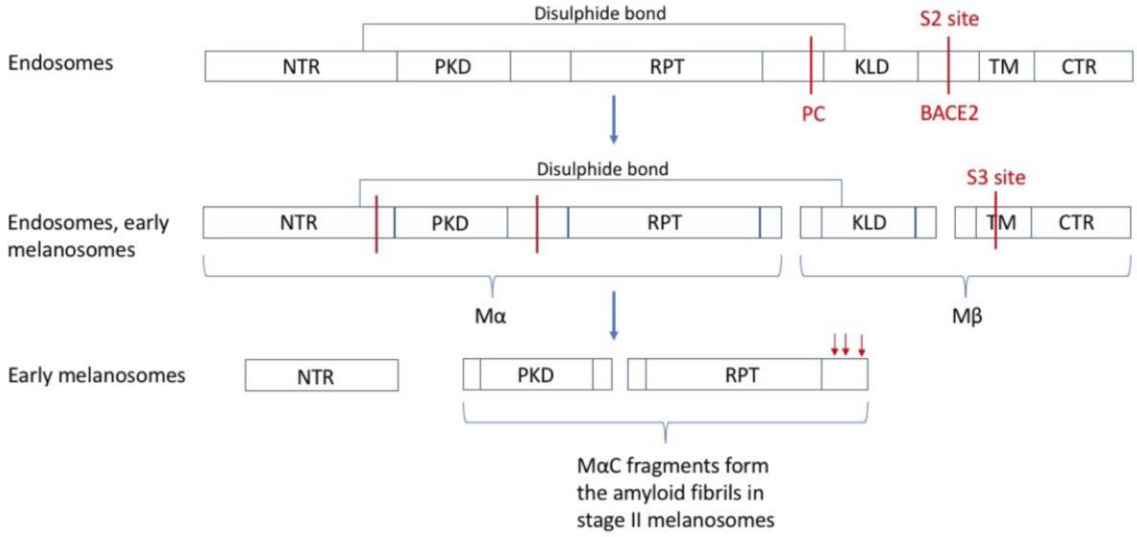

Figure 1.3. Pmel17 proteolytic processing steps with locations

NTR: N-terminal region, PKD: polycystic kidney disease region, RPT: repeat domain, KLD: kringle-like domain, TM: transmembrane domain, CTR: C-terminal region.

Following modification in the Golgi, the P2 form undergoes several proteolytic cleavage steps in post-Golgi endosomes and early melanosomes (Figure 1.3). Delivery to early sorting endosomes most likely occurs by arrival of the protein at the plasma membrane and subsequent internalisation (Watt *et al.*, 2009). Once internalised vesicles fuse with early endosomes, further invagination of the endosomal membrane produces multivesicular bodies. Firstly, while on route to the plasma membrane, Pmel17 is cleaved into two fragments, Mα and Mβ, by a furin-like proprotein convertase (Berson *et al.*, 2003). The Mα fragment includes the N-terminal region, PKD-like region and RPT domain, while the Mβ fragment includes the KLD, transmembrane and C-terminal regions. These two fragments remain tethered to each other via the disulphide bond between the RPT domain and KLD. Berson *et al.* (2003) investigated the cleavage of Pmel17, and identified a furin-like recognition site, which was conserved between species (human, chicken, bovine, equine and mouse). Introducing a mutation at this site resulted in the accumulation of P2 and complete absence of Mα and Mβ, as well as the inability to form Pmel17 derived striations in the endosomal compartments of HeLa cells, confirming that this is the target site for cleavage,

and demonstrating the necessity of cleavage for the generation of fibrils and melanogenesis. Subsequently, Mβ is further cleaved by a sheddase between the KLD and transmembrane domain in order to release the protein from the intraluminal vesicle membrane. This cleavage step is mediated by BACE2 at the S2 site, as demonstrated by Rochin *et al*. (2013). In MNT-1 cells depleted of BACE2, a great decrease in the number of type II and III striated melanosomes and a significant six-fold increase in the number of rounded melanosomes containing unstructured aggregates was observed. Furthermore, treatment of cells with BACE2 siRNA resulted in a significant increase in intact Mβ fragments and a significant decrease in cleaved C-terminal fragments over time. The cleavage event occurs between amino acids Glutamine-583 and Leucine-584 (Kummer *et al.*, 2008). The remaining C-terminal fragment in the membrane of intraluminal vesicles is rapidly degraded by a γ-secretase, through cleavage at the S3 site within the transmembrane region (Kummer *et al*., 2008).

Once released from internal membranes, the Mα-Mβ fragment undergoes further proteolytic processing into fragments which can be incorporated into the intralumenal fibrils. The Mα fragment is cleaved to produce MαN and MαC subfragments, corresponding to the N-terminal region, and the RPT and KLD regions respectively (Hoashi *et al*., 2006; Harper *et al.*, 2007; McGlinchey *et al*., 2009; Hee *et al.*, 2017). Cleavage products of the Mα fragment contribute to the formation of the melanosome amyloid fibrils. First, a core amyloid fragment (CAF) is formed, onto which MαC fragments accumulate. The CAF has been identified as a 76aa-long fragment derived from part of the NTR and adjacent region, extending from aa148 to aa223 (Hee *et al*., 2017). Deletion mutants within the NTR of Pmel17, while not affecting trafficking of Pmel17 between different cellular compartments or proteolytic processing, lead to fragments which form an unstable fibrillar matrix and are degraded (Leonhardt *et al*., 2013). This demonstrates the importance of NTR in the formation of the CAF and amyloid fibrils. Once the CAF has formed, MαC fragments are deposited onto it to increase the surface area for subsequent melanin deposition. These fragments may either be composed of intact PKD and RPT domains in tandem, or PKD and RPT domains separated by cleavage (Harper *et al*., 2007). The cleavage sites and enzymes responsible for the generation of MαC fragments are not yet known, and thus more scientific investigation is required to uncover them. Possible C-terminal cleavage sites are indicated by arrows in Figure 1.3.

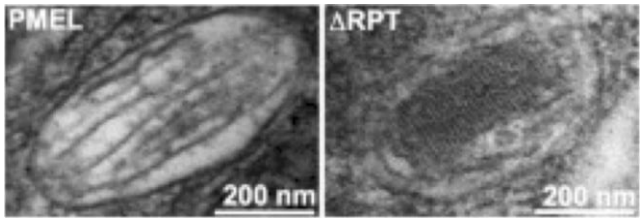

Figure 1.4. TEM of Mel220 cells expressing wild type PMEL (left) and ΔRPT mutant (right).

Source: Figure 1B, Graham et al., 2019.

The RPT domain in MαC fragments has been shown to be indispensable in the correct assembly of intraluminal fibrils (Hoashi *et al*., 2006). HeLa cells were induced to overexpress physiological Pmel17 and a ΔRPT mutant. Cells expressing physiological Pmel17 formed many melanosome-like fibrillated structures, however cells expressing the ΔRPT mutant produced only one fibrillated organelle. Furthermore, several different mutants of the RPT domain were generated, eliminating or altering specific repeats within the original 10. These were transfected into HeLa cells, and lysates were immunoblotted with HMB45 antibody. Observed detection and migration of MαC fragments between the RPT mutants demonstrated the variable proteolytic cleavage of these fragments for incorporation into amyloid fibrils. Another study by Graham *et al*. (2019) found that O-glycosylation, and not primary amino acid sequence, of the RPT domain is most important in the correct formation of amyloid fibril sheet morphology. Researchers firstly generated a ΔRPT mutant and stably expressed it in melanoma cell line Mel220, which lacks endogenous Pmel17. They found that, although amyloid fibrils still formed (slightly reduced compared to wild type), they adopted a block-like appearance compared to physiological sheet morphology (Figure 1.4). The researchers also observed that, while the RPT domain primary sequence is not conserved between species (human, mouse, chicken, snake, frog and zebrafish), it is predicted to be highly O-glycosylated in all of these species. Transfection of human cells with mutant Pmel17 constructs containing RPT sequences from different species produced largely physiological melanosomes. Mouse, chicken and snake RPT domains produced fewer than 7% of melanosomes with the block-like fibril phenotype, while frog Pmel17 produced 19% of melanosomes with this phenotype, compared to the human ΔRPT mutant which produced 100% of melanosomes with this phenotype. Finally, researchers treated human Mel220 cells with an O-glycosylation inhibitor for four days. While Pmel17 expression and trafficking was not affected, between 82% and 87% of melanosomes displayed the block-like fibril phenotype. These results demonstrate that O-

glycosylation of the RPT domain, and not primary protein structure, is the main driver of physiological sheet-like fibril formation for effective melanin deposition. This may be due to physical forces between each of the proteins, whereby the protruding O-glycans may prevent physical proximity of the individual fibres, and thus maintain the sheet-like fibrillar structure. Further investigation is needed to clarify this.

MART-1 has also been implicated in the correct trafficking and processing of Pmel17. It was initially found to be enriched in early stage melanosomes (Kushimoto *et al*., 2001), leading to investigations regarding its function (Hoashi *et al*., 2005). Firstly, MART-1 is a 22-24kDa type III membrane-bound protein which has been localised to the ER, trans-Golgi and melanosomes. Comparison between different melanocyte cell lines found that MART-1 is expressed at a negligible level in WM266-4 cells, in which Pmel17 is also only expressed in its immature form found in early stage melanosomes, and appears to degrade more easily than in highly pigmented MNT-1 melanoma cells. When compared to SK-MEL-28 cells, which express higher levels of MART-1, degradation of the P100 form of Pmel17 in WM266-4 cells was more rapid, indicating a role for MART-1 in the stability of Pmel17. Subsequent immunoprecipitation analysis showed that MART-1 clearly forms a complex with Pmel17 in MART-1 positive cells, which was not seen in negative control WM266-4 cells, but not with Tyr, Tyrp1 or Tyrp2. Furthermore, these complexes were localised to the Golgi, ER and stage I melanosomes, determined by immunoprecipitation and immunoblotting of subcellular fractions from SK-MEL-28 cells. Confocal immunohistochemistry confirmed this, showing MART-1 and Pmel17 colocalisation in the perinuclear area. Researchers then knocked down MART-1 expression in normal melanocytes and SK-MEL-28 cells using MART-1 siRNA, which resulted in a significant decrease in MART-1 expression, as expected, and a concomitant decrease in the levels of the P100 and P26 (C-terminal tail) forms of Pmel17. RT-PCR showed that Pmel17 mRNA levels were not affected by the knockdown of MART-1, indicating that the reduction in Pmel17 protein levels was due to the lack of MART-1 protein. Moreover, expression of MART-1 in MART-1-negative WM226-4 cells led to an increase in P100 levels, and prolonged the stability of this form. In these cells, MART-1 colocalised with Pmel17 in the perinuclear area, and an increase in the number of striated organelles was observed compared to MART-1-negative WM226-4 cells. Finally, researchers determined that Pmel17 is not trafficked to early melanosomes as efficiently in MART-1 negative cells, as shown by reduced colocalisation with LAMP-2, an early melanosome marker, while colocalisation

with ER marker KDEL was comparable in both MART-1 positive and negative cells. These results suggest a significant role for MART-1 in the stabilisation and effective trafficking of Pmel17.

1.2 TRP2

Once the intraluminal fibrils are fully formed in early stage melanosomes, progression to stages III and IV is mediated by the synthesis and deposition of melanin upon the fibrils. The synthesis of melanin is catalysed by three main enzymes: Tyr, TRP1 and TRP2 (Serre, Busuttil and Botto, 2018; Kushimoto *et al*., 2001). TRP2, also known as dopachrome tautomerase, catalyses the conversion of dopachrome to DHICA (5,5-dihydroxyindole-2-carboxylic acid), an intermediate product in eumelanin synthesis (Olivares *et al*., 2001; Tsukamoto et al., 1992). This enzyme is expressed as a 60kDa transmembrane protein (UniProt-P40126, Figure 1.5), but glycosylation increases its size to approximately 75kDa (Jackson *et al*., 1992). It specifically localises to stage II melanosomes, which is thought to be mediated by the Rab6/ELKS secretory pathway (Patwardhan *et al*., 2017). ELKS denotes a Rab6 accessory protein rich in amino acids E, L, K and S. In their study, Patwardhan *et al*. (2017) show that GFP-Rab6 associates with melanosomes, as detected by mCh-VAMP7, in live MNT1 cells. They also showed that lysates from melanosome enriched fractions contain TRP2 and other melanosome-specific components together with Rab6. Depletion of Rab6 also led to a reduction in pigmentation. In mice, a mutation in codon 194 changing arginine to glutamine produces the *slaty* phenotype (Jackson *et al*., 1992), characterised by a decrease in eumelanin and increase in pheomelanin (Hirobe et al., 2006). The *slaty* mutation has been shown to have a detrimental effect on melanosome maturation and morphology (Hirobe and Abe, 2006). Overall, it is clear that the melanosome-specific protein TRP2 plays an essential role in melanogenesis and melanosomal development.

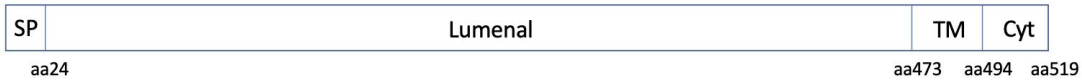

Figure 1.5. Structure of the 519-amino acid TRP2 protein, including the positions of each domain within the protein

SP: signal peptide, TM: helical transmembrane domain, Cyt: cytoplasmic domain, aa: amino acid.

1.3 Melanosome trafficking

Fully matured stage IV melanosomes then initially traffic along microtubules, and are captured by actin filaments for local transport in the periphery of the cell. Melanosome transport and attachment to the actin cytoskeleton is mediated by Rab27a, recruited to the membrane of stage IV melanosomes. Rab27a is part of a family of proteins which cycle between inactive GDP-bound and activated GTP-bound states. These states determine its affinity to proteins it interacts with. It binds to membranes via geranylgeranyl groups bound to its C-terminus by ester linkages to cysteine residues. Rab27a does not bind directly to actin filaments, but instead interacts with Melanophilin (Mlph) and Myosin VA (MyoVA) via N-terminal switch I and II regions, which undergo GDP and GTP-dependent conformational changes. Initially, Rab27a binds to the N-terminal slack homology domain (SHD) of Mlph via its switch I and II regions. MyoVA then attaches to the myosin-binding domain (MBD) in the middle region of Mlph via its C-terminal globular domain. The N-terminal region of MyoVA binds to actin and moves towards the (+) end of the filament. An actin-binding domain at the C-terminus of Mlph mediates the efficient transfer of the complex from microtubules to the actin filament in the cell periphery (Kuroda, Ariga and Fukuda, 2003; Wu, Tsan and Hammer, 2005; Lopes *et al*., 2007). A schematic representation of the Rab27a-Mlph-MyoVA complex can be seen in Figure 1.6. Knockdown of any one component of the complex results in perinuclear aggregation of melanosomes, indicative of its role in melanosome motility (Wu *et al.*, 2001; Hume *et al*., 2002; Kuroda, Ariga and Fukuda, 2003; Lopes *et al*., 2007).

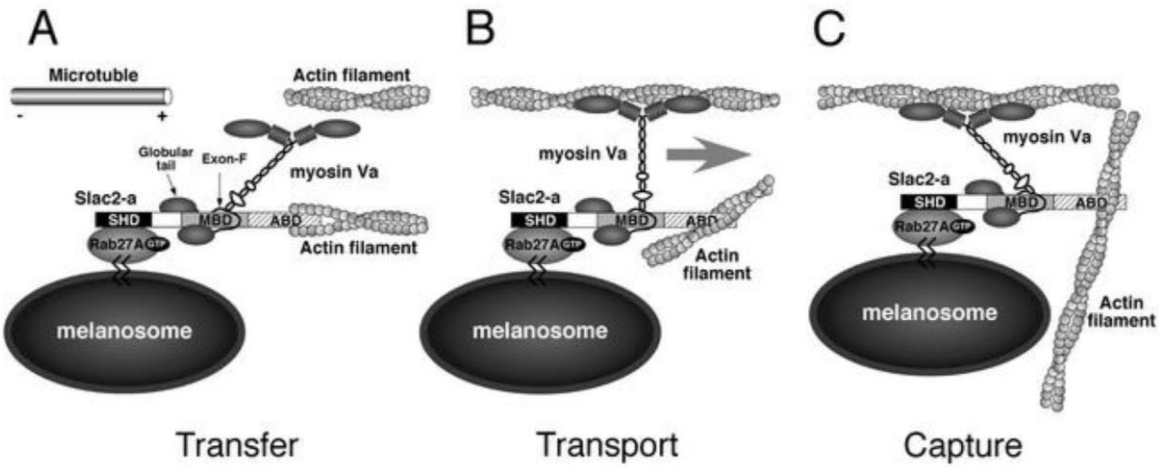

Figure 1.6. The Rab27a-Mlph-MyoVA complex in melanosome transport

Mlph binds to the switch I and II regions of Rab27A via its slack-homology domain (SHD) and MyoVA attaches to Mlph via its myosin-binding domain (MBD). The C-terminal actin-binding domain (ABD) of Mlph interacts with actin and the N-terminal heads of MyoVA track along actin filaments. Source: Kuroda, Ariga and Fukuda (2003).

The mechanism by which Rab27a targets specifically to end-stage melanosomes has been elusive, however research undertaken by Booth *et al*. (2014) aimed to uncover the proteins involved. Initially, the researchers tagged wild type Rab27a and Rab27a$^{SF1/F4}$ mutant with a Hemagglutinin-TEV-FLAG protein purification tag. In the Rab27a$^{SF1/F4}$ mutant, the native RabSF1/RabF4 effector binding motifs are replaced with the respective motifs of Rab3, which prevents interaction with melanosome transport effectors such as Mlph, while binding to melanosomes is unaffected (Tarafder *et al*., 2011). They transfected these constructs into Rab27a-null murine melanocytes and performed immunoprecipitation of Rab27a. Following subsequent analysis, ATP1a1 was identified as a candidate for regulation of Rab27a localisation. ATP1a1 is a ubiquitously expressed isoform of the α subunit of a Na^+/K^+-ATPase, which has not been previously implicated in any transport events. They then knocked down this protein in wild type melanocytes using siRNA probes. The most effective of these probes produced a 94% depletion in ATP1a1 protein, with 56±7% of cells displaying perinuclear clustering of melanosomes. This suggests a role for this protein in Rab27a-mediated melanosome transport, although the scale of perinuclear clustering indicates the involvement of other factors. Further pulldown experiments using native melanocyte Rab27a or his_6-tagged Rab27a from bacteria showed Rab27a interacting with the intracellular loop of ATP1a1 that resides between transmembrane domains 4 and 5. The

levels of activated GTP-bound Rab27a were found to be 50% lower in ATP1a1 siRNA-treated cells than in control cell, indicating that ATP1a1 is involved in Rab27a activation. However, as there is only a 50% reduction, it is clear there are undetermined factors at play. The authors also looked at the effect of knocking down Rab3GEP (R3G) in combination with ATP1a1. R3G has been shown to be a non-redundant nucleotide exchange factor for Rab27a (Figueiredo *et al*., 2008), and may be involved in Rab27a targeting to melanosomes (Tarafder *et al*., 2011). R3G knockdown produces an effect on active Rab27a levels comparable to ATP1a1 knockdown. Confocal immunofluorescence microscopy showed that ATP1a1, R3G and simultaneous ATP1a1+R3G knockdown caused Rab27a to localise to non-melanosome intracellular vesicles. Analysis of purified melanosomes revealed that ATP1a1, R3G and ATP1a1+R3G knockdown significantly impacted Rab27a association with melanosomes, with -22±5%, -33±10% and -50±5% reduction respectively. Mlph association was also affected (-62±7%, -79±3 and -72±3 respective reduction). Finally, pre-loading Rab27a with either GDP or GTP did not affect ATP1a1 binding, suggesting that it is not a Rab27a effector. These results provide substantial evidence for the involvement of ATP1a1 in Rab27a targeting to melanosomes, possibly aided by R3G.

1.4 Melanosome transfer

Following Rab27a-mediated trafficking to the cell membrane, melanosomes are transferred to surrounding keratinocytes. Although the precise mechanism of transfer has not been fully elucidated, four models have been put forward (Figure 1.7). The first describes melanin transfer by exocytosis. This would involve melanosome membrane fusion with the plasma membrane and release of “naked” melanin into the intracellular space, for subsequent phagocytosis by neighbouring keratinocytes. The presence of several SNARE and Rab GTPase proteins in melanocytes, as well as the relation of melanocytes to neuronal and haematopoietic cells for which exocytosis has great functional significance, support this model. The second model is cytophagocytosis, by which projections of the melanocyte plasma membrane containing melanosomes are engulfed by neighbouring keratinocytes. The third model is membrane fusion, which would involve direct fusion of melanocyte and keratinocyte plasma membranes, forming a channel through which melanosomes can be transferred to keratinocytes. Finally, the fourth model of transfer is by the formation of melanosome-containing vesicles budding off from the melanocyte plasma membrane, and

subsequent endocytosis by keratinocytes (Van Den Bossche, Naeyaert and Lambert, 2006). Although it has been reported that certain models of transfer have been directly observed, technological limitations have precluded the establishment of a definitive answer. Singh *et al*. (2008) reported observing melanosome transfer via cytophagocytosis and membrane channel formation using immunofluorescent staining of Pmel17 and electron microscopy. Their findings include fluorescent melanocytic components in adjacent keratinocytes, which are given as evidence for the cytophagocytosis model. However, this observation may also be attributed to melanosome transfer by membrane vesicles or a combination of both, which has not been taken into account in this study. Electron microscopy images showed melanosomes within melanocyte membrane projections moving towards the keratinocyte cell membrane, providing evidence for the membrane channel model. However, keratinocyte membrane ruffling prevented the detailed observation of melanosome entry into keratinocytes.

One of the molecules recognised as being involved in melanosome transfer is protease-activated receptor-2 (PAR-2). This G protein-coupled receptor on the surface of keratinocytes has been shown to mediate phagocytosis of melanosomes *in vitro* and *in vivo*. Inhibiting the activation of the receptor results in depigmentation, as melanosome transfer to keratinocytes is reduced. Electron microscopy images of keratinocytes with activated PAR-2 showed increased membrane ruffling and actin polymerisation beneath the membrane compared to inactivated PAR-2. Scott *et al*. (2003) found that Rho, a member of a family of proteins which are involved in cytoskeletal remodelling during phagocytosis, is activated downstream of PAR-2 activation, and PAR-2-mediated phagocytosis is Rho-dependent, suggesting a role for Rho in melanosome uptake.

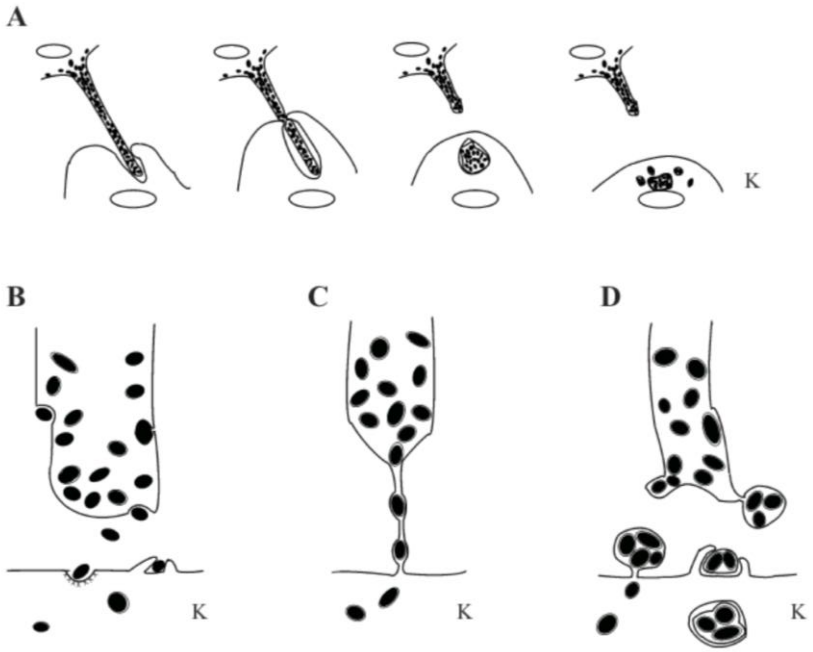

Figure 1.7. The four models of melanosome transfer

A. Cytophagocytosis, B. exocytosis, C. membrane fusion and channel formation, D. melanosome-containing vesicle budding. K: keratinocyte. Source: Van Den Bossche, Naeyaert and Lambert (2006).

1.5 Rationale

The study of melanosome formation and transfer holds significant interest for potential therapeutic advances. Although physiological melanogenesis is vital for the protection of the skin, including melanocytes themselves, from potentially cancer-causing UV damage, melanin pigment can also be deposited in the skin irregularly. A number of genetic or acquired disorders are responsible for these disorders of hyperpigmentation. The most commonly observed acquired hyperpigmentation disorders include melasma, post-inflammatory hyperpigmentation, solar lentigines, ephelides, erythema dyschromicum perstans and friction melanosis, while different pigmentation disorders are associated with different age groups (Plensdorf and Martinez, 2009; Pandya and Guevara, 2000).

One of the most commonly diagnosed hyperpigmentation disorders is melasma. It is characterised by macular and irregular, light to dark brown areas of hyper-melanosis. Melasma affects skin that is exposed to the sun, and UV exposure is considered a risk factor, in addition to genetic predisposition (Grimes, 1995). The majority of patients show

hyperpigmentation on facial skin in a symmetrical pattern, but it can also appear on forearms. Women are proportionally more affected than men, and diagnosis is often associated with pregnancy, oral contraceptive use, hormone therapy and anticonvulsant medication use. Individuals with darker skin corresponding to types IV-VI on the Fitzpatrick scale are also disproportionately affected (Plensdorf, Livieratos and Dada, 2017; Hexsel *et al*., 2013; Grimes, 1995).

Other common hyperpigmentation disorders are similar in phenotype but differ in characteristics or pathogenesis. For example post-inflammatory hyperpigmentation appears as irregular areas of darker skin but occurs as a consequence of inflammation, leading to melanocyte hypertrophy and increased melanin deposition in the epidermis. Similarly to melasma, it affects darker skin types III to VI more than lighter skin types (Plensdorf and Martinez, 2009). On the other hand, solar lentigines predominantly appear after chronic sun exposure due to localised proliferation of melanocytes and are more common in older individuals, as well as skin types I-III (Plensdorf, Livieratos and Dada, 2017). Ephelides are similar to solar lentigines but usually appear in younger individuals after sun exposure. While these disorders do not cause physical problems, affected people often report adverse psychological effects and significant reduction in quality of life (Maymone *et al*., 2017; Amatya, Jha and Shrestha, 2020). As a result, effective and safe treatments should be available for patients needing to correct hyperpigmented areas.

The methods of treatment currently available are similar for several of the acquired hyperpigmentation disorders. They include topical depigmentation compounds such as hydroquinone, used as a first-line treatment for melasma and post-inflammatory hyperpigmentation, retinoids and tretinoin, as well as ablative methods such as chemical peels, cryotherapy and laser treatment (Grimes, 1995; Zubair *et al*., 2019; Plensdorf and Martinez, 2009). However, these treatments are often costly and do not prevent recurrence of the conditions. They are also often accompanied by several distressing side-effects, including hypersensitivity, redness, burning, pain and hypopigmentation, while even post-inflammatory hyperpigmentation can itself be a side-effect of laser treatments for different conditions (Plensdorf and Martinez, 2009). As a result, further research into melanogenesis is needed in order to produce more effective and safe treatments for disorders of hyperpigmentation.

1.6 Thesis aims

As described in the above introduction, a large proportion of melanogenesis research has utilised static methods of imaging melanin formation and transfer. The advent of novel brighter fluorescent proteins, such as mNeonGreen, have made live imaging at a higher spatial and temporal resolution possible. Consequently, the main aims of this thesis were:

1. To successfully generate and validate novel fluorescent probes created by fusing melanosome-specific proteins with bright fluorescent probes such as mNeonGreen
2. To visualise melanosome movement in real-time, from biogenesis to stage IV
3. To observe the effect of bioactive compounds on the activity of melanosome-specific fluorescent probes

2 Materials and methods

2.1 Cell culture

2.1.1 SKMEL28 cell line

SKMEL28 cells were originally obtained from ATCC (https://www.atcc.org/products/htb-72). These are lightly pigmented immortalised melanocytes isolated from a human male, identified as a good candidate for experiments due to their highly dendritic morphology. They were grown in Dulbecco's Modified Eagle Medium (DMEM, Gibco) supplemented with foetal bovine serum (FBS) to a final concentration of 10%, glutamax (Gibco) to a final concentration of 2 mM and penicillin with streptomycin (Gibco) to a final concentration of 100 U/ml. The culture vessels used were either T75 or T25 flasks (TPP). Cells were maintained in an incubator at a temperature of 37 °C and 5% CO_2. Cells were passaged two to three times a week, approximately every three days, once the cells had reached ~ 95% confluence. Passaging the cells began by removing all media from the cells and washing once with 6 ml of room temperature Phosphate Buffered Saline ($PBS^{-/-}$, Gibco) if the cells are cultured in a T75, and 3 ml of PBS if the cells are cultured in a T25 flask. The PBS was taken up and 1 ml of 0.05% Trypsin (Gibco) pre-warmed to 37 °C (~ 0.6 ml if the cells were cultured in a T25) is used to cover the cells initially, with half the initial volume (0.5 ml) then being taken up before the flask was returned to the incubator. After 3-5 min once the cells have detached, they are re-suspended in 10 ml of fresh medium (5 ml if in a T25) pre-warmed to 37 °C, gently mixing with the stripette in order to ensure all cells were detached. Either 2 ml or 1 ml of the suspension was added to a new T75 or T25 flask respectively such that the confluence of the cells once settled would be 20-25%. The total volume in a T75 flask was then made up to 10 ml with fresh medium, or 5 ml in a T25 flask. The culture vessel was marked with the cell line name, date passaged, passage number and seeding density.

2.1.2 MNT1 cell line

The MNT1 cell line was obtained from ATCC (https://www.atcc.org/products/crl-3450). These are highly pigmented immortalised melanocytes containing very dark pigment,

isolated from a melanoma. Cells were grown in DMEM supplemented with 20% FBS, 10% AIM-V (Gibco) medium to a final concentration of 10% and 0.1 mM nonessential amino acids (NEAA, Gibco), according to the cell line supplier's instructions. The culture vessels used were either T75 or T25 flasks (TPP). Cells were maintained in an incubator at 37 °C under 5% CO_2. Cells were passaged twice a week, once the cells had reached ~ 80% confluence, as these cells did not grow past this level of confluence. Passaging was done as described above, with the exception of re-seeding in the new flask, which was done such that the settled cell confluence would be 25-30%.

2.1.3 HT1080 cell line

HT1080 cells were obtained from ATCC (https://www.atcc.org/products/ccl-121). This human immortalised fibroblast cell line was isolated from fibrosarcoma tissue in a white male. They were cultured in DMEM, supplemented with 10 % FBS, 2 mM glutamax, 100 U/ml penicillin with streptomycin. The culture vessels used were either T75 or T25 flasks (TPP). Cells were maintained at 37 °C and 5% CO_2. Cells were passaged two to three times a week, approximately every three days, once the cells had reached ~ 95% confluence, and passaging was done exactly as described above for SKMEL28 cells.

2.2 Cell stock revival and cryopreservation

2.2.1 Revival

For long-term storage, cells were maintained in cryogenic storage vials (Sarstedt) in the vapour phase of liquid nitrogen, or at -80 °C for shorter-term storage. Before reviving a stock, the appropriate medium was warmed to 37 °C and a 15 ml tube (Sarstedt) was filled with 10 ml of medium. The vial containing the cells was then removed from storage and held in a 37 °C water bath until it had almost completely thawed, in order to minimise the time spent by the cells in the freezing medium containing DMSO. The contents were then pipetted into the 15 ml tube containing 10 ml of warmed medium, and this was centrifuged at 200 g for 5 min using a Sigma 3K18 centrifuge. As much of the cell-free supernatant as possible was then removed without disturbing the cell pellet, and the cells were re-suspended in 10 ml of warmed medium for culture in a T75 flask, or 5 ml for culture in a T25 flask,

pipetting up and down with a stripette in order to disperse the cells. The cell suspension was then transferred to a flask and placed into an incubator at 37 °C and 5% CO_2. One or two days later the cells were checked, and the medium replaced with fresh warmed medium if necessary to maximise cell survival.

2.2.2 Cryopreservation

Before commencing the freezing process, cryogenic storage vials were labelled with the passage number of the cells to be frozen down, the date they were frozen, the cell line, and the culture vessel into which they should be revived (T25 or T75 flask). Freezing medium was also prepared in advance, which is composed of 90 % FBS containing 10 % DMSO. Growth medium was removed from the cells to be frozen down prior to washing once with $PBS^{-/-}$ (6 ml if in a T75 and 3 ml if in a T25). Cells were covered in 0.05% trypsin as described in section 1.1 for cell passaging, and allowed to incubate for 3-5 min. Once the cells had detached from the culture vessel, they were re-suspended in the appropriate volume of growth medium specific to the cell line, 10 ml for a T75 and 5 ml for a T25. The contents of the flask were transferred to a 15 ml tube and centrifuged at 200 g for 5 min in a Sigma 3K18 centrifuge. The cell-free supernatant was carefully removed and the remaining cell pellet was re-suspended in an appropriate volume of cold freezing medium for the number of vials to be frozen down (1 ml per vial). Vials were then quickly transferred to a cryo-freezing container, “Mr. Frosty” (Nalgene, Sigma-Aldrich), which was placed in a -80 °C freezer. The “Mr. Frosty” limits the cooling rate of the vials to 1 °C/min, which is the optimal rate for maximal cell survival. The cryogenic storage vials were transferred after 24 hr from the “Mr. Frosty” to long-term storage.

2.3 Cell lysis

Cell lysis was used to prepare samples for use in SDS Polyacrylamide Gel Electrophoresis (PAGE) and native PAGE. Firstly, 6 cm cell culture dishes (TPP) were seeded with cells at 50% confluence. Twenty four-48 hours later (depending on cell growth), cells were either transfected as described in section 1.5, treated with a bioactive compound as described in section 1.4, or directly lysed once the cells had reached 100 % confluence. MNT lysis buffer

(20 mM MES, 30 mM Tris, 100 mM NaCl, pH 7.4) was prepared from a 10X MNT stock and supplemented with 1x Protease Inhibitor (Sigma-Aldrich) and 1 % Triton X-100. The 10X MNT stock was prepared with 3.904g of MES, 4.73g of Tris HCL and 5.84g of NaCl, and was then adjusted to pH 7.4 before making up to 100 ml with deionised water. Once made up, the lysis buffer was kept on ice and used on the same day. The cells in 6 cm dishes used for lysis were firstly washed in room temperature $PBS^{+/+}$ (phosphate buffered saline with 1 mM calcium and 0.5 mM magnesium) twice, after careful removal of the medium. All excess PBS was removed using a 1 ml pipette, and 150-200 µl of lysis buffer was added while the dishes were kept on ice, ensuring they were kept level for even distribution of the lysis buffer. Approximately 20 min later, the cells were examined under a bright field microscope to assess the degree of lysis. A cell scraper (Fisher Scientific) was used to scrape the entire surface of the 6 cm dish, in a downwards motion while spinning the dish around in one hand, ensuring all the material was collected. The suspension was collected into a 1.5 ml tube (Eppendorf) and centrifuged at 13,300 g in a VRW Micro Star 17R centrifuge pre-cooled to 4 °C for 10 min. The supernatant was transferred to a fresh, labelled 1.5 ml tube and flash-frozen in liquid nitrogen before storing in a -20 °C freezer. For lysis using RIPA buffer, a 50 ml stock solution was made with 5 ml of 10X Triton-X100, 0.394g Tris HCl, 0.438g NaCl, 0.25g Sodium deoxycholate and 0.5 ml of 10% SDS. Directly prior to lysis, Protease Inhibitor (Sigma-Aldrich) was added to the required volume of RIPA buffer stock for a final concentration of 10%. All subsequent steps were completed identically to the protocol for MNT lysis.

2.4 Bio-active compound preparation and cell treatment

2.4.1 Sepiwhite

Sepiwhite (undecylenoyl phenylalanine) stock solution was prepared by weighing out 6 mg of the powder and dissolving in 1 ml of sterile DMSO, to produce a final concentration of 0.6% w/v. Aliquots (150 µl) were made in sterile 1.5 ml tubes, and were stored at -20 °C. For treatment of cells in 35 mm glass-bottom dishes (ibidi), one tube was thawed and 1.6 µl of the stock solution was added to 2 ml of warmed medium specific to the cells being treated, for a working solution final concentration of 0.001% w/v. Existing, untreated medium was removed and replaced with the working solution and cells were incubated with the bioactive

for 48 hr prior to imaging. For treatment of cells in 12-well plates, the same concentration of Sepiwhite was applied, making up the solution in 12 ml of warmed medium, 1 ml per well. After 48 hr, the cells were fixed for further examination by immunofluorescence e.g. to determine endogenous Pmel17 levels.

2.4.2 Sucrose Dilaurate

Sucrose Dilaurate was supplied in crystal form, thus a primary stock solution was prepared by selecting a small crystal weighing 0.12 g and dissolving in 1 ml of sterile DMSO, to produce a final concentration of 12% w/v. Then, 200 µl of the 12% stock was diluted further in 1 ml of sterile DMSO, for a final concentration of 2% w/v. 100 µl aliquots of the 2% solution were kept in 1.5 ml tubes. Both the 12% stock and the 2% stock solutions were stored at -20 °C. For a working solution of 0.001% w/v, or 56 µM, 1 µl of the 2% stock solution was added to 2 ml of warmed medium specific to the cells being treated. For a working solution of 0.002% w/v, 2 µl was added to 2 ml of medium, and for a working solution of 0.004% w/v, 4 µl was added to 2 ml of medium. Cells in a 35 mm glass-bottom dish were treated with the specified working solution of Sucrose Dilaurate 48 hr prior to imaging. For treatment of cells in 12-well plates, a 0.004% w/v solution was made up in 12 ml of warmed medium, 1 ml per well. After 48 hr, the cells were fixed for further examination by immunofluorescence e.g. to determine endogenous Pmel17 levels.

For the experiments in which the effects of Sucrose Dilaurate were examined at the point of treatment, the bioactive was applied differently. 35 mm glass-bottom dishes were seeded with cells, and the untreated medium was replaced with 1.5 ml of specialised imaging media (Fluorobrite, Gibco) immediately prior to imaging. At this time, a 1.5 ml tube was prepared containing 1 ml of bioactive at double the concentration of the desired treatment. During imaging, 750 µl of medium on the cells was removed without disturbing the dish, and an equal volume of the prepared bioactive solution was used to replace it.

2.5 Transfection

JetPei transfection reagent (Polyplus)

The jetPei transfection kit includes 50 ml of 150 mM NaCl and 1 ml of the jetPei reagent, and was stored at 4 °C as per manufacturer's instructions. For transfection of 2 x 35mm glass-bottom dishes (ibidi), two sterile 1.5 ml tubes were prepared in a sterile tissue culture flow hood. Each tube was filled with 200 µl of the provided NaCl solution, 100 µl per dish to be transfected. DNA plasmid (6 ug) was then deposited into one tube, 3 µg per dish, while 12 µl of jetPei reagent was placed into the second tube, 6 µl per dish. The tube containing the jetPei solution was vortexed for 10 s, and the contents were added to the tube containing the DNA, in that order. The combined solution was vortexed for 15 s and allowed to incubate for 20 min. After incubation, 200 µl of the approximately 400 µl solution was applied to the cells in each dish, in a dropwise manner, ensuring equal distribution of the solution around the dish. The dishes were incubated with the solution for 24 hr prior to imaging. For transfection of 1 x 6cm dish, each tube was instead filled with 250 µl of the NaCl solution, and 5 µg of plasmid DNA and 10 µl of jetPei solution were used per dish. Cells were allowed to reach 95-100% confluence on the day of transfection.

Lipofectamine transfection reagent (Invitrogen)

The Lipofectamine 3000 transfection kit includes one vial of Lipofectamine 3000 reagent and one vial of P3000 enhancer reagent, and was stored at 4 °C as per manufacturer's instructions. Transfection using Lipofectamine also requires specialised Opti-MEM medium (Gibco), which was pre-warmed to 37 °C before each transfection. For transfection of 1 x 35 mm glass-bottom dishes (ibidi), first two sterile 1.5 ml tubes were prepared in a sterile tissue culture flow hood. For each dish to be transfected, 125 µl of Opti-MEM was pipetted into each tube. Three µg of plasmid DNA were then pipetted into one tube, together with 4 µl of P3000 enhancer reagent. Six µl of Lipofectamine 3000 Reagent was then pipetted into the second tube. Each tube was vortexed for 5 s and the contents of the tube containing the DNA and P3000 reagent were added to the tube containing Lipofectamine 3000 Reagent, importantly in that order. The combined solution was vortexed for 5s before incubation at room temperature for 10 min. The 250 µl solution was then pipetted onto the cells with existing media present, in a dropwise manner to ensure even distribution of the transfection solution. The dish was incubated with the transfection material for 2 hr, before all the medium was removed, the cells were washed once in 1.5 ml of room temperature sterile $PBS^{-/-}$, and the cells were covered with fresh, pre-warmed normal medium. Twenty-four hr

post-transfection, the cells were imaged. Cells were allowed to reach 95-100% confluence on the day of transfection.

2.6 Microscopy

2.6.1 Live cell imaging

Immediately prior to live imaging of cells in 35mm glass-bottom dishes (ibidi), existing medium was replaced with 1.5 ml of Fluorobrite medium (Gibco) pre-warmed to 37 °C. This medium reduces background fluorescence signal, allowing clearer visualisation of the fluorophore being imaged. All live cell imaging was performed on a Zeiss LSM 880 confocal microscope with Airyscan. Before imaging, the environmental control settings on the microscope were set to 37 °C and 5% CO_2, and the peltier stage temperature was set to 37 °C. For all experiments using GFP and mNeonGreen fluorescence probes, a 488 nm laser was used for excitation. For experiments using tdTomato, a 543 nm laser was used for excitation. The objective used for most experiments was the x63 NA 1.4 oil immersion lens, with the x40 NA 1.30 oil immersion lens being used for some experiments.

For quantification of the effect of bio-active compounds on the behaviour of the mNG-Pmel17 (MαC) probe, representing the cells' melanin production levels, two 35 mm glass-bottom ibidi dishes were seeded with SKMEL28 cells per replicate of the experiment. One of these dishes was treated with the bio-active, as described in sections 1.4.1 and 1.4.2, and the other was untreated. During imaging, ~20 cells were selected per dish, and a 50-100 frame time-lapse was taken of each one, with frames being approximately 300-600 ms apart.

For examination of the effect of Sucrose Dilaurate on actin organisation, for each experiment one 35 mm glass-bottom ibidi dish was seeded with stable SKMEL28 tdTomato-LifeAct expressing cells for a confluence of approximately 75 % on the day of imaging. For imaging, the x43 oil immersion lens was selected to enable larger cells to be imaged as whole cells. The eyepiece was used to select one representative cell, and its location was noted in the ZEN (black edition) software. First, an image of the untreated cell was captured using the

Airyscan detector, before treatment was applied as described in section 1.4.2, without moving the dish. After application of treatment, an image was taken of the cell every 5 min.

2.6.2 Fixed cell imaging

Most of the imaging of fixed cells was performed on a Zeiss LSM 880 confocal microscope with Airyscan, with a small number of imaging done on a Zeiss LSM 800 confocal microscope with Airyscan, and a Zeiss Axioskop 40 light microscope. For imaging of cells stained with Alexa Fluor 488-conjugated secondary antibody, the 488 nm laser was used on both the LSM 880 and the LSM 800, and the appropriate Alexa Fluor 488 filter was used on the Axioskop 40. For imaging of cells stained with Alexa Fluor 594-conjugated secondary antibody, the 594 nm laser was used on the LSM 880. For imaging of fixed cells transfected with constructs containing tdTomato on the Axioskop 40, the Alexa Fluor 546 excitation filter was used.

For experiments to examine the effect of bioactive compounds on endogenous Pmel17 levels, cells were treated as described in section 1.4, fixed, and stained with Pmel17 primary antibody and Alexa Fluor 488 secondary antibody. During imaging on the Zeiss LSM 880, 20 images were taken for each repeat of each condition, using the exact same image capture settings for all treatment conditions.

2.7 Immunofluorescence

In preparation for fixed cell immunofluorescence, 13 mm coverslips (VWR) were placed in a 12-well tissue culture plate (TPP), one per well to be used. The wells were then seeded with cells for a confluence of approximately 50 %, with a proportion of these settling onto the coverslips. Any treatment or transfection was applied 24 hr later. Once the cells had reached 85% confluence, the coverslips were first washed twice in 2 ml of room temperature $PBS^{+/+}$. The cells were then fixed in 1 ml per well of 4% PFA for 10 min at room temperature, before being washed twice in 2 ml $PBS^{+/+}$ for 5 min each time on a rocker. 4% PFA was prepared by diluting 10 ml of 16 % PFA (Agar Scientific) in 30 ml $PBS^{+/+}$. Cells were then permeabilised in 1 ml of 0.1% Triton X-100 for 10 min on a rocker, before a further three

washes in 2 ml $PBS^{+/+}$. The coverslips were then blocked within the wells, in 1 ml of 2% BSA per well for 30 min. Two% BSA was prepared by dissolving 1g of BSA(Sigma-Aldrich) in 50 ml of $PBS^{+/+}$, vortexing at high speed to aid dissolution. The final solution was then filter-sterilised using a sterile 0.2 μm filter (Fisher Brand) and a sterile 5 ml syringe (Henke Sass Wolf), and collected into a fresh 50 ml tube (Sarstedt), to be stored at 4 °C. During the 30-min block, primary antibody dilutions were prepared in 2% BSA. A list of antibodies used in immunofluorescence can be found in Table 2.1 along with the concentrations used for each. Dilutions were prepared allowing for 50 μl of liquid per coverslip. The antibody incubation chamber was prepared with strips of Parafilm M (Heathrow Scientific, VWR) onto which 50 μl droplets of antibody dilution were placed, approximately 5 cm apart. After blocking, each coverslip was turned onto one droplet, cell side facing the liquid. A wet paper towel was placed into the incubation chamber away from the coverslips in order to maintain humidity, and the coverslips were incubated overnight at 4 °C. Following incubation, the coverslips were returned to their original wells in the 12-well plate with the cells facing upwards, and they were washed in 2 ml $PBS^{+/+}$ each three times for 5 min on a rocker. During the washes, the secondary antibody dilutions were prepared in 2% BSA, 50 μl per coverslip (Table 2.1). Antibody dilution droplets were placed on clean strips of Parafilm M as described for the primary antibody dilution, taking care to shield both the secondary antibodies and the dilutions from the light to prevent bleaching. After the washes, excess $PBS^{+/+}$ was removed from the wells and the coverslips were turned onto the antibody dilution droplets, cell side down, using a wet paper towel to maintain humidity as with the primary antibody incubation. Coverslips were incubated in the humidity chamber for 1 hr at room temperature. The coverslips were then washed in $PBS^{+/+}$ in the original wells, three times for 5 min each on a rocker, covering the 12-well plate in foil to prevent bleaching of the fluorescent secondary antibody. During the washes, 50 μl droplets of DAPI solution were placed on clean Parafilm M strips, one for each coverslip, taking care to protect the DAPI droplets and solution from the light to prevent bleaching. DAPI solution was prepared by diluting 10 μl of 1 mg/ml stock in 250 ml of $PBS^{+/+}$ and adding 2.5 ml of 0.02% sodium azide. The coverslips were then turned onto the DAPI droplets, and incubated for 10 min at room temperature. During this time, glass slides were prepared for the coverslips by first cleaning with 70% ethanol, and then pipetting two 5 μl droplets of antifade mounting medium (Vectashield) onto each, one droplet for each coverslip. The coverslips were then washed by briefly dipping once in $PBS^{+/+}$, and were placed onto the mounting

medium droplets. A sheet of clean paper towel was placed on the bench and the slides were carefully pressed down onto this, coverslip side down, in order to remove excess mounting medium. The slides were covered to prevent bleaching, and after 20 min, nail varnish was placed around the edges of the coverslips, in order to seal them. The slides were labelled and placed in a slide holder at 4 °C until imaging. If any salt crystals remained on the top of the coverslips from the $PBS^{+/+}$, these were removed by carefully wiping with a paper towel soaked in deionised water.

Table 2.1. All of the antibodies used, including concentrations used for both immunofluorescence and western blotting.

Antibody	1º or 2º	Host	Clonality	Manufacturer	Cat. number	IF conc.	WB conc.
Anti-Rab27A	1º	Rabbit	Polyclonal	Proteintech	17817-1-AP	1:100	1:1000
Anti-DCT	1º	Rabbit	Polyclonal	Proteintech	13095-1-AP	1:100	1:1000
Anti-SILV	1º	Rabbit	Polyclonal	Proteintech	27329-1-AP	-	1:500
Anti-Pmel17 (E-7)	1º	Mouse	Monoclonal	Santa Cruz Biotechnology	Sc-377325	1:100	1:500
Anti-HMB45	1º	Mouse	Monoclonal	BioLegend	911504	1:100	1:1000
Anti-tdTomato	1º	Goat	Polyclonal	SICGEN	AB8181-200	-	1:1000
Anti-PDI	1º	Rabbit	Polyclonal			1:100	-
Anti-beta Actin	1º	Mouse	Monoclonal	Abcam	ab8224	-	1:10,000
Anti-mNeonGreen	1º	Mouse	Monoclonal	Chromotek	32F6	-	1:1000
Anti-LAMP1	1º	Rabbit	Polyclonal	Santa Cruz Biotechnology	Sc-5570	1:100	-
Anti-Mouse IgG/HRP	2º	Goat	Polyclonal	DakoCytomation	P0447	-	1:3000
Anti-Rabbit IgG/HRP	2º	Swine	Polyclonal	DakoCytomation	P0217	-	1:3000
Alexa Fluor 594 anti-Mouse IgG	2º	Donkey	Polyclonal	Invitrogen	A21203	1:500	-
Alexa Fluor 488 anti-Mouse IgG	2º	Goat	Polyclonal	Invitrogen	A11001	1:500	-
Alexa Fluor 594 anti-Rabbit IgG	2º	Donkey	Polyclonal	Invitrogen	A21207	1:500	-
Alexa Fluor 488 anti-Rabbit IgG	2º	Donkey	Polyclonal	Invitrogen	A21206	1:500	-

2.8 BCA protein assay

After producing cell lysates, their concentrations were determined using a Pierce BCA protein assay kit (Thermo Scientific). Firstly, standard solutions were prepared as per the manufacturer's instructions by dissolving the provided BSA vial in differing volumes of deionised water to produce 9 different protein concentrations, ranging from 0 to 2000 μg/ml. The final dilutions were made up in 1.5 ml tubes (Eppendorf) and stored at -20 °C. For the protein assay, the proteins standards were thawed on ice, and 10 μl of each was pipetted per well into the first two rows of a 96-well plate (Thermo Scientific), for two repeats of each concentration. The samples to be assayed were also thawed on ice, and 10 μl of each was pipetted into two wells for two repeats. Two blank wells for the final analysis were also included using 10 μl of MNT lysis buffer or RIPA buffer depending on the lysis buffer used in the samples. The working reagent was then prepared by mixing working reagent A (WRA) with working reagent B (WRB) together, for a ratio of 50:1 WRA:WRB, and accounting for 200 μl of solution per well. Once the 200 μl of working solution were pipetted onto the samples and protein standards, the 96-well plate was covered and incubated at 37 °C for 30 min with slight agitation. Once incubation was complete, the 96-well plate was read using a plate reader with a 570 nm filter (540-570 nm range can be used). A standard curve was plotted with the average absorbance value for each of the protein standards against their known concentrations, after subtracting the absorbance value of the blank. Concentrations of unknown samples were determined by comparing their average absorbance values against the standard curve, after also subtracting the blank value from each.

2.9 Gel electrophoresis

2.9.1 SDS-Polyacrylamide Gel Electrophoresis (SDS-PAGE)

Sample preparation:

Firstly, the lysates to be examined using SDS-PAGE were thawed on ice, and the appropriate volume to be used was calculated using the results of a BCA protein assay, such that an equal amount of protein would be loaded into each well. In order to load 20 μl of sample in each well, for each of the samples the appropriate volume of lysate was pipetted into a 1.5

ml tube, along with an equal volume of 2x SDS Laemmli sample buffer (Bio-Rad), 2 µl of DTT, and, if required, an appropriate volume of the lysis buffer used to collect the sample in order to make up to a total volume of 20 µl. Laemmli sample buffer is composed of 65.8 mM Tris-HCl, 2.1% SDS, 26.3% (w/v) glycerol, 0.01% bromophenol blue. The samples were boiled for 5 min at 95 °C using a dry bath (Thermo Scientific) before being centrifuged at 13,300 g for 5 min at room temperature. The samples were then kept at room temperature until loading. The lysates were flash-frozen in liquid nitrogen and returned to -20 °C for storage.

Gel preparation:

In order to prepare one 10% gel, 15 ml of the running gel solution was prepared in a 50 ml tube (Sarstedt). The components for this are 7.2 ml of deionised water, 3.75 ml of 40% Acrylamide (Severn Biotechnology) 3.75 ml of 1.5M Tris, 150 µl of 10% SDS and 150 µl of 10% APS. A further 3 ml of stacking gel solution was prepared in a second 50 ml tube, using 2.2 ml of deionised water, 400 µl of 40% acrylamide, 400 µl of 1.0 M Tris, 30 µl of 10% SDS and 23 µl of 10 % APS. Once these solutions were prepared, but not yet induced to polymerise, the gel casting equipment (Mighty Small, Hoefer) was assembled. An 8x10cm glass plate and a white ceramic plate of the same size were assembled, separated by two narrow and thin plastic pieces on the left and right sides of the plates, to form the border for gel casting. Once assembled, deionised water was pipetted between the glass and ceramic plates to ensure the casting setup was completely sealed. The running gel solution was then induced to polymerise by adding 6 µl of TEMED in a chemical flow cabinet, inverting to mix, and immediately pipetting between the glass and ceramic plates, such that the top of the liquid was 1cm below the top of the glass plate. Deionised water was pipetted carefully on top in order to ensure the top of the running gel was level. While the running gel was polymerising, the sample preparation was initiated, as described above. Once the running gel had completely polymerised, the water was removed from the top, and 2 µl of TEMED was added to the stacking gel solution to induce polymerisation. After inverting to mix, the solution was pipetted above the running gel, reaching the top of the glass plate, and a 10-well comb was inserted. Once fully polymerised, the glass and ceramic plates containing the gel were moved to the gel electrophoresis kit (Hoefer), and running buffer was poured in such that the entire gel was covered. Running buffer was made by diluting 100 ml of 10x

Tris/Glycine/SDS buffer (Bio-Rad) with 900 ml of deionised water, for final concentrations of 25 mM Tris, 192 mM Glycine and 0.1% SDS, and a pH of 8.3. A second singular glass plate was clipped to the opposite side of the gel in order to contain the running buffer, if only one gel was being run. A 10-well stencil was placed onto the glass to mark the positions of the wells, and the 10-well comb was removed. The samples and 5 µl of protein ladder (Precision Plus Protein Dual Colour Standards, Bio-Rad) were pipetted into the wells, aligning the pipette tip against the inside of the glass plate to ensure the sample was entering the well uniformly, and the gel was run at 40 mA using a Bio-Rad power source for approximately 30 min, or until the laemmli sample buffer had reached the bottom of the gel.

2.9.2 Native/Non-reducing PAGE

Sample preparation:

The lysates to be examined were thawed on ice, and the appropriate volumes to be used were calculated using the results of a BCA protein assay, in order to load 40 µl of sample in each well. After centrifugation to remove residual insoluble material, the required volumes of lysate were pipetted into individual 1.5 ml tubes, along with an equal volume of sample buffer (Novex Tris-Glycine Sample Buffer 2x, Invitrogen), as well as the appropriate lysis buffer corresponding to the lysate if necessary to make a total volume of 40 µl per well. Once prepared, the samples were kept on ice to prevent denaturation, and the lysates were flash-frozen in liquid nitrogen and returned to -20 °C.

Gel preparation:

All native gel electrophoresis was done using pre-cast gels (Novex WedgeWell 10% Tris-Glycine Gel, Invitrogen) with 10x Novex Tris-Glycine Native Running Buffer (Invitrogen), at 4 °C. Firstly, the pre-cast gel was removed from the packaging immediately prior to use and placed into the gel electrophoresis tank (Bio-Rad). Running buffer was prepared by diluting 50 ml of the 10x running buffer with 450 ml of deionised water, pre-chilling at 4 °C. This was poured into the gel electrophoresis tank such that all of the gel was covered, and the 12-well comb was then removed from the top of the gel. Five µl of ladder and 40 µl

of sample was then loaded into the wells, and the gel was run at 200 V for approximately 70 min at 4 °C.

Gel imaging:

After completion of electrophoresis, the gel was removed from the plastic casing and transferred to a clear thin sheet of plastic, cut to be slightly larger than the gel. The gel on the plastic sheet was placed onto a Typhoon 94000 laser-scanning gel imager, and a 488 nm laser was used to detect fluorescent protein (non-denatured mNeonGreen) in the gel. Exposure and laser power settings were adjusted in the software to obtain optimum resolution and signal. The gel was then retained for further examination by western blotting, as described below.

2.10 Western blotting

2.10.1 Protein transfer

After electrophoresis of the gels was complete, the protein transfer kit was assembled. First, four equally sized 11x8 cm squares of chromatography paper (Whatman) were cut, to the same size as the transfer support sponges, along with an 11x8 cm square of PVDF transfer membrane (Merck, Immobilon-P). The support sponges and filter paper squares were placed in a tray and covered in transfer buffer. Transfer buffer was prepared by dissolving 2.9g of Trizma base and 14.5g of glycine in 700 ml of deionised water, adding 200 ml of methanol and making up to a total volume of 1L with deionised water. The final concentrations were 25 mM Tris, 190 mM glycine and 20% methanol. The PVDF membrane was activated by submerging in pure methanol for 20 seconds, and then placed into transfer buffer, in the tray with the support sponges and filter paper. The gel was then removed from the electrophoresis tank, and the glass plate was carefully prised away from the gel. The gel was detached from the ceramic plate by sliding the plastic beneath it. The gel was guided on top of the PVDF membrane submerged in transfer buffer, and two of the filter paper squares submerged in buffer were placed on top of the gel, securing it in place. Using tweezers, the filter paper-gel-PVDF membrane “sandwich” was flipped onto one of the support sponges, and the remaining two filter paper squares were placed on top of the PVDF membrane, ensuring any

air bubbles were removed that would prevent even protein transfer. The complete "sandwich" was as follows: support sponge – 2x filter paper – gel – PVDF membrane – 2x filter paper – support sponge. This was placed into a transfer cassette, and then into a protein transfer tank (Bio-Rad), ensuring that the PVDF membrane was on the correct side of the gel, in the same direction as protein transfer. A -20 °C cold pack was placed into the tank next to the cassette, and the transfer cassette was submerged in transfer buffer. The proteins were then transferred at 150 mA for 2.5 hr. After transfer, the "sandwich" was disassembled and the PVDF membrane was removed using tweezers, with the top left corner being trimmed in order to mark which side the proteins were facing.

2.10.2 Blocking

The PVDF membrane was then placed into a small plastic tray and blocked in a 5% w/v milk solution. This was made by dissolving 2.5g of standard milk powder in 50 ml of TBST buffer. TBST was prepared by dissolving 8 g NaCl, 0.2 g KCl and 3 g Trizma base in 800 ml of deionised water, before adjusting the pH of the solution to 8.0, and then making up the total volume to 1L with further deionised water. One ml of Tween 20 (Sigma-Aldrich) was then added, pipetting slowly due to the high viscosity of the liquid. The PVDF membrane was blocked in the milk solution overnight at 4 °C, or at room temperature for 1 hr. After blocking, the milk solution was removed and approximately 20 ml of TBST was poured into the tray in order to wash the membrane. The first wash was done by shaking the tray to vigorously wash the membrane, and four subsequent 5 min washes were performed, placing the tray on a rocker.

2.10.3 Primary antibody

After the completion of the 5 washes following blocking, the membrane was incubated with the primary antibody. First, a total of 3 ml of antibody dilution was made up in a 50 ml tube. A list of antibodies used in western blotting can be found in Table 2.1. The antibody incubation solution consisted of 2.7 ml TBST and 0.3 ml 5% w/v milk solution pre-prepared for blocking, along with the appropriate volume of antibody. If using two different antibodies, the membrane was cut in half at this stage using a scalpel. The membrane was then transferred from the tray into the 50 ml tube containing the antibody dilution, using

tweezers to lift the membrane, sliding into the tube protein side up. The tube was labelled, placed on a roller, and incubated with the antibody for 1hr at room temperature. After incubation, the membrane was washed five times as described after blocking (section 1.10.2), with the first wash using a larger volume of TBST and manually shaking to remove most of the excess antibody solution.

2.10.4 Secondary antibody

During the primary antibody washes, the secondary antibody dilution was prepared in a clean 50 ml tube by mixing 2.7 ml of TBST, 0.3 ml of 5% w/v milk solution and the appropriate volume of secondary antibody. The secondary antibodies can be found in Table 2.1. For primary antibodies raised in a mouse, anti-mouse secondary antibody was used, and for those raised in a rabbit, anti-rabbit secondary antibody was used. Using tweezers, the membrane was then transferred from the primary antibody tube to the labelled secondary antibody tube, and was incubated for 1 hr at room temperature on a roller. After incubation, the membrane was washed five times, as detailed after primary antibody incubation.

2.10.5 ECL application and film exposure

During the final secondary antibody washes, two 30x30cm sheets of Sarogold plastic film were spread onto a bench, using a ball of dry paper towel to remove any wrinkles. The ECL (Amersham) solution was prepared, mixing 0.5 ml of Reagent A with 0.5 ml of Reagent B in a 1.5 ml tube to make 1 ml of total solution per membrane. The solution was then vortexed to ensure complete mixing of the reagents. After the secondary antibody washes were complete, the membrane was placed onto the lower half of one of the Sarogold sheets using tweezers. The 1 ml ECL solution was then pipetted dropwise onto the protein side of the membrane, evenly over its surface. The upper half of the Sarogold sheet was then lowered onto the top of the membrane, using dry paper towel to smooth out any wrinkles and ensure even coverage of the solution. The membrane was then covered to protect it from the light and incubated with the ECL solution for 5 min. The top half of the Sarogold sheet was then lifted off the membrane, which was transferred to the bottom half of the clean sheet of Sarogold, touching the edge of the membrane against a dry paper towel to remove excess ECL solution. The upper half of the Sarogold sheet was lowered onto the membrane, using

dry paper towel to smooth out wrinkles, and a scalpel was used to cut around the membrane. A fluorescent sticker (Agilent Technologies) was placed in the top left corner of the Sarogold sheet containing the membrane, and the membrane was placed in an exposure cassette (Kodak). All subsequent steps were carried out in the dark under red light. One 20x25cm sheet of CL-X Posure film (Thermo Scientific) was placed on top of the membrane. An initial exposure was made for 1-5 min followed by multiple exposures if required. The film was then developed either by hand, or using an OPTIMAX 2010 developer machine. If developing by hand, the film was first placed in x-ray developer fluid (RG) for 1 min, then briefly in clean water, and finally in x-ray fixative solution (RG) for 5 min, before being washed again with distilled water and allowed to dry.

2.11 Plasmid preparation

All plasmid preparations were made using a Qiagen plasmid purification Maxi Prep Kit. Firstly, the bacterial stock was streaked onto an agar plate containing appropriate antibiotic for bacterial selection, using a Bunsen burner and sterile tips to maintain aseptic conditions. If streaking from a bacterial stock frozen in glycerol, a pipette tip was used to dislodge a small chunk of ice, which was dropped onto the outer edge of the agar plate in order to streak. The plate was kept facing up for approximately 10 min, or until it had almost completely dried. Plates were then incubated at 37 °C for around 16 hr, or until individual colonies were large enough to be selected. Two individual colonies were selected for each construct, and inoculated into a Rohre 13 ml tube (Sarstedt) containing 3 ml LB broth (manufacturer) for the starter culture, with the appropriate selection antibiotic. Sterility was maintained by pushing the pipette tip against the wall of the tube and lowering slowly to avoid the pipette touching the sides. For selection using ampicillin, a concentration of 100 µg/ml was used. The inoculated starter cultures were incubated at 37 °C for 8 hr with vigorous shaking at approximately 280 rpm. Duran flask were prepared, one for each starter culture, with 100 ml of LB broth and the appropriate selection antibiotic. One hundred-200 µl of the starter culture was dispensed into a flask, and incubated at 37 °C for 12-16 hr with vigorous shaking at approximately 280 rpm. The contents of each flask were then poured into 50 ml tubes. The bacteria were harvested by centrifuging the tubes at around 3,901 x g for 30 min at 4 °C, using an Allegra X-22R centrifuge (Beckman Coulter). The bacterial pellets were re-suspended in 10 ml of Buffer P1. The pellet was fully dispersed by pipetting

up and down. Ten ml of buffer P2 was then added and mixed by inverting the tube 4-6 times, or until the solution had turned entirely blue, due to the addition of LyseBlue to Buffer P1, and this was incubated at room temperature for 5 min. 10 ml of pre-chilled Buffer P3 was then added, and the solution mixed thoroughly by inverting 4-6 times, or until the solution had turned from blue to white. The solution was then incubated on ice for 20 min. After incubation, the solution was poured from the original 50 ml tube into a specialised centrifuge tube (Nalgene), and was centrifuged at ≥20,000 x g for 30 min at 4 °C using an Avanti- J-26 XP centrifuge (Beckman Coulter). During this step, a QIAGEN-tip 500 was equilibrated by applying 10 ml of Buffer QBT and allowing the column to empty by gravity flow, placing a plastic box underneath to collect the waste. The supernatant after centrifugation was then applied to the QIAGEN-tip and allowed to pass through by gravity flow. The QIAGEN-tip was then washed with 2 x 30 ml of Buffer QC an allowed to empty into the waste box by gravity flow. The plasmid DNA was then eluted from the column with 15 ml of Buffer QF, which was collected into a clean centrifuge tube (Nalgene). The eluted DNA was precipitated by adding 10.5 ml of room temperature isopropanol, and the solution was mixed by inverting 4-6 times before centrifuging at ≥15,000 x g for 30 min at 4 °C using an Avanti-J-26 XP centrifuge. The supernatant was carefully poured out, holding the tube such that the DNA pellet was facing upwards. The pellet was then washed in 5 ml of room temperature 70% ethanol and centrifuged at ≥15,000 x g for 10 min using the same centrifuge. The supernatant was collected from the tube using a 10 ml stripette until a small volume remained, taking care not to disturb the pellet. As much remaining supernatant as possible was then removed using a pipette, and the pellet was left to air dry under a Bunsen burner flame. Once dry enough, the pellet was re-dissolved in 100-200 µl of sterile TE buffer, and its concentration was determined using a Thermo Scientific NanoDrop Lite Spectrophotometer.

2.12 Stable cell lines

The following protocol was used to produce an SKMEL28 cell line stably transfected with tdTomato-LifeAct. Firstly, SKMEL28 cells were seeded in a 6-well plate (TPP), and were transfected with the tdTomato-LifeAct plasmid, leaving an untransfected control well. The following day, the cells were treated with G418 (neomycin) antibiotic at a concentration of 750 µg/ml, made up in the regular medium for SKMEL28 cell culture. Every 2-3 days, the

medium was replaced with fresh antibiotic treatment. The cells in the plate were examined periodically for fluorescence. Once all the control cells had died, after approximately 10-14 days, one of the transfected wells was further split into a 24-well plate (TPP), and the other was split into a T75 flask (TPP) for expansion. The 24-well plate was treated with G418 at 750 μg/ml , while the T75 flask was split once the cells had reached 100% confluence, with 4 vials of cells being retained for cryopreservation of the mixed population, as described in section 1.2.2. The remaining cells from the T75 flask were transferred into a freshT25 flask (TPP) for further culture. This protocol was replicated for attempted generation of an SKMEL28 cell line stably expressing the mNG-Pmel17 (MaC) construct, an MNT1 cell line stably expressing the tdTomato-LifeAct construct, and an MNT1 cell line stably expressing the mNG-Pmel17 (MaC) construct; however stable populations of these cells could not be obtained.

3 Results

3.1 Endogenous Rab27A staining in SKMEL28 cells vs SKMEL28 cells transfected with Rab27A-GFP construct

Among the protein candidates identified as being the most relevant in melanosome development and trafficking, Rab27A was examined first due to the extensive knowledge surrounding its role in melanosome transport, as well as the readily available sequence information for a tagged GFP construct for use in live imaging (Addgene plasmid # 89237; http://n2t.net/addgene:89237; RRID: Addgene 89237; Westbroek et al., 2008). As discussed in the introduction (see 1.2), Rab27A targets to the membrane of mature stage IV melanosomes, recruiting MyoVA and Mlph to mediate transport along microtubules in the cell body and actin filaments in the cell periphery. Rab27A is, however, not specific to melanosomes and binds to a variety of intracellular vesicles.

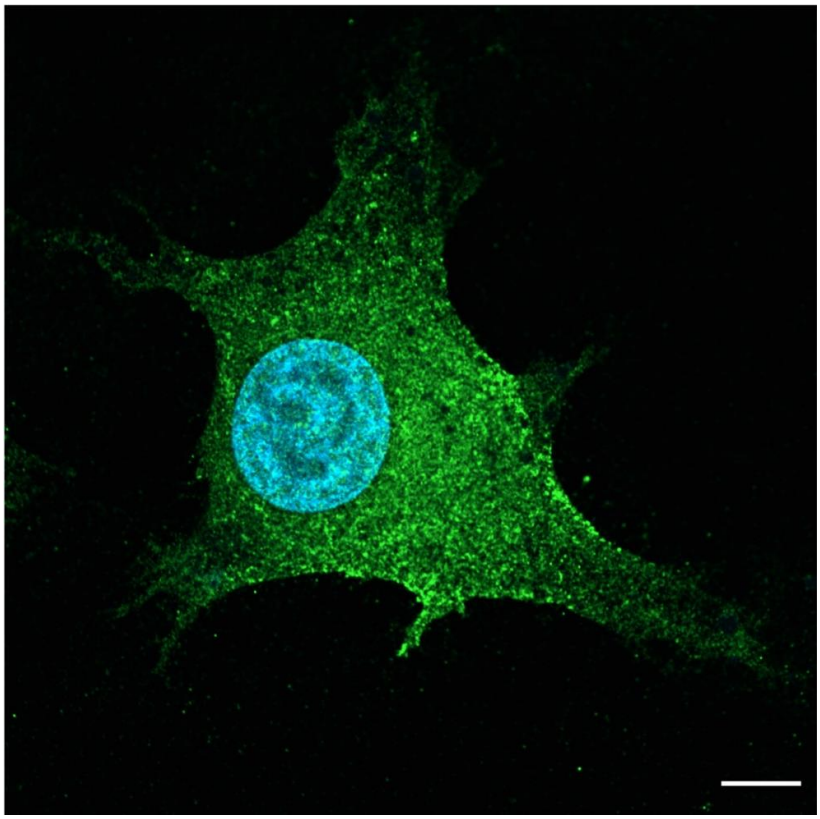

Figure 3.1. Localisation of endogenous Rab27A in an SKMEL28 cell detected by immunofluorescence and confocal microscopy as described in materials and methods. The cells were stained with mouse primary anti-Rab27A antibody and alexa-fluor 488 secondary antibody (green). The nucleus is shown by DAPI staining in blue. Scale bar = 10 μm.

Endogenous Rab27A localisation was detected in SKMEL28 cells by immunofluorescence (Figure 3.1). Cells were fixed and stained with primary anti-Rab27A antibody (Proteintech) as described in materials and methods. Rab27A staining appears punctate and does not appear to localise to a particular area of the cell, revealing the entire shape of the cell. The signal appears to be stronger towards the centre of the cell compared to the dendrites.

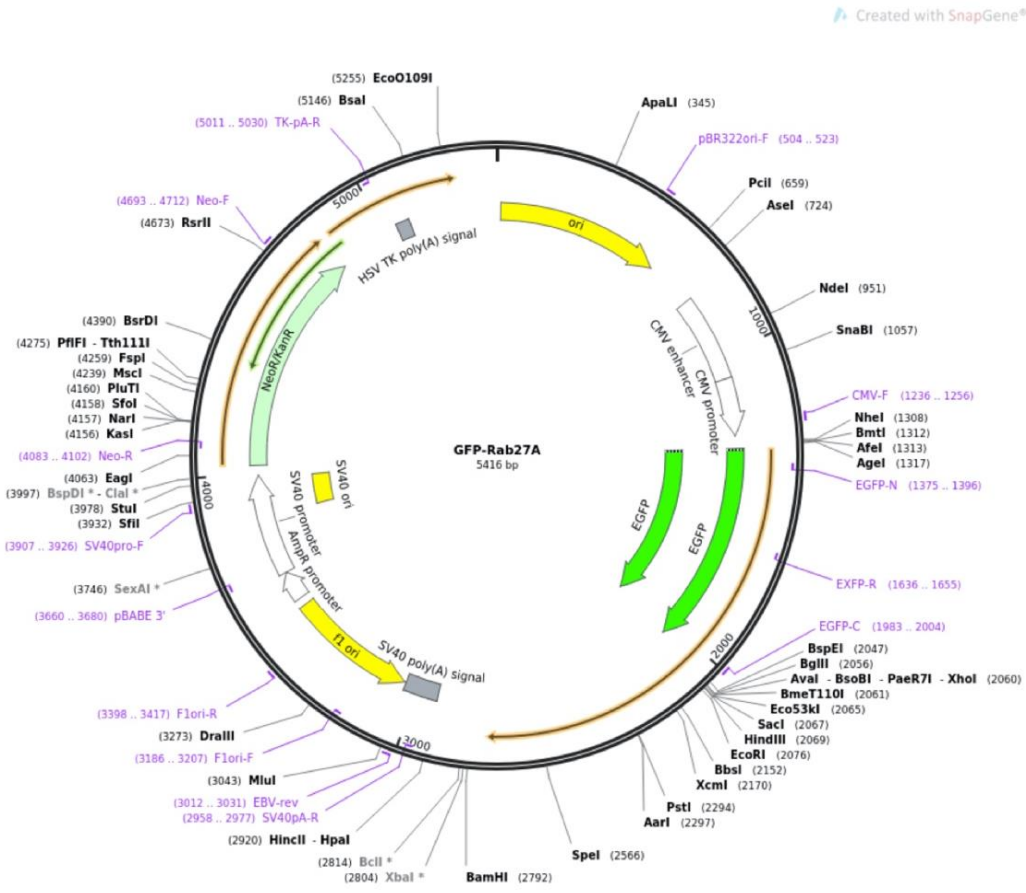

Figure 3.2. Plasmid map of GFP-Rab27A construct

The sites at which the cDNA can be cut by restriction enzymes are shown. A CMV promoter is upstream of the GFP-Rab27A sequence for constitutive expression, and kanamycin and neomycin resistance genes are included for bacterial selection and stable transfection selection in cells respectively.

Following examination of endogenous Rab27A in fixed cells, the subcellular localisation of the protein in live cells was observed using a GFP-tagged Rab27A protein construct (Figure 3.2). The construct was obtained from AddGene as a bacterial stab culture and contains a CMV promoter for constitutive expression of the protein, as well as a gene for kanamycin resistance for bacterial selection during plasmid preparation. The plasmid used was obtained using a QIAGEN Maxiprep kit, and had a concentration of 2.6 µg/µl. SKMEL28 cells were seeded on 35 mm glass-bottom dishes (ibidi) and transfected at high confluence using JetPei reagent 24 hours prior to imaging. Directly before imaging, regular DMEM media was replaced with specialised Fluorobrite media to improve detection of the fluorescent signal

and reduction of background fluorescence. The GFP signal appears to localise to vesicles of varying sizes, along with some generalised signal dispersed within the cells (Figure 3.3). GFP-Rab27A-encircled vesicles ranged from 0.2 μm to 2.5 μm in diameter, with one large vesicle measuring 8.2 μm identified in the cell (Figure 3.3, white box). It is possible that this larger vesicle may be part of the nucleus, with the connection being on a different z-plane and thus not visible in the image. Some background fluorescence was visible within the nucleus, whereas the large vesicle had no background signal at all. There was no specific GFP signal within the nucleus, which is to be expected as Rab27A protein should not enter the nucleus.

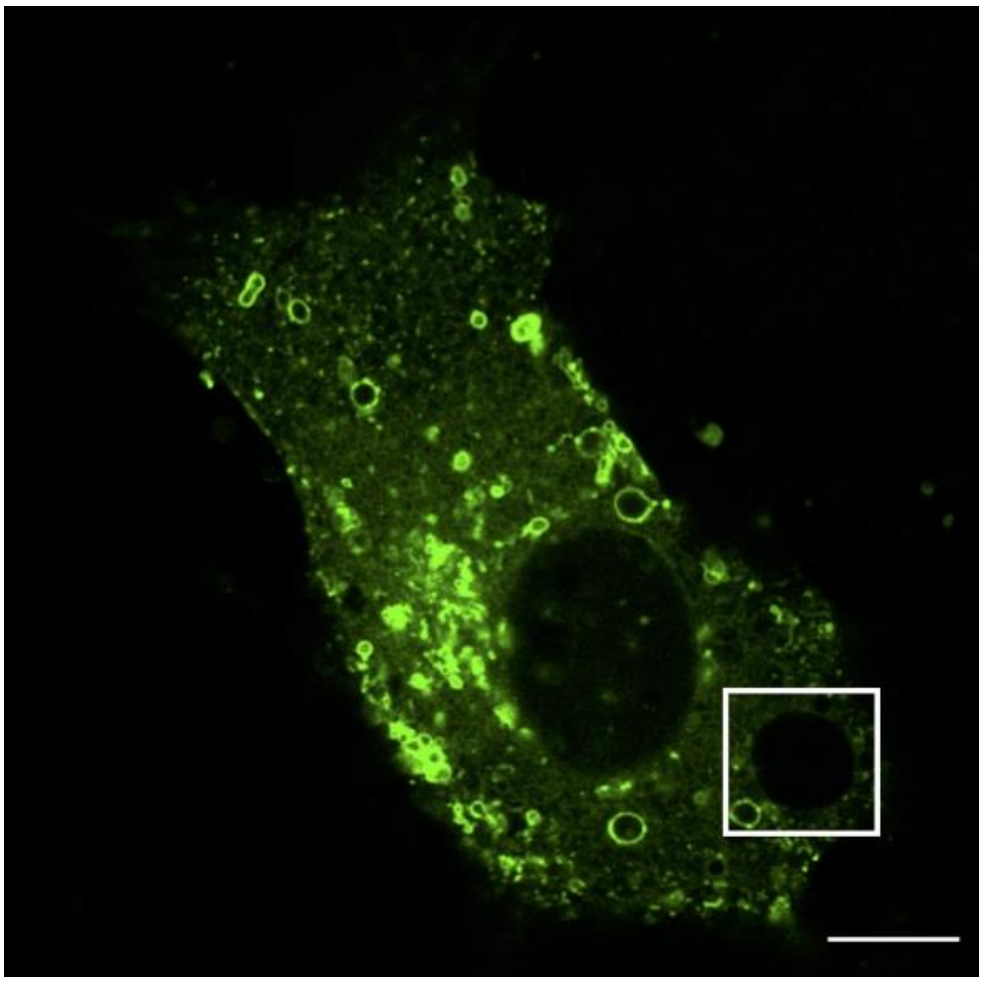

Figure 3.3. SKMEL28 cell transfected with the GFP-Rab27A construct

SKMEL28 cells were transfected with 3 μg of DNA and 6 μl of JetPei reagent. The expression of GFP-Rab27a was captured using a 488 nm laser on a confocal microscope (green). A particularly large vesicle is highlighted in a white box. Scale bar = 10 μm.

3.1.1 Intact Rab27A-GFP construct and endogenous Rab27A detected by western blotting

Following transfection of the construct in SKMEL28 melanocytes, transfected lysates were examined by western blotting. Cells were first seeded onto 6 cm dishes and were allowed to settle. Once they had reached a high confluence they were transfected using JetPei reagent and 5 µg of plasmid DNA, as described in Materials and Methods. After 24 hours, the cells were lysed and the lysate concentrations determined before performing SDS-PAGE and western blotting. Probing the resulting membrane with anti-Rab27A antibody (Proteintech) firstly revealed a band at around 27 kDa in both transfected and untransfected cell lysates (Figure 3.4). This band represents endogenous Rab27A protein, with a molecular weight corresponding with what is expected from the literature. In lane 2, containing transfected cell lysate, there was a second strong band at around 55 kDa. This represents intact GFP-RAb27A protein, as GFP alone has a molecular weight of approximately 27 kDa. This result provides evidence that the construct remains intact in transfected cells, and the vast majority of the GFP signal observed when live-imaging in SKMEL28 cells corresponds to Rab27A protein.

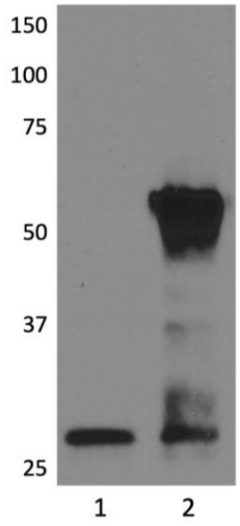

Figure 3.4. Intact GFP-Rab27A detected in transfected SKMEL28 cells by western blotting

Lane 1 contains a sample of untransfected SKMEL28 cell lysate, with a band visible at around 27 kDa corresponding to endogenous Rab27A. The sample in lane 2 is a lysate of SKMEL28 cells transfected with the GFP-Rab27A construct, lysed 24 hours post transfection. Endogenous Rab27A is detected as a band at 27 kDa, and an additional band at around 55 kDa represents intact GFP-Rab27A protein.

3.1.2 GFP-Rab27A does not appear to co-localise with reflectance signal at 633nm

After examining the GFP-Rab27A signal alone, it was imaged in conjunction with confocal reflectance microscopy. Reflectance microscopy using a laser wavelength of 633 nm has previously been shown to identify melanin in skin cells and hair follicles (Thompson, 2019). Live imaging of the cells (Figure 3.5) with a 633 nm laser showed a limited number of small particles spread around the cell, with clusters in some areas. These particles did not appear to co-localise with GFP-Rab27A vesicles of any size. Measurements taken of a number of particles from 5 different cells gave an average particle diameter of 250 nm, which is marginally smaller than expected for melanosomes, around 350-550 nm, as determined by electron microscopy. The lack of co-localisation with GFP-Rab27A and small size of these particles, combined with their apparently random distribution, may suggest that the reflectance at 633 nm highlights a different type of vesicle.

Due to the possible lack of specificity of the GFP-Rab27A protein for detection of melanosomes, as well as the lack of co-localisation of the protein with the reflectance signal, no further research was undertaken using this construct. However, it remains a useful tool for future studies.

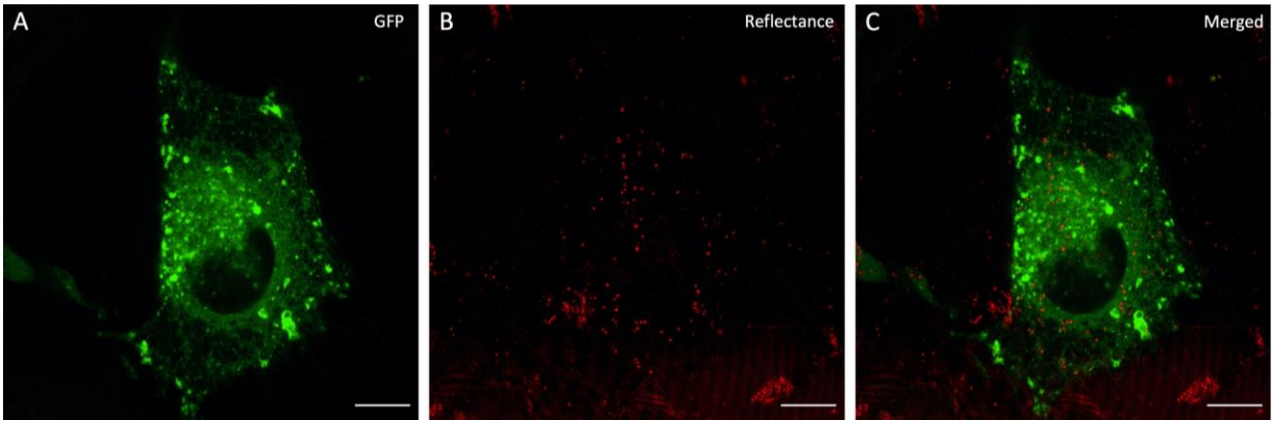

Figure 3.5. SKMEL28 cell transfected with GFP-Rab27A combined with reflectance imaging

A. Still image of GFP-Rab27A in SKMEL28, imaged using a 488 nm laser. B. Reflectance signal in the same cell using a 633 nm laser for identification of pigmentation. C. Merged image with both the GFP-Rab27A and reflectance signal. Scale bars = 10 μm.

3.2 tdTomato-TRP2 construct imaged in SKMEL28 cells

Next, the tdTomato-TRP2 construct was examined. As discussed in the introduction, TRP2 protein is involved in the biosynthesis of melanin, and is thus specifically associated with stage II and III melanosomes. This construct was designed by fusing tdTomato fluorescent protein to the N-terminal region of full-length TRP2. Specifically, tdTomato was inserted after amino acid 24 in the TRP2 protein (Figure 3.6), as amino acids 1-23 of the protein form the signal peptide and are required for correct localisation of the protein (UniProt, P40126). The linker sequence used before and after tdTomato was GGA-TCC, which codes for glycine-serine and provides flexibility in the linkage. tdTomato was selected for fusion with TRP2 in order to be able to image simultaneously with green fluorescent protein constructs for co-localisation purposes. It was chosen over other red fluorescent proteins as it is more photostable, meaning that it is able to resist photobleaching for a longer period of time, allowing for longer time-course imaging.

Figure 3.6. Diagram of TRP2 protein with the addition of the tdTomato tag, shown in orange.

The tdTomato coding sequence was added downstream of the signal peptide (SP). TM denotes the transmembrane domain and Cyt denotes the cytosolic domain.

Following design of the fusion protein, the open reading frame was inserted into a pre-made vector for construction and expression by VectorBuilder (Figure 3.7). Two plasmids were designed, one with a CMV promoter for constitutive protein expression, and the other with a tetracycline-inducible promoter. The constitutive plasmid contains an ampicillin-resistance gene for bacterial selection, as well as a neomycin-resistance gene for selection of mammalian cell clones stably expressing the fluorescently-tagged protein. The inducible plasmid contains the same ampicillin-resistance gene, but in this case a blasticidin-resistance gene was included for stable cell selection. A different antibiotic-resistance gene was selected for the inducible plasmid to allow for the possibility of creating a stable cell line expressing both this plasmid and a second plasmid with a neomycin-resistance gene.

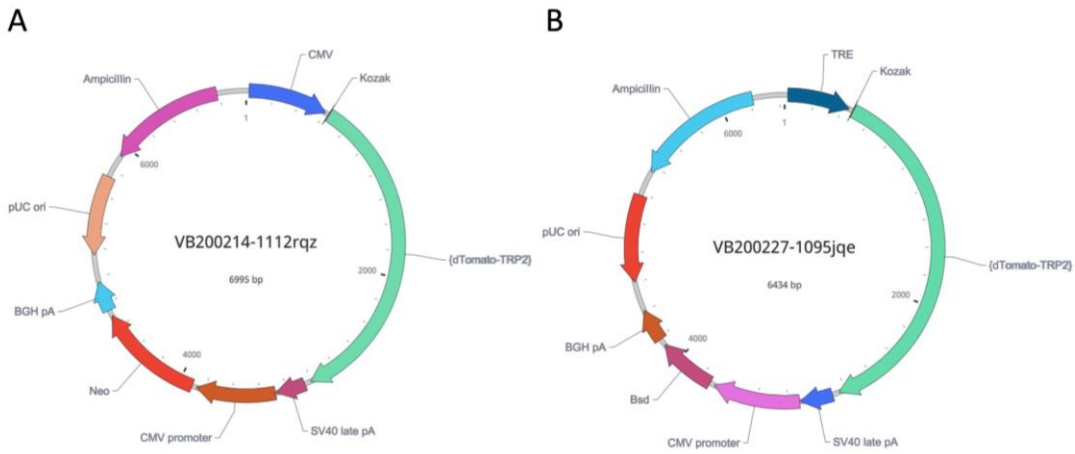

Figure 3.7. Diagram of the finalised vectors containing the tdTomato-TRP2 construct, produced in VectorBuilder

A. The constitutive tdTomato-TRP2 plasmid with a CMV promoter, neomycin resistance gene in red for stable transfection selection and ampicillin resistance gene in pink for bacterial selection. B. The tetracycline inducible tdTomato-TRP2 plasmid with a TRE promoter, blasticidin resistance gene in dark pink for stable transfection selection and ampicillin resistance gene in light blue for bacterial selection.

The plasmids were transfected into SKMEL28 cells using JetPei reagent and, 24 hours later, the cells were fixed onto glass slides and imaged (Figure 3.8). TRP2 protein localises to the membrane of stage II melanosomes to catalyse the synthesis of melanin, and we would thus expect to see tdTomato signal appearing as melanosome-sized particles or ringlets. The tdTomato signal appeared diffuse within the cytoplasm of the cell, with no distinguishable punctate structures that may correspond to melanosomes. The fluorescent protein was distributed equally within the majority of the cell, with a stronger signal directly around the nucleus and ER region. The diffuse nature of the signal suggests that the tdTomato-TRP2 protein may not be expressed as expected. Because of this, the construct was not used in any further experiments.

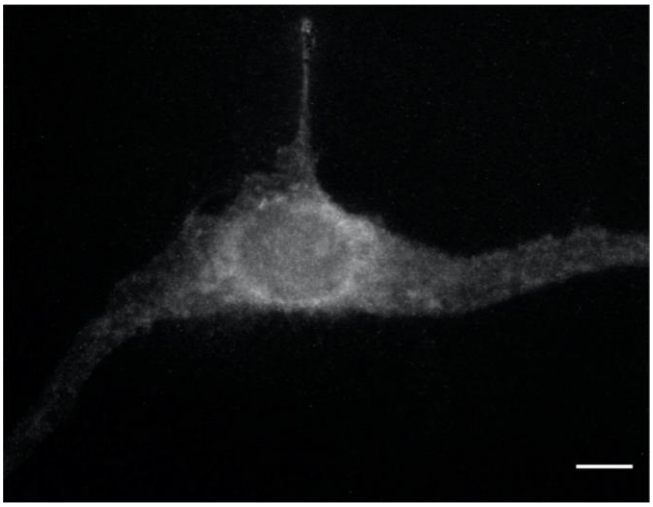

Figure 3.8. SKMEL28 cell transfected with tdTomato-TRP2

The cell was transfected and fixed 24 hours later, before imaging on an Axioskop 40 microscope. Scale bars = 10 μm.

3.3 Design and examination of mNeonGreen-Pmel17 constructs in SKMEL28 cells

After examining the expression of Rab27A and TRP2 proteins, the final candidate for melanosome tracking was the Pmel17 protein. As discussed in the Introduction, Pmel17 undergoes several proteolytic cleavage steps to form the mature protein found in melanosomes. Initially, the full-length protein is comprised of 6 regions: The N-terminal region, the PKD region, the RPT region, the KLD region, the transmembrane domain and the C-terminal region (Figure 3.9). The core amyloid fragment forming the fibril scaffold is derived from sections of the N-terminal region and the PKD region, while the MαC fragments are derived from cleavage of the PKD and RPT regions at one of a number of cleavage sites, producing fragments of varying lengths. Due to the extensive processing that occurs to produce the mature fibrils, the position of fluorescent marker placement within the protein was critical to avoid degradation of the protein or cleavage of the marker in transfected cells.

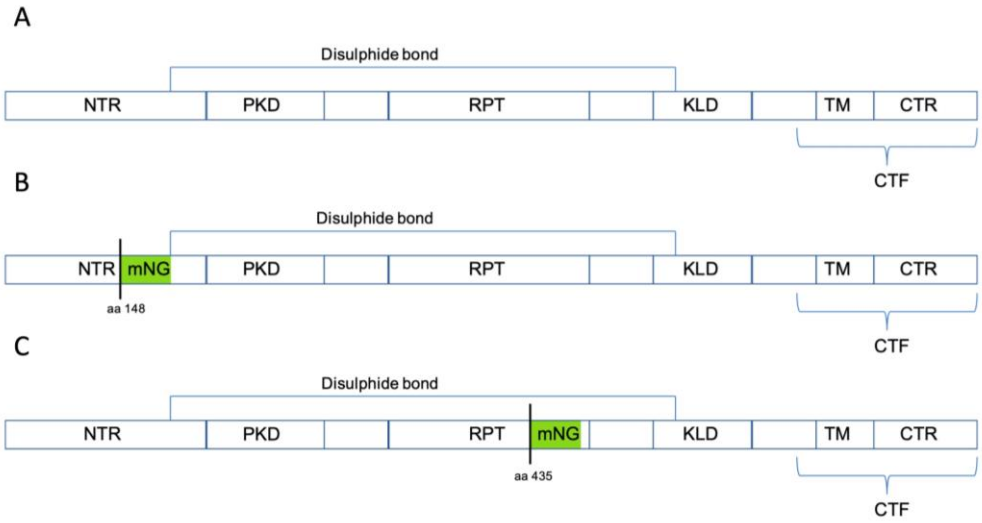

Figure 3.9. Diagram illustrating Pmel17 protein structure and tagged construct design. A. Native Pmel17 protein structure, where NTR denotes the N-terminal region, PKD denotes the polycystic kidney domain, RPT denotes the repeat domain, KLD denotes the Kringle-like domain, TM denotes the transmembrane domain and CTR denotes the C-terminal region. The C-terminal fragment (CTF) encompasses the CTR, TM and adjacent region. B. Pmel17 protein with mNG tagged to the CAF. C. Pmel17 protein with mNG tagged to the MαC fragments.

Two different constructs were designed in order to cover both potential sites for melanosome tracking and maximise the chances of producing a successful construct with correct processing in the cells (Figure 3.9). The first construct was designed with the mNG marker adjacent to the core amyloid fragment (mNG-Pmel17, CAF), and the second construct was designed with the marker adjacent to the MαC fragments (mNG-Pmel17, MαC). For mNG-Pmel17 (CAF), mNG was placed directly to the right of amino acid 148, which is reported to be the first amino acid in the core amyloid fragment, in order for it to be retained within the fragment once it is cleaved from the full-length protein. For mNG-Pmel17 (MαC), mNG was placed downstream of amino acid 435 within the RPT region, upstream of the reported cleavage sites in order for it to be retained in the MαC fragments once these are cleaved from the full-length protein. Both the CAF and MαC fragments are present in very early stage melanosomes through to stage IV melanosomes which are transported to keratinocytes. As a result, mNG tagging of these segments of Pmel17 should allow the tracking of melanosomes throughout their life cycle, to establish a more complete picture of melanosome trafficking.

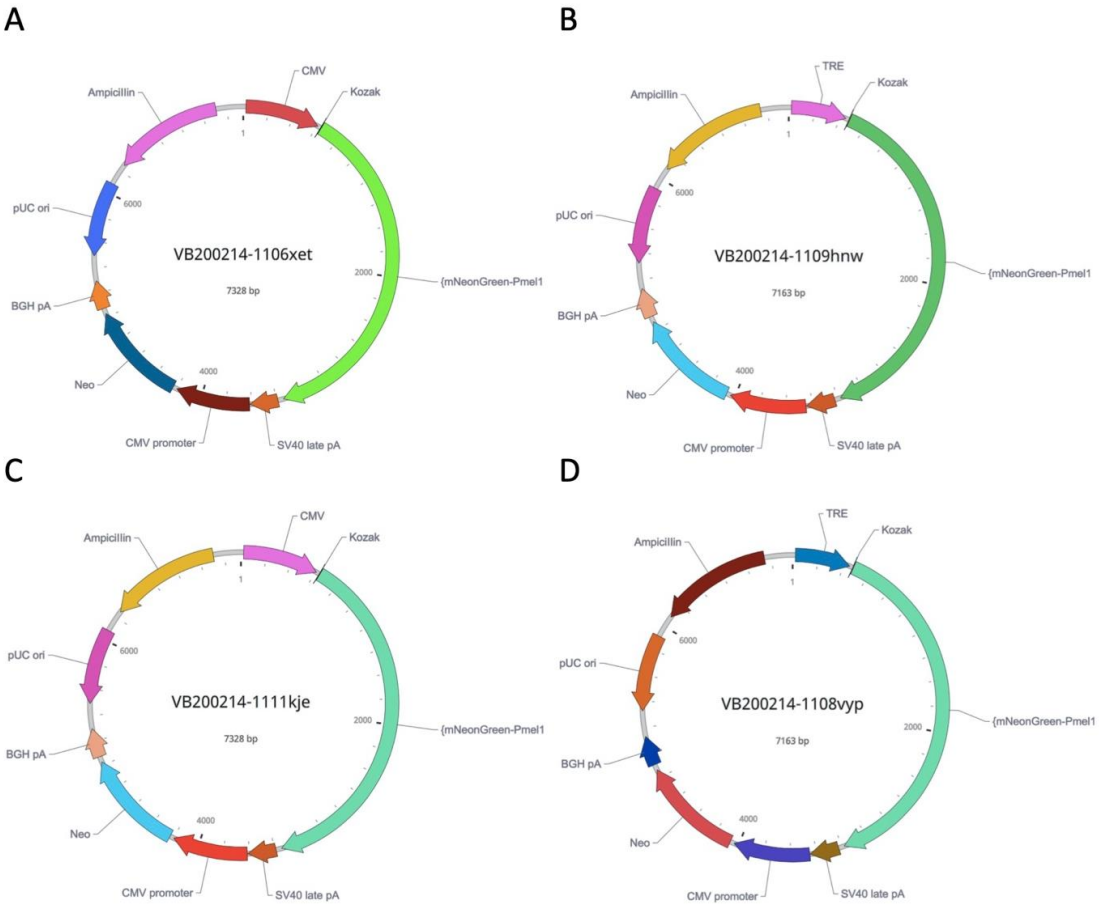

Figure 3.10. Four vectors containing the mNG-Pmel17 variants

A. The constitutive mNG-Pmel17 (CAF) construct, with a CMV promoter, neomycin resistance gene in dark blue for stable transfection selection and ampicillin resistance gene in pink for bacterial selection. B. The tetracycline-inducible mNG-Pmel17 (CAF) construct, with a TRE promoter, neomycin resistance gene in blue for stable transfection selection and ampicillin resistance gene in yellow for bacterial selection. C. The constitutive mNG-Pmel17 (MαC) construct, with a CMV promoter, neomycin resistance gene in blue for stable transfection selection and ampicillin resistance gene in yellow for bacterial selection. D. The tetracycline-inducible mNG-Pmel17 (MαC) construct, with a TRE promoter, neomycin resistance gene in pink for stable transfection selection and ampicillin resistance gene in dark red for bacterial selection.

Two variations of each of the constructs were made, one with a constitutively active CMV promoter and the other with a tetracycline-inducible promoter (Figure 3.10). All of the plasmids contain an ampicillin-resistance gene for bacterial selection, as well as a neomycin-resistance gene for selection of plasmid-containing cells during stable cell line development.

3.3.1 Western blot of cells transfected with construct shows overlap of mNG signal with Pmel17 antibody signal and mNG antibody signal

Once prepared, the protein expression from each plasmid was examined by western blot. SKMEL28 cells were seeded onto 6 cm culture dishes and were allowed to reach a high confluency. They were then transfected with the two constitutively active variants of the mNG-Pmel17 constructs. Twenty-four hours later the dishes were lysed as described in the materials and methods, and samples were then run on a non-reducing gel (Figure 3.11). The gel was imaged using a Typhoon imager in order to detect mNG in the samples (panel A). An mNG bacterial lysate was included as a positive control. Small but distinct bands can be seen at the top of lanes 2 and 3 in both repeats, as well as lower down in the gel, indicated by arrows in the figure. Lanes 2 and 3 correspond to lysates of cells transfected with mNG-Pmel17 (MαC) and mNG-Pmel17 (CAF) respectively. Two bands were also seen in lane 6 which contains the positive control, one at the same level as in lanes 2 and 3, and the other mid-way through the gel, indicated by arrows. As expected, no mNG bands were seen in the negative controls in lanes 4 and 5, untransfected SKMEL28 cell lysate and untransfected HaCaT lysate respectively. The mNG signal is however stronger in lane 2, and the band lower down is only present in lane 2 and not lane 3. This indicates that the mNG-Pmel17 (CAF) construct examined in lane 3 may not remain intact or be processed correctly in transfected cells.

The proteins in the gel were then transferred onto a PVDF membrane, as described in the materials and methods. The membrane was first probed with anti-HMB45 antibody (BioLegend) in order to detect Pmel17 protein (panel B). anti-HMB45 detects a sequence in the RPT region of Pmel17, and thus detects the processed form of the protein which is present in maturing melanosomes. As expected, Pmel17 bands were detected in lanes 2, 3 and 4, containing the two transfected SKMEL28 lysates and the untransfected SKMEL28 lysate respectively. The bands are indicated by black arrows. In lane 2, the Pmel17 bands overlap with the mNG signal seen in panel A, indicating that the mNG-Pmel17 (MαC) tagged protein remains intact after processing. The Pmel17 band in lane 3 is comparable in size to the band in lane 2, however the absence of mNG signal at the same level in panel A suggests this is Pmel17 that is not attached to mNG. The band in lane 4 is weaker than the previous two lanes, reflecting lower Pmel17 protein amount in the untransfected cells

compared to transfected cells which express higher levels. There is no band in lane 5 as expected, as this contains untransfected HaCaT lysate as a negative control.

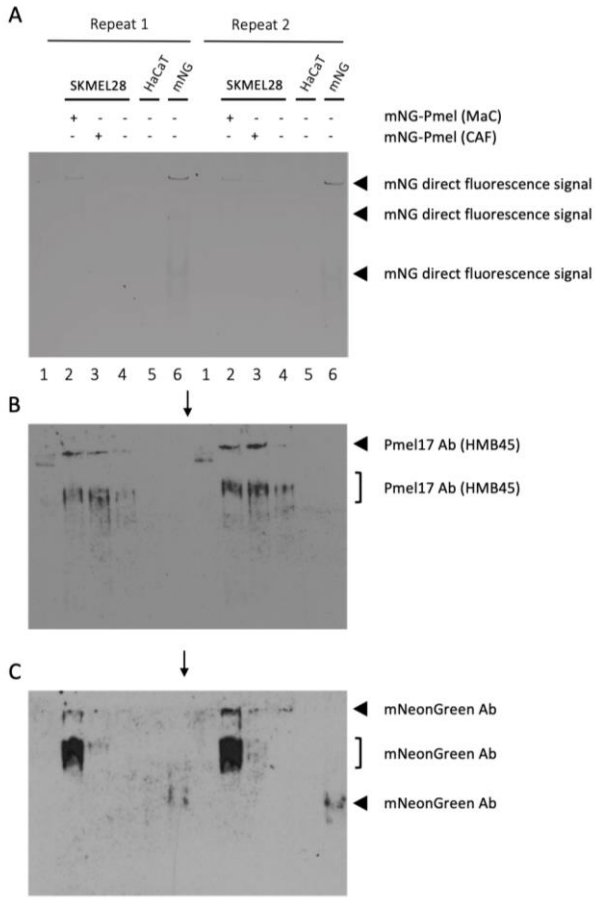

Figure 3.11. Non-reducing gel electrophoresis and subsequent western blotting of lysates from transfected SKMEL28 cells

A. Non-reducing gel imaged using a Typhoon imager for detection of fluorescence. Lane 1 contains a ladder, lane 2 contains SKMEL28 cell lysate transfected with the mNG-Pmel17 (MαC) construct, lane 3 contains SKMEL28 cell lysate transfected with the mNG-Pmel17 (CAF) construct, lane 4 contains untransfected SKMEL28 cell lysate, lane 5 contains untransfected HaCaT cell lysate and lane 6 contains mNG bacterial lysate. B. Western blot using the gel from (A), stained with anti-Pmel17 antibody. C. Re-staining of the membrane from (B) with anti-mNG antibody. Arrows and brackets indicate antibody bands.

The PVDF membrane was then stripped and re-probed with anti-mNG antibody (Chromotek). Bands are again indicated with black arrows. Firstly, a band can be seen in lane 6 containing the mNG bacterial lysate positive control, confirming the antibody is identifying mNG. Two bands can be seen in lane 2, one at the top and the second lower down, which overlap with both the Pmel17 protein signal in panel B and the mNG signal in

panel A. This provides further indication that the mNG remains attached to the Pmel17 protein after processing. A much fainter and smaller band is present in lane 3, indicated by the middle arrow, which may reflect a small amount of intact mNG-Pmel17 (CAF) protein. Taken together, non-reducing gel and western blot analysis of both mNG-Pmel17 proteins indicate that the MαC fragment remains intact, while the majority of the CAF product may be degraded in transfected cells.

3.3.2 mNG-Pmel17 (CAF) CMV construct has a diffuse appearance in SKMEL28 cells

The constructs protein expression was then examined visually by transfection in SKMEL28 cells, starting with the constitutively active mNG-Pmel17 (CAF) construct. SKMEL28 cells were seeded in glass-bottom ibidi dishes and were allowed to reach high confluence before transfection using JetPei reagent. Twenty-four hours later, they were imaged live in fluorobrite imaging medium using a confocal microscope. Environmental controls on the microscope ensured the cells were maintained at optimal temperature and CO_2 conditions during imaging. The transfection efficiency of the construct was approximately 20%. The mNG signal in the cell appeared to accumulate around the ER region, as well as near the periphery of the cell (Figure 3.12). It also appeared to faintly highlight an unidentified network in the bottom left region of the cell. The signal is slightly diffuse and does not form melanosome-like structures, but rather granular structures. Taken together with the western blot analysis, this is a strong indication that the majority of the mNG-Pmel17 (CAF) protein is not able to form the closely packed core amyloid fibril and may be degraded as a result.

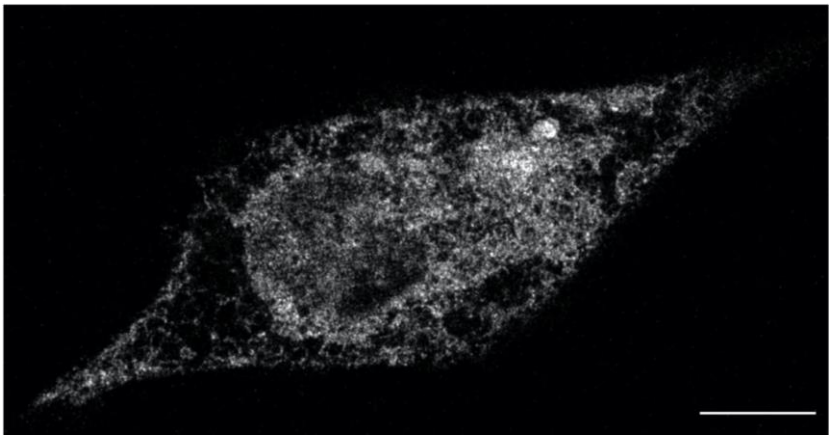

Figure 3.12. Still image of SKMEL28 cell transfected with mNG-Pmel17 (CAF)
The cell was imaged 24 hours after transfection on a confocal microscope. Scale bar = 10 μm.

3.3.3 mNG-Pmel17 (MαC) CMV construct produces melanosome-sized particles in SKMEL28 cells

Having observed the mNG-Pmel17 (CAF) construct, the MαC fragment tag variation was examined next. JetPei reagent was used to transfect cells in glass-bottom ibidi dishes, and imaging was done in fluorobite medium using a confocal microscope. Environmental controls were maintained at optimum for cell viability as above. Transfection efficiency was approximately 35%. The appearance of the protein expressed by this construct was noticeably different to that of the CAF construct (Figure 3.13 A). Firstly, the mNG was punctate, with the particles being approximately equal in size throughout the cell. The particles appeared to accumulate principally at the tips of dendrites and around the nucleus. Measurements taken from 5 different cells from different experiments showed an average particle size of 445nm (Figure 3.14). This number is consistent with existing data on the size of melanosomes, collected through static imaging such as electron microscopy (Sturm, Box and Ramsay, 1998). The accumulation of particles at dendrite tips provides further indication that the fusion protein is being processed correctly, as mature melanosomes would accumulate in these regions before transfer to keratinocytes.

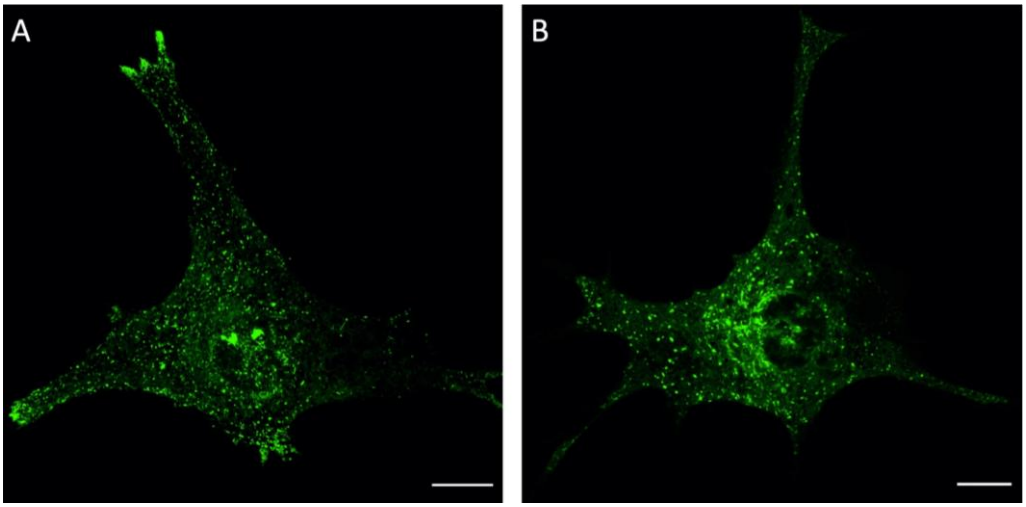

Figure 3.13. SKMEL28 cells transfected with the mNG-Pmel17 (MαC) constructs

A. SKMEL28 cell transfected with the constitutive construct, imaged 24 hours post-transfection. B. SKMEL28 cell transfected with the tetracycline-inducible construct, imaged before treatment with tetracycline.

The tetracycline-inducible MαC construct was also examined in live SKMEL28 cells (Figure 3.13 B). The localisation of the Pmel17 particles was analogous to that seen with the constitutively active construct. A tetracycline-inducible construct was produced with the aim of observing melanosome maturation from the earliest stages by following the full-length Pmel17 protein as it is produced and trafficked to early sorting endosomes. However, the construct was determined to be "leaky" as the protein was expressed even prior to the addition of tetracycline. The majority of the cells expressed the same amount of protein 24 hrs post transfection as the constitutively active version, and thus the tetracycline-inducible construct was not used in any further experimentation.

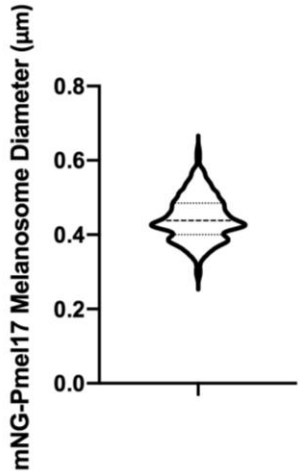

Figure 3.14. Violin plot illustrating the distribution of mNG-Pmel17 (MαC) particle diameter

The average diameter of Pmel17 particles measured in 5 cells is approximately 455nm. The darker dashed line denotes the median while the lighter dotted lines denote the interquartile range.

Figure 3.15 highlights the dynamics of the movement of the mNG-Pmel17-MaC particles. Panel B follows a particular particle highlighted in panel A, indicated by a white arrow, from its position near the periphery of the cell back towards the nucleus. This direction of movement may reflect an early stage in the maturation of Pmel17 protein, whereby it is trafficked to the plasma membrane before endocytic vesicles transport it to early sorting endosomes to become melanosomes. Over a time-course of 9.79 seconds, the particle travelled approximately 14 µm, giving it a rough speed of 1.44 µm/s for this particular time-course. Panel C shows the movement of all the particles in the cell over a 100-frame time-course spanning 69.94 seconds. The particles are colour-coded such that the colour of each

particle reflects its position in the time-course. The darker the particle is coloured, the earlier the frame in which it appears, and the lighter the particle the later it appears. Overall, live cell imaging with this construct showed very dynamic particles, with some travelling from the peri-nuclear region to the cell periphery and others travelling in the opposite direction.

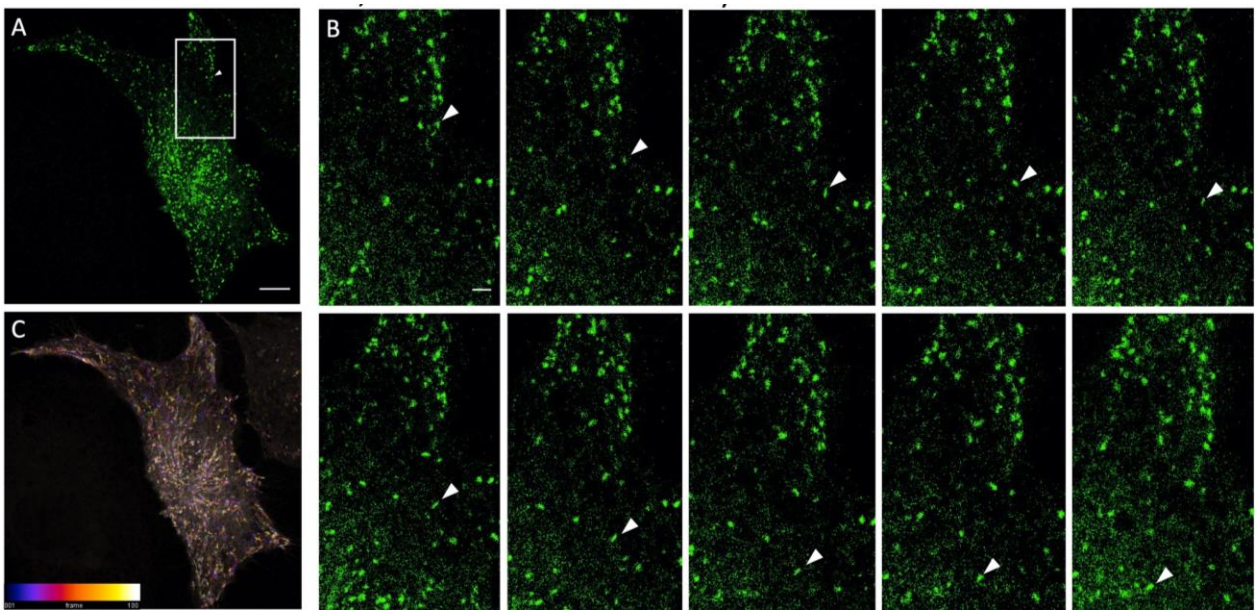

Figure 3.15. mNG-Pmel17 vesicle movement in SKMEL28 cells

A. An SKMEL28 cell transfected with the mNG-Pmel17 (MαC) construct, imaged 24 hours post-transfection. Scale bar = 10 μm. B. A particular mNG-Pmel17 vesicle from the section highlighted by a white box in panel A (indicated by white arrow) is tracked from the periphery of the cell towards the centre, over a time course of 9.79 seconds between the first and last frame. Scale bar = 2 μm. B. temporal colour-coding of all mNG-Pmel17 vesicle movement, over a time course of 69.94 seconds covering 100 frames.

3.3.4 Comparison with SKMEL28 cells probed for endogenous Pmel17 protein by immunofluorescence

Alongside imaging the mNG-Pmel17 constructs in live cells, endogenous Pmel17 localisation was examined in fixed cells. SKMEL28 cells were seeded onto glass coverslips, fixed and then stained with anti-Pmel17 antibody (Santa Cruz Biotechnology). The concentrations of antibodies used can be found in Table 2.1 of Materials and methods. Endogenous Pmel17 protein localisation appears to be very similar to that of the mNG-Pmel17 (MαC). The Pmel17-containing vesicles were dispersed throughout the cell, with the strongest signal being in the peri-nuclear region and at the tips of the dendrites (Figure

3.16). The clustered Pmel17 vesicles at the dendrite tips are likely mature melanosomes prepared for transfer to keratinocytes. The high degree of similarity between the distribution of endogenous Pmel17 in fixed cells and that of the mNG-Pmel17 (MαC) construct in live cells provides further indication that the construct truly reflects Pmel17 protein.

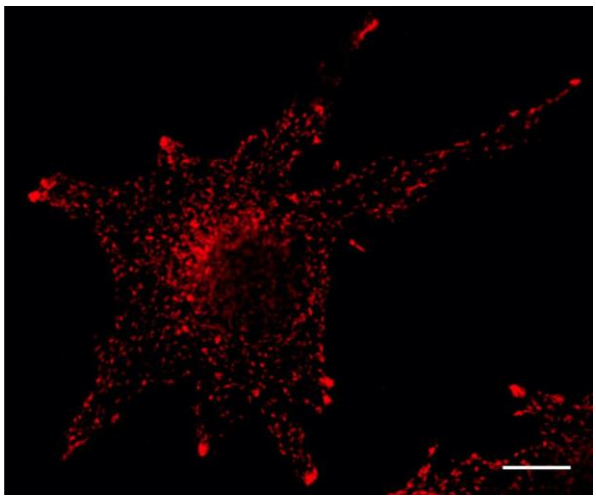

Figure 3.16. Endogenous Pmel17 protein distribution in an SKMEL28 cell detected by immunofluorescence

SKMEL28 cells were fixed and stained with anti-HMB45 antibody to detect Pmel17. Scale bar = 10 μm.

3.3.5 mNG-Pmel17 vesicles show very limited co-localisation with lysotracker stain

Having established that the mNG-Pmel17 (MαC) construct behaves very similarly to endogenous Pmel17 protein, transfected SKMEL28 cells were stained with lysotracker, which stains lysosomal compartments in the cell. Lysosomes are responsible for degradation of biomolecules from endocytic, phagocytic and autophagic pathways in the cell (Trivedi, Bartlett and Pulinilkunnil, 2020). Panels A and B in Figure 3.17 show portions of a cell where lysosomal compartments are stained red. Co-localisation of the lysosomes with the mNG-Pmel17 (MαC) was very limited, shown by very few instances of yellow colour in both images. This absence of co-localisation provides additional encouragement that the tagged protein is being processed and trafficked correctly, in the same way as endogenous Pmel17, and is not being transferred to lysosomal compartments for degradation. A small degree of co-localisation is to be expected, as Pmel17 is trafficked to early sorting endosomes and multivesicular bodies to trigger their development into melanosomes (Watt *et al.*, 2009). Lysotracker specifically targets acidic organelles, and while early sorting

endosomes and multivesicular bodies have an acidic pH, melanosome pH is closer to neutral. Thus, the vesicles transitioning to stage I melanosomes may be targeted by the lysotracker stain.

Alongside the live imaging experiments with mNG-Pmel17 (MαC) and lysotracker, endogenous Pmel17 co-localisation with lysosomes was also examined. SKMEL28 cells were fixed onto glass coverslips and stained with both anti-HMB45 antibody and anti-LAMP1 antibody, which functions as a lysosomal marker. In Figure 3.17 C green secondary antibody denotes Pmel17 and red secondary antibody denotes lysosomal compartments. As observed in the live cells, endogenous Pmel17 also showed very limited co-localisation with lysosomes. This illustrates that the mNG-Pmel17 protein construct again reflects endogenous Pmel17 trafficking with respect to lysosomal degradation, providing further confidence that it behaves in the same way as endogenous Pmel17 in live cells.

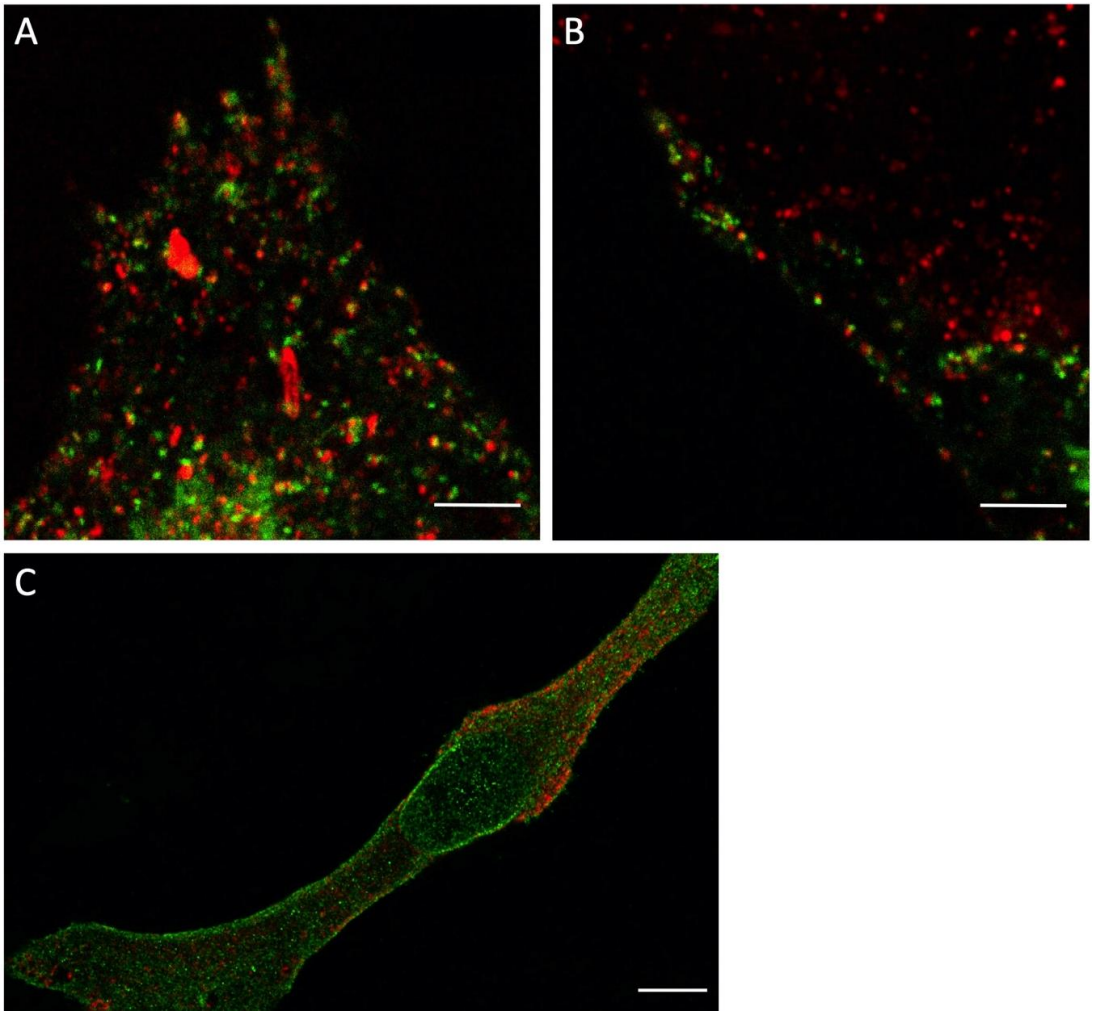

Figure 3.17. Co-localisation of transfected and endogenous Pmel17 protein with lysosomal markers

A. Live SKMEL28 cell transfected with mNG-Pmel17 (MαC) and stained with lysotracker (red) to detect lysosomes. Scale bar = 5 μm. B. An alternative region in the cell shown in (A). Scale bar = 5 μm. C. A fixed SKMEL28 cell stained with anti-HMB45 antibody with alexa-fluor 488 secondary antibody (green), and anti-LAMP1 antibody with alexa-fluor 594 secondary antibody (red). Scale bar = 10 μm.

3.4 mNG-Pmel17 vesicles in SKMEL28 cells appear to co-localise with the actin network, detected by SiR actin, at the cell periphery

In order to further validate the mNG-Pmel17 (MαC) construct, it was evaluated in conjunction with the actin network in live cells. Firstly, live SKMEL28 cells were stained for actin using a probe which targets filamentous actin, SiR actin (Spirochrome). The SiR actin probe is cell-permeable, non-toxic and can be used for live cell imaging over extended

time periods with low phototoxicity due to its excitation wavelength in the far red (Lukinavičius et al., 2014; Müller *et al*., 2019; D'Este *et al*., 2015; Klementieva *et al*., 2016). Figure 3.18 A illustrates the specificity of the probe and its ability to highlight the actin network in great detail. A gradated lookup table has been applied to emphasize the detailed stress fibres visible in this cell, with the lighter colour signifying stronger actin signal. This probe is very valuable for observing actin cytoskeletal health and cell morphology, and its red colour allows it to be used in cells transfected with the mNG-Pmel17 (MαC) construct. This is particularly useful as melanosomes are captured by the actin network at the cell periphery in order to be transferred to keratinocytes. Figure 3.18 B shows the SiR actin probe in red and the Pmel17 construct in green. The peripheral actin network can be seen, with a clearly defined cell morphology, and several Pmel17 particles in close proximity, appearing to be guided towards the tips of the cell's projections by the actin network. This is the behaviour expected from mature melanosomes being captured by the peripheral actin network for transfer (Wu *et al.*, 2001; Hume *et al*., 2002; Kuroda, Ariga and Fukuda, 2003; Lopes *et al*., 2007). These observations suggest that the mNG-Pmel17 (MαC) protein does not alter the behaviour of melanosomes at the latter stages of their development, and will allow the observation of melanosomes throughout their lifecycle and at the point of transfer to keratinocytes.

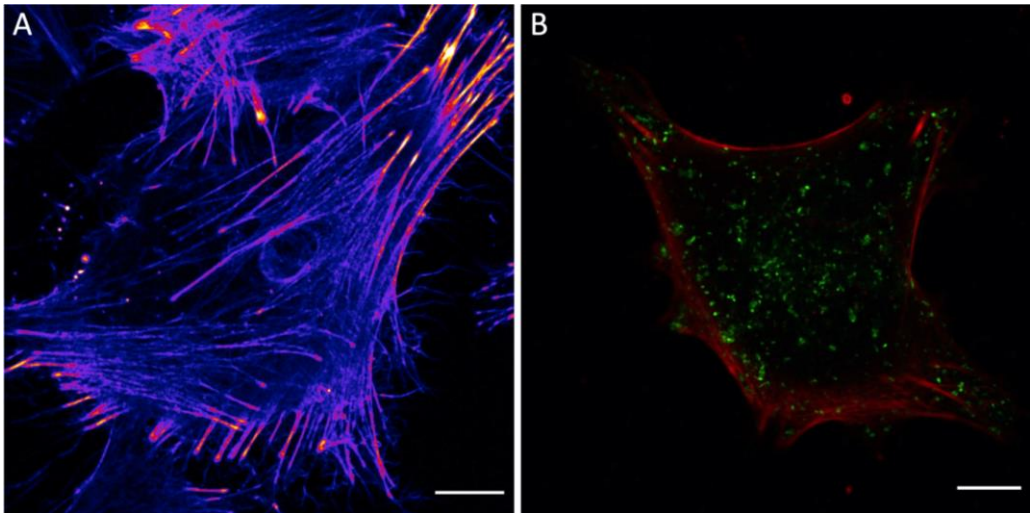

Figure 3.18. Use of the SiR actin probe in live imaging of SKMEL28 cells

A. An untransfected SKMEL28 cell imaged with the SiR actin probe, with the "Inferno" lookup table applied in FiJi to highlight the cell's stress fibres. B. An SKMEL28 cell transfected with the mNG-Pmel17 (MαC) construct, imaged with the SiR actin probe. Scale bars = 10 μm.

3.4.1 mNG-Pmel17 (MαC) vesicles appear to co-localise with tdTomato-LifeAct network at the cell periphery in SKMEL28 cells

Having observed that the mNG-Pmel17 (MαC) vesicles cluster around the peripheral actin network of SKMEL28 cells stained with SiR actin probe, the next step was to observe how the tagged Pmel17 interacts with actin filament produced within the cell. To this end, SKMEL28 cells were co-transfected with the Pmel17 construct and a tdTomato-LifeAct construct (Figure 3.19). Transfection efficiency of the LifeAct construct was considerably higher than that for the Pmel17 construct, at approximately 90%. Transfection efficiency of the Pmel17 construct was slightly lower than what had been seen for a single transfection, likely due to the increased stress of constitutively producing two proteins causing a reduction in cell viability. Panel A in Figure 3.19 shows the tdTomato-LifeAct protein alone after Airyscan processing and highlights the construct's brightness, which allows a very detailed image of the actin cytoskeleton to be captured even at low laser power. This LifeAct construct is thus a very valuable tool for the observation of cell morphology and cytoskeletal health in SKMEL28 cells, both of which are vital for their function in transporting melanosomes to keratinocytes. In panel B of the figure, the Pmel17 protein is shown alone, with a cyan lookup table applied in order to increase the contrast with grey-coloured actin in the merged image. The distribution of Pmel17 particles corresponds to that seen in transfections with the mNG-Pmel17 (MαC) construct alone, with particle clustering in the peri-nuclear region and in the tips of cellular projections. The merged image in panel C shows that these groups of clustered particles in the tips of projections map onto bright LifeAct filaments, suggesting that the particles are being captured by these filaments at the periphery. Two of these areas are highlighted in panels D and E of Figure 3.19, with a particularly large cluster of Pmel17 particles in panel E appearing to be guided outwards by the bright actin filament.

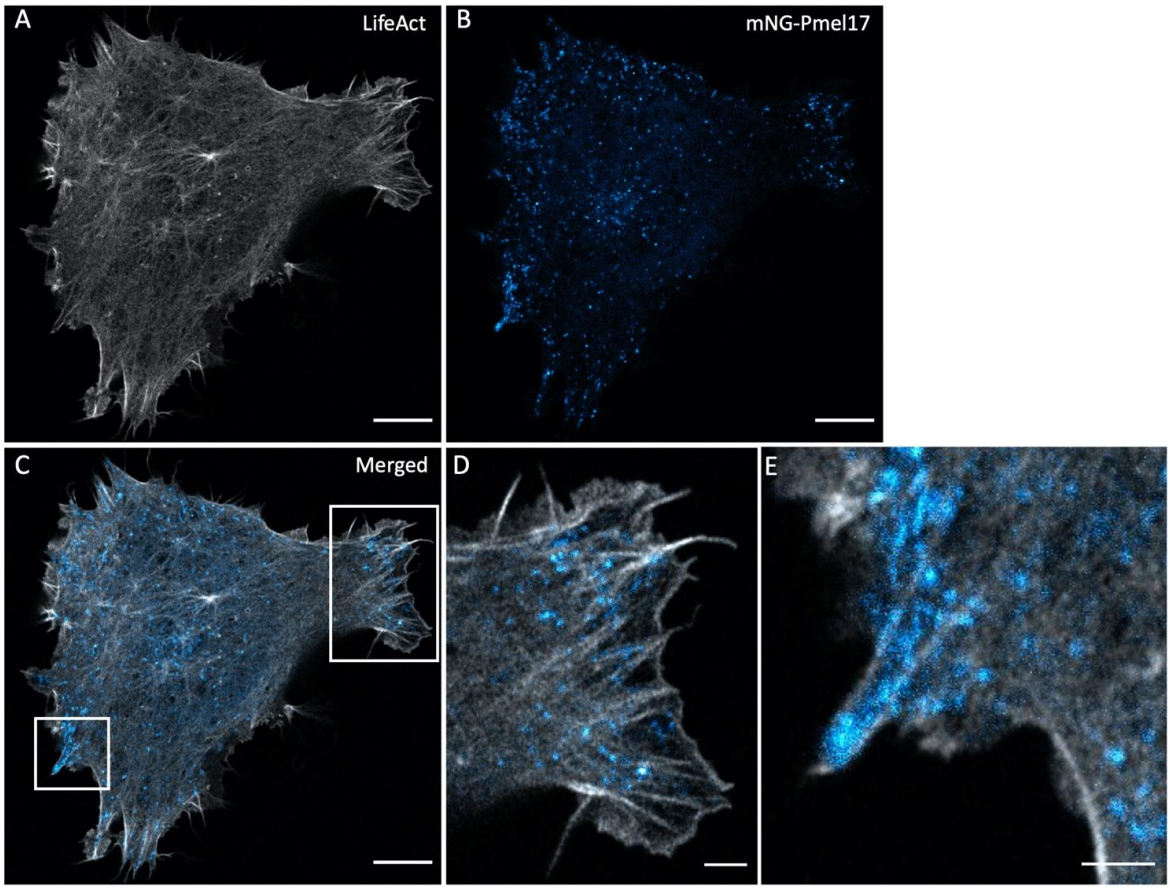

Figure 3.19. Co-transfection of an SKMEL28 cell with mNG-Pmel17 (MαC) and tdTomato-LifeAct

A. The tdTomato-LifeAct construct imaged alone, using Airyscan processing to capture the details of the actin cytoskeletal organisation. Scale bar = 10 μm. B. Still of the mNG-Pmel17 (MαC) protein in the cell, with a cyan lookup table applied. Scale bar = 10 μm. C. Merged image with both fluorescent proteins, with regions of substantial clustering highlighted in panels D and E. Scale bar for C = 10 μm, scale bar for D = 2.5 μm, scale bar for E = 2 μm.

3.4.2 Examining endogenous Pmel17 localisation with respect to actin in fixed SKMEL28 cells by immunofluorescence

After observing mNG-Pmel17 co-localisation with actin in live SKMEL28 cells, a parallel experiment was conducted in fixed cells to ascertain whether the same distribution is seen with endogenous Pmel17 and actin filaments. Cells were seeded and fixed onto coverslips, and stained with anti-HMB45 antibody as well as phalloidin, which specifically stains filamentous actin. Images were captured using a confocal microscope with Airyscan processing. Figure 3.20 A shows the phalloidin staining alone, with clear detection of stress fibres within the cell as well as the peripheral actin network, also illustrating an additional

benefit in providing a clear picture of cell morphology. Panel B of the figure shows Pmel17 staining alone, with melanosomes displaying typical distribution with clustering around the nucleus and cell periphery and in the tips of dendrites. The merged image in panel C shows an example of how areas of increased melanosome clustering co-localise with bright actin filaments in the cell periphery, indicating the melanosomes are being captured by the actin. Panels D and E highlight two areas with particularly dense clusters of melanosomes, which appear to be travelling along the projecting actin filaments. The interaction of endogenous Pmel17 with endogenous actin filaments thus reflects the interaction seen between both the mNG-Pmel17 (MαC) protein and SiR probe, and the mNG-tagged Pmel17 and tdTomato-LifeAct. Overall, the live imaging experiments with actin and supporting fixed cell experiments with endogenous protein provide additional support that mNG-tagged Pmel17 behaves in the same manner as endogenous Pmel17.

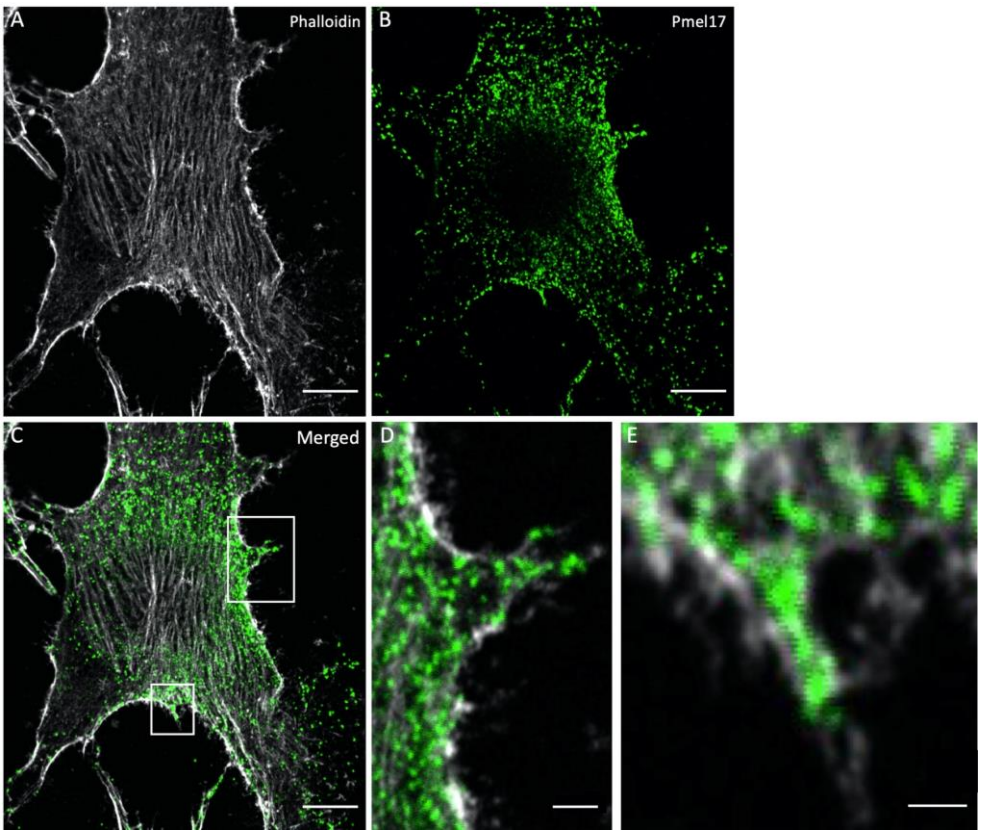

Figure 3.20. Co-localisation of endogenous Pmel17 protein with the actin cytoskeleton A. Phalloidin staining of a fixed SKMEL28 cell, with Airyscan processing. Scale bar = 10 μm. B. Pmel17 staining in the same cell with anti-HMB45 antibody. Scale bar = 10 μm. C. Merged image of both phalloidin and Pmel17 staining (scale bar = 10 μm), with regions of high notable co-localisation highlighted in panels D (scale bar = 1 μm) and E (scale bar = 1 μm).

3.5 Evaluating MNT1 cells as an additional melanocyte cell line

After validating the mNG-Pmel17 (MαC) construct in SKMEL28 cells alone and observing expression in relation to lysosomes and the actin cytoskeleton, an additional melanocyte cell line, MNT1, was obtained to compare the results reported in SKMEL28 cells (Figures 3.14, 1.16). SKMEL28 cells were easily transfectable and thus valuable for the evaluation of the construct, however these cells are lightly pigmented meaning they do not naturally produce a lot of melanin. On the other hand, MNT1 cells are very darkly pigmented, and were thus chosen in order to observe the behaviour of the construct in cells which naturally produce large amounts of melanin. Figure 3.21 illustrates the differences between these cell lines as observed in bright field images. The majority of MNT1 cells are fibroblast-like in shape, narrow and long with no projections, while SKMEL28 cells have a tendency towards being more dendritic. In this regard, using SKMEL28 cells is more beneficial for downstream studies, as the dendrites mediate transfer of the melanosomes to keratinocytes, meaning that a more dendritic cell line would be more suitable for co-culture experiments involving melanocytes and keratinocytes. Furthermore, the majority of MNT1 cells are smaller than SKMEL28 cells, which may also impact their melanosome transfer ability by reducing their range. The melanosomes are much more easily visible in MNT1 cells; however, their large number means that it is difficult to capture them in the same focal plane. Despite these differences in morphology, the MNT1 cells' high degree of visible pigmentation made them an ideal candidate for validation of the mNG-Pmel17 (MαC) construct in an additional cell line.

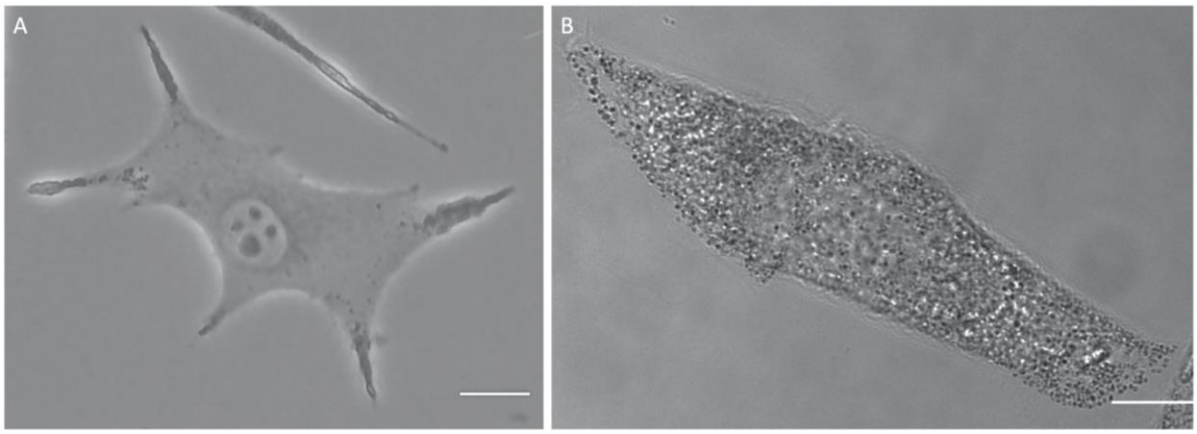

Figure 3.21. Bright field image of SKMEL28 and MNT1 melanocytes

A. Bright field image of an SKMEL28 cell, with visible melanosomes at the tips of dendrites. Scale bar = 10 μm. B. Bright field image of an MNT1 cell, with melanosomes dispersed throughout the cytoplasm. Scale bar = 10 μm.

3.5.1 mNG-Pmel17 (MαC) validation in MNT1 melanocyte cell line

MNT1 cells were transfected using JetPei reagent, with the same protocol used with SKMEL28 cells. The cells were incubated with the transfection reagent for 24 hours and were then imaged on a confocal microscope, with environmental controls maintaining temperature and CO_2 at optimal levels. The transfection efficiency achieved with the MNT1 cells was considerably lower than that for SKMEL28 cells, at approximately 5-10%. The appearance and distribution of the mNG-Pmel17 protein was similar to that seen in the SKMEL28 cells, with particles dispersed throughout the cell but concentrated near the nucleus and peripheral regions (Figure 3.22). The diameter of the particles also corresponded with the average particle size in SKMEL28 cells. There were generally fewer particles in MNT1 cells relative to their size than were observed in SKMEL28 cells, which may be related to the cell line's lower transfectability compared to SKMEL28 cells. Co-localisation of the particles with melanosomes that were located using a bright field channel was made difficult due to the sheer number of melanosomes. The large number of pigmented granules hindered the ability to focus on even a small fraction of them, as can be seen in Figure 3.22 A. Panel C of the figure shows both the bright field and fluorescence channels merged and, while it is likely there was some co-localisation, this was difficult to identify. Overall, as the characteristics of the mNG-Pmel17 (MαC) protein seen in lightly pigmented SKMEL28 cells were confirmed in darkly pigmented MNT1 melanocytes, this adds further confidence that the construct is correctly labelling melanosomes through Pmel17.

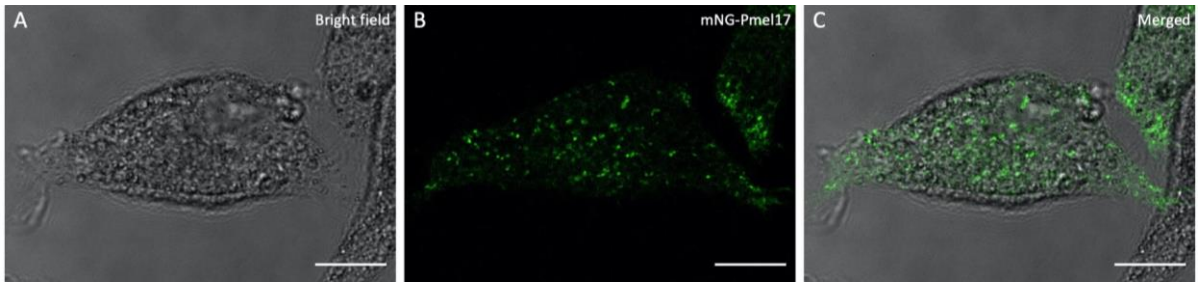

Figure 3.22. MNT1 cell transfected with mNG-Pmel17 (MαC)

A. Bright field image of the transfected cell with visible melanosomes. Scale bar = 10 μm. B. The mNG-Pmel17 (MαC) construct in the MNT1 cell. Scale bar = 10 μm. C. Merged bright field and fluorescent protein image. Scale bar = 10 μm.

Having seen low transfection efficiency with the mNG-Pmel17 (MαC) construct, MNT1 cells were transfected with an additional construct in order to further investigate their ability to be transfected. As the tdTomato-LifeAct construct had shown very high transfection efficiency in SKMEL28 cells, this construct was chosen. Three μg of plasmid DNA and 6 μl of Jetpei reagent were used per ibidi dish. After 24 hours, the cells were imaged in fluorobrite medium on a confocal microscope. Even with a construct showing high transfection rates in other cell lines, the MNT1 cell transfection efficiency was low, at approximately 25%. Therefore, even though it has been shown that the MNT1 cell line can be transfected, it has a much reduced transfectability compared to SKMEL28 cells.

3.6 0.001% w/v (6 μM) Sepiwhite treatment significantly decreases the number of mNG-Pmel17 vesicles in SKMEL28 cells

From the previously described experiments with the mNG-Pmel17 (MαC) construct in SKMEL28 melanocytes and subsequent test in MNT1 melanocytes, the construct was established as an appropriate tool for the observation of melanosomal behaviour. This construct could also be used to record the effects of various biological compounds on melanosomal activity in melanocytes. Two compounds were chosen as they were of interest to the industrial sponsor. The first compound to be examined was Undecylenoyl Phenylalanine (Sepiwhite, Figure 3.23 B). Sepiwhite is a lipoamino acid reported to act as an αMSH and beta-adrenergic receptor antagonist (Katoulis et al., 2014), resulting in

reduced pigmentation in cells due to diminished activation of the MC1R and downstream effectors discussed in section 1. Consequently, it was expected that Sepiwhite would decrease the number of melanosomes in melanocytes transfected with the mNG-Pmel17 (MαC) construct. As described in materials and methods, 6 ibidi dishes in total over three individual experiments were seeded with SKMEL28 cells and transfected, 3 treated with Sepiwhite and 3 untreated. After 48 hours of treatment, the cells were imaged on a confocal microscope and 10-20 cells from each dish were selected for a 100-frame time course. The average number of Pmel17 particles from 3 frames of each time course was divided by the surface area of the cell to establish a standardised average number of melanosomes for that cell. These figures were then combined and an average number was derived for the Sepiwhite-treated and the untreated cells. Figure 3.23 A illustrates these numbers graphically, and an un-paired T test determined this difference to be statistically significant, with a value of $p \leqq 0.01$. Untreated and Sepiwhite-treated cell representative examples are shown in panels C and D respectively, where the treated cell contains visibly fewer Pmel17 particles but the distribution of particles is similar to the untreated cell. This experiment illustrates the value of this construct for the direct examination of melanosome production in response to biological compounds at the cellular level.

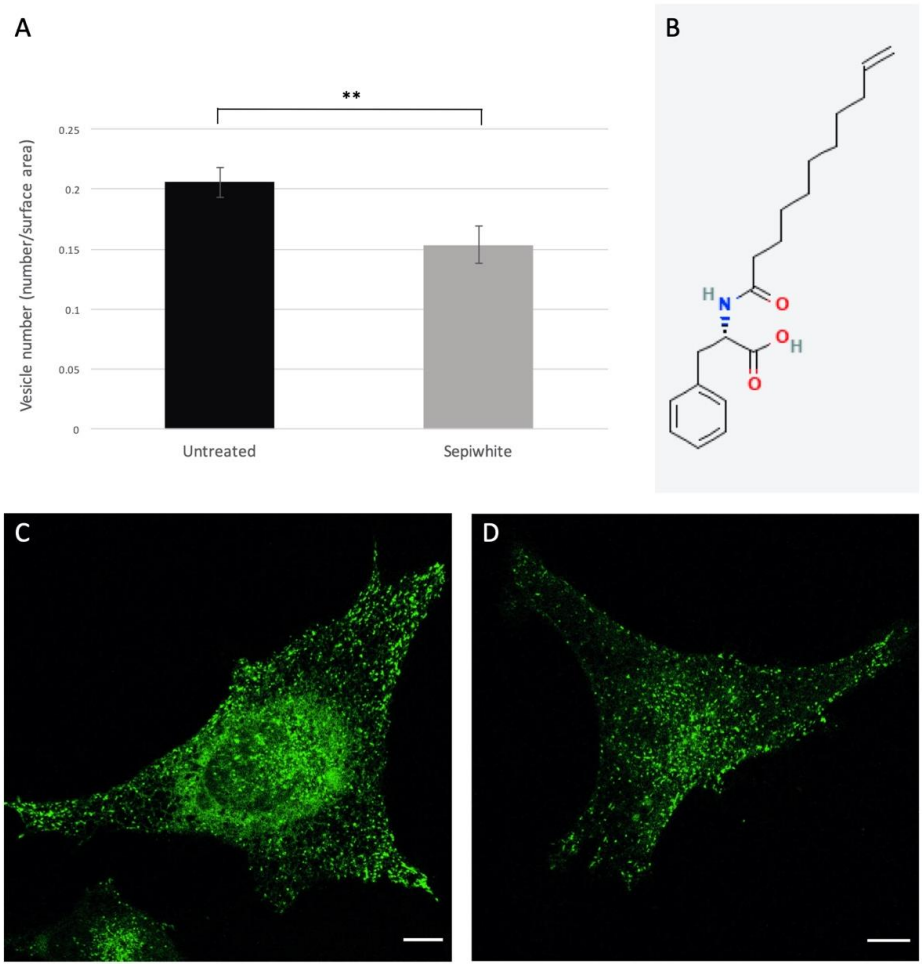

Figure 3.23. Sepiwhite treatment (0.001% w/v) in live SKMEL28 cells transfected with mNG-Pmel17 (MαC)

A. Graphical illustration of the decrease in the number of Pmel17 particles per surface area of the cell in Sepiwhite-treated cells (N=40) compared to untreated cells (N=39). ** signifies statistical significance with $p \leqq 0.01$. Error bars represent standard error. B. Chemical structure of Sepiwhite. C. Untreated SKMEL28 cell example. Scale bar = 10 μm. D. Treated SKMEL28 cell example. Scale bar = 10 μm.

3.6.1 0.001% w/v (6 μM) Sepiwhite treatment significantly decreases the intensity of endogenous pmel17 antibody signal

Alongside the live imaging Sepiwhite experiments, endogenous Pmel17 levels were evaluated in response to Sepiwhite treatment in order to validate the results obtained with the mNG-Pmel17 (MαC) construct. SKMEL28 cells were seeded onto coverslips and a proportion of the coverslips were treated with Sepiwhite. 48 hours after treatment, the cells were stained with anti-Pmel17 antibody (Santa Cruz Biotechnology), and images of 20 cells

per coverslip were captured. All of the microscope settings were kept constant for imaging the coverslips in order for any variation in fluorescence to directly reflect differences in endogenous Pmel17 levels. The average fluorescence of the cells for untreated and Sepiwhite-treated cells is plotted in the graph in panel A of figure 3.24. There was an obvious reduction in endogenous Pmel17 levels for the Sepiwhite-treated cells, which was confirmed to be statistically significant by an un-paired T test ($p \leqq 0.001$). Panels B and C provide examples of untreated and treated cells respectively, with the treated cells exhibiting noticeably lower fluorescence than the untreated cells. The brightness was adjusted in both images by an equal amount for illustrative purposes. This result confirms the observations made with the mNG-Pmel17 (MαC) construct in live cells, suggesting the decrease in Pmel17 particles is not specific to the Pmel17 protein tagged to mNG.

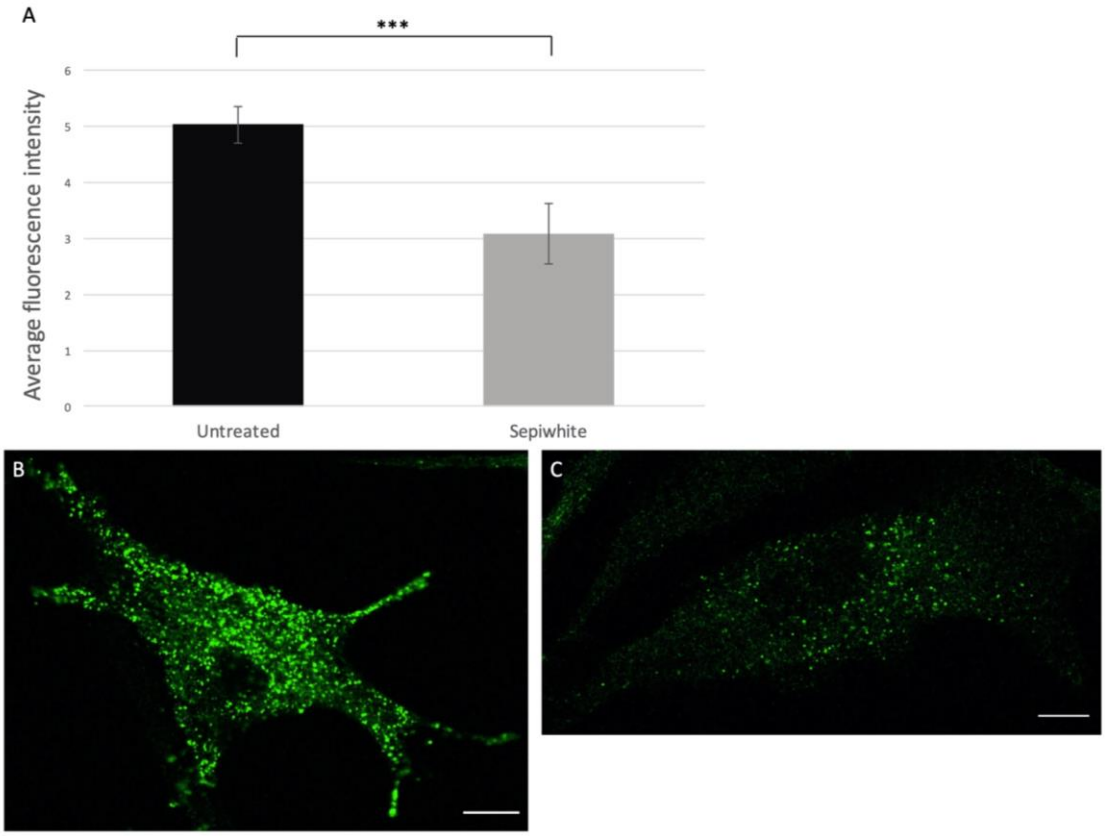

Figure 3.24. Sepiwhite treatment effects on endogenous Pmel17 protein levels

A. Graphical illustration of the decrease in the average fluorescence intensity of Sepiwhite-treated cells (N=70) compared to untreated cells (N=80). *** signifies statistical significance with $p \leqq 0.001$. Error bars represent standard error. B. Untreated SKMEL28 cell example. Scale bar = 10 μm. C. Treated SKMEL28 cell example. Scale bar = 10 μm.

3.7 0.004% w/v (56 μM) sucrose dilaurate treatment significantly decreases the number of mNG-Pmel17 vesicles in SKMEL28 cells

Having successfully used the mNG-Pmel17 construct to evaluate the effect of Sepiwhite on the number of melanosomes in SKMEL28 cells, a second bioactive compound was tested: Sucrose 1,6'-dilaurate (sucrose dilaurate), otherwise known as alpha-D-Glucopyranoside, 1-O-(1-oxododecyl)-beta-D-fructofuranosyl, 6-dodecanoate (Figure 3.25 B). Sucrose dilaurate is a diester of lauric acid and sucrose which is used in a number of skincare products, and acts as a surfactant (PubChem: CID 91864488, Sucrose 1,6'-dilaurate). The experiment was conducted in the same way as for Sepiwhite, with 6 ibidi dishes in total; 3 treated with 0.004% w/v (56 μM) sucrose dilaurate and 3 untreated. The cells were imaged 48 hours after treatment, and 20 cells were selected from each dish for a 100-frame time course. The average number of Pmel17 particles from 3 frames of each time course was divided by the surface area of the cell to establish a standardised average number of melanosomes for that cell. These figures were then combined and an average number was derived for the treated and untreated cells. The graph in Figure 3.25 shows a clear decrease in the number of Pmel17 particles in the treated cells compared to the untreated cells. This difference was interrogated by an un-paired T test which found it to be statistically significant, with $p \leqq 0.0001$. Representative examples of cells from each of the conditions are shown in panels C and D of the figure. Panel D shows a lot fewer Pmel17 vesicles in the cell treated with Sucrose Dilaurate compared to the untreated cell in panel C.

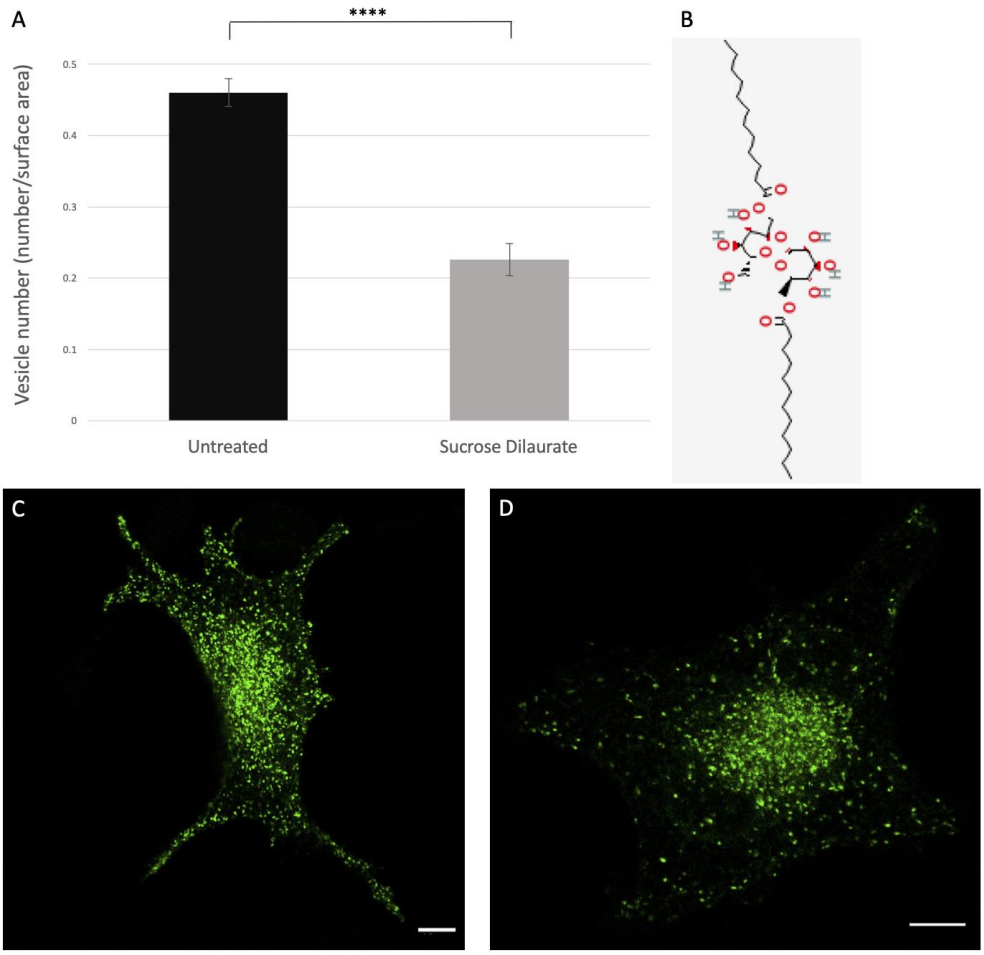

Figure 3.25. Sucrose dilaurate treatment (0.004% w/v) in SKMEl28 cells transfected with mNG-Pmel17 (MαC)

A. Graphical illustration of the decrease in the number of Pmel17 particles per surface area of the cell in sucrose dilaurate-treated cells (N=62) compared to untreated cells (N=58). **** signifies statistical significance with $p \leqq 0.0001$. Error bars represent standard error. B. Chemical structure of sucrose dilaurate. C. Untreated SKMEL28 cell example. Scale bar = 10 μm. D Treated SKMEL28 cell example. Scale bar = 10 μm.

3.7.1 Treatment of SKMEL28 cells with 0.004% w/v (56 μM) sucrose dilaurate does not appear to decrease endogenous Pmel17 protein levels

In addition to the live imaging experiments with sucrose dilaurate, endogenous Pmel17 protein levels were examined in treated cells. SKMEL28 cells were seeded onto coverslips and treated with 0.004% w/v (56 μM) Sucrose Dilaurate. After 48 hours, the cells were fixed and stained with anti-Pmel17 antibody (Santa Cruz Biotechnology). As with the fixed-cell Sepiwhite experiments, 20 cells were imaged from each coverslip, and the microscope

settings were kept constant in order to determine the true effect of the compound on fluorescence. The average values of fluorescence for treated and untreated cells are plotted in Figure 3.26 A. Although there appeared to be a slight decrease in fluorescence in the treated cells, this difference was not significant because the variation, indicated by the error bars, was very large. Examples of each condition are shown in panels B and C, and the brightness of the images was increased by the same relative amount for illustrative purposes. There did not appear to be a difference in fluorescence visually, reflecting the data shown in the graph. The cause of the discrepancy between the live imaging and fixed cell results is not clear, but may be due to effects of transfection in the live imaging experiments, or non-linear loss of antibody recognition in the fixed cell experiments.

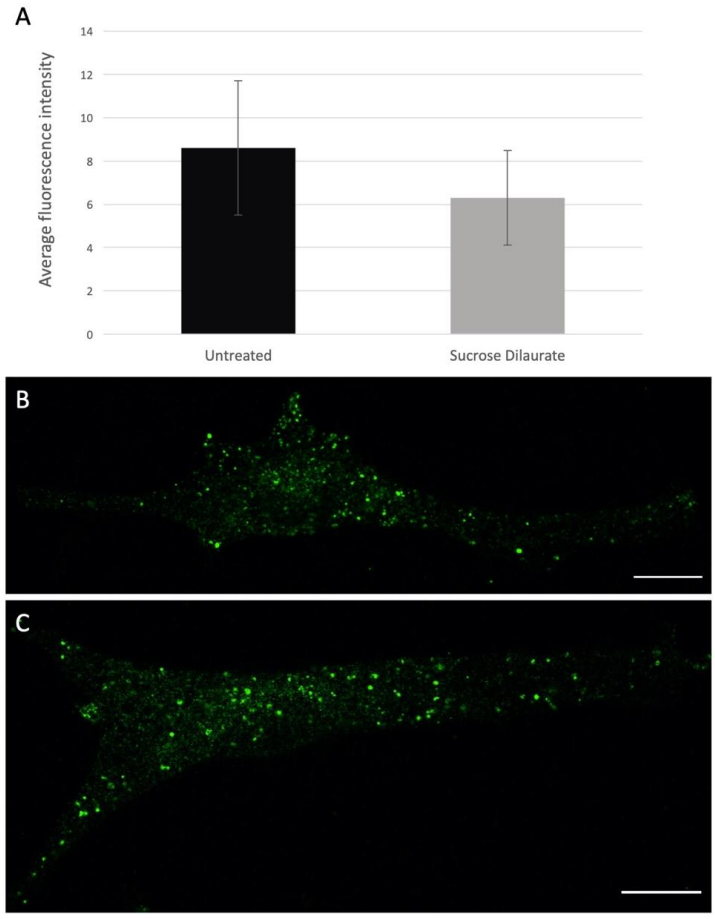

Figure 3.26. Sucrose dilaurate treatment effects on endogenous Pmel17 protein levels
A. Graphical illustration of the decrease in the average fluorescence intensity of Sucrose Dilaurate-treated cells (N=93) compared to untreated cells (N=94). Error bars represent standard error. B. Untreated SKMEL28 cell example. Scale bar = 15 μm. C. Treated SKMEL28 cell example. Scale bar = 15 μm.

3.8 Developing an SKMEL28 cell line stably expressing the tdTomato-LifeAct construct

The tdTomato-LifeAct construct has already been shown to be a valuable tool for the detailed visualisation of the cytoskeleton and cell morphology (Figure 3.19). An SKMEL28 cell line stably expressing this construct would thus be particularly useful for experiments involving actin and the physical appearance of the cells, as well as for co-transfections such as with the mNG-Pmel17 (MαC) discussed in section 1.4.1. The high transfection efficiency of the tdTomato-LifeAct construct in SKMEL28 cells facilitated the production of this cell line, as the process of bacterial selection of fluorescent protein-expressing cells was simpler. The selection marker included in this construct was neomycin. A mixed-clone population of fluorescent cells was established; however SKMEL28 cells grow best when surrounded by other cells, which prevented the isolation and growth of a single colony within the timeframe of these experiments. However, a mixed population is also beneficial as variation in the expression levels of the construct protein and the effect on melanosome appearance can be evaluated. Examples of stably transfected cells from a mixed pool can be seen in Figure 3.27. These examples highlight the natural variation in SKMEL28 cell morphology, as well as the different actin structures present in the cells. These stable transfectants are a valuable addition to the existing toolbox, for initial screening of future bioactives that may modulate melanosome dynamics.

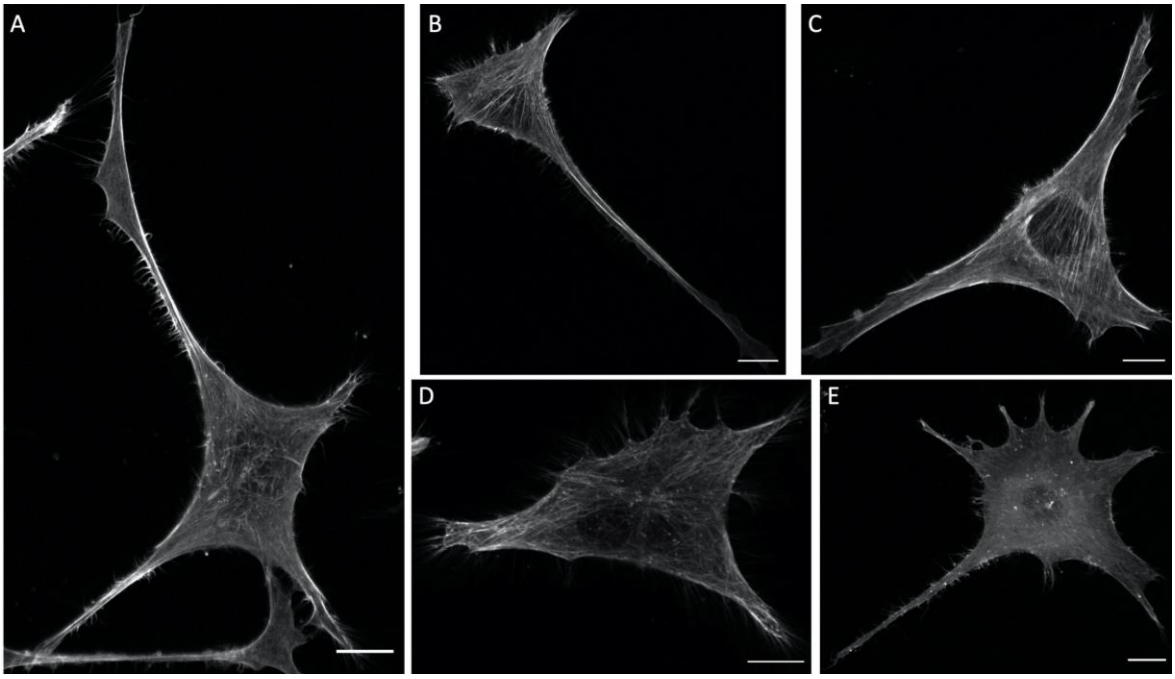

Figure 3.27. Illustrative examples of the SKMEL28 cell line stably expressing tdTomato-LifeAct

A-E. Examples demonstrating the variability in SKMEL28 cell morphology, with all of the cells possessing dendrites which are necessary for their function in providing keratinocytes with melanin. Images were processed using Airyscan. Scale bars = 15 μm.

3.8.1 0.001% w/v (14 μM) sucrose dilaurate disrupts actin organisation in SKMEL28 cells transfected with tdTomato-LifeAct

Having established a stably transfected SKMEL28 cell pool with the tdTomato-LifeAct construct, this was used in order to examine the effect of Sucrose Dilaurate on the actin cytoskeleton and cell morphology. It has been reported that Sucrose Dilaurate may hinder melanosome transfer between melanocytes and keratinocytes by affecting melanocyte dendrites (personal communication with P&G). The tdTomato-LifeAct cells were used for these experiments. The cells were seeded at a high confluency in ibidi dishes, and 24 hours later they were imaged. The sucrose dilaurate treatment was applied to the dish once a representative cell had been located and imaged pre-treatment. The dish was not moved in order for images to be taken of the cell at various time points to determine the immediate effect of sucrose dilaurate on actin and cell morphology. Within 5 minutes of application of the treatment, the actin cytoskeleton visibly began to rearrange itself, with extensive changes in actin organisation being seen within 30 minutes (Figure 3.28). The actin appeared to form

clusters throughout the cell where the organised filaments were breaking down, and the cellular dendrites shortening. The cells became smaller overall, and their outline became disorganised.

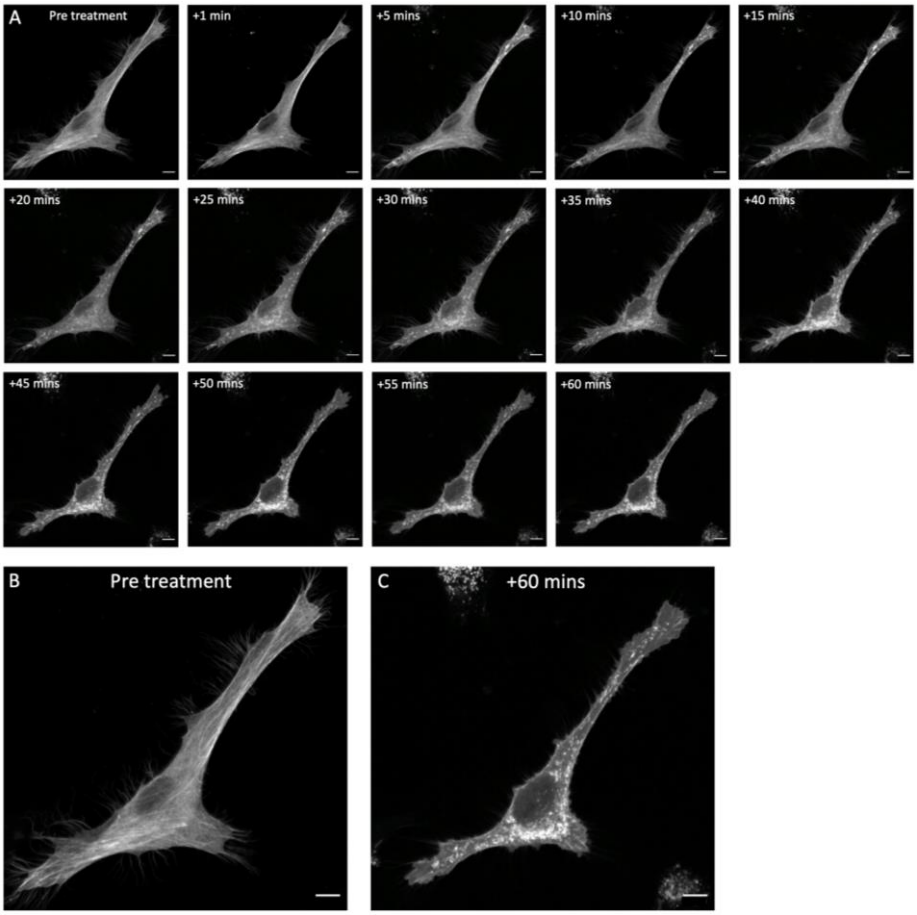

Figure 3.28. An SKMEL28 cell stably expressing tdTomato-LifeAct, treated with 0.001% w/v (14 μM) sucrose dilaurate

A. Time course before and for 60 minutes after treatment with sucrose dilaurate, with images captured every 5 minutes. Scale bars = 10 μm. B. A larger image of the cell before addition of treatment, showing a large cell with a healthy cytoskeleton. Scale bar = 10 μm. C. A larger image of the cell 60 minutes after addition of the treatment, showing extensive actin disorganisation, with clumping and shortening of the cell's projections. Airyscan processing was applied to the images. Scale bar = 10 μm.

3.8.2 0.05% DMSO does not cause actin disruption in SKMEL28 cells similar to that seen with Sucrose Dilaurate treatment

In order to rule out any contribution of the drug carrier DMSO to the cytoskeletal rearrangement seen with sucrose dilaurate treatment, the same experiment was repeated with DMSO alone. One µl of DMSO was added to 2 ml of imaging medium and the cells were treated in the same way, after finding a representative cell to image. Over a time period of 30 minutes, very little change in morphology of the cell was seen, with a very minor degree of cell shrinkage which may be attributed to the exchange of fluid on the dish upon treatment, or phototoxicity from prolonged imaging (Figure 3.29). There was no clumping or reorganisation of actin at all, which was seen within 5 minutes in the Sucrose Dilaurate treatment condition. This control experiment suggests that the cytoskeletal disorganisation observed after Sucrose Dilaurate treatment is due to the Sucrose Dilaurate itself, and not due to non-specific imaging or drug carrier effects.

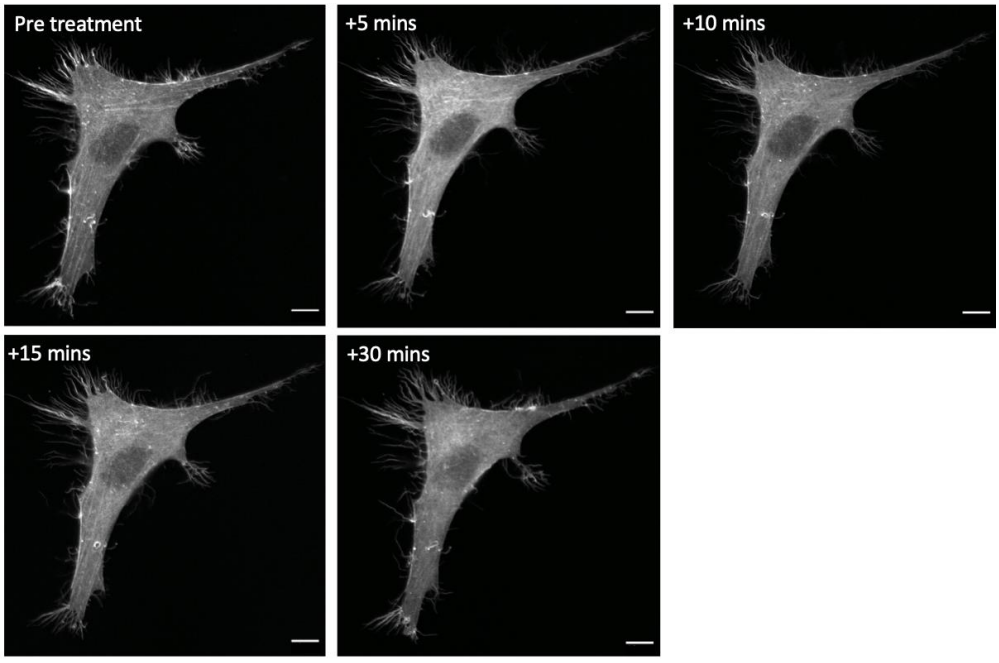

Figure 3.29. An SKMEL28 cell stably expressing tdTomato-LifeAct, treated with 0.05% DMSO

Images were captured before and for 30 minutes after addition of treatment. Airyscan processing was applied to the images. Scale bars = 10 µm.

Overall, the most useful construct for the investigation of melanosome dynamics proved to be mNG-Pmel17 (MαC), allowing a detailed view of Pmel17 movement. Although not specific to melanosomes, the GFP-Rab27A construct remains a useful tool which could be used in conjunction with a melanosome-specific reporter of a different colour. The tdTomato-LifeAct construct proved to be equally valuable, especially for the observation of the interaction of Pmel17 with actin. Both mNG-Pmel17 (MαC) and tdTomato-LifeAct are also useful reporters for the evaluation of the effects of bioactives, with Sepiwhite and sucrose dilaurate producing a decrease in mNG-tagged Pmel17 and the latter also disrupting the actin cytoskeleton.

4 Discussion

4.1 Investigation of the Rab27A protein for melanosome tracking

As discussed in Results, endogenous Rab27A staining appears diffuse throughout the cell (Figure 3.1), reflecting its widespread use for vesicle trafficking in melanocytes. The GFP-Rab27A protein construct also localises to vesicles of varying sizes throughout the cell (Figure 3.3). Western blot analysis of SKMEL28 melanocytes transfected with the GFP-Rab27A protein showed the protein to remain intact in these cells (Figure 3.4), suggesting that the GFP signal detected reflects true Rab27A protein localisation. The appearance of endogenous Rab27A differed to that seen with the GFP-tagged construct, with endogenous Rab27A appearing more punctate and evenly spread. While larger Rab27A-coated vesicles are also highlighted with the GFP-Rab27A construct, endogenous Rab27A vesicle size appears homogeneous throughout the cell. An EGFP-Rab27A probe used by Ostrowski *et al*. (2009) to investigate the role of Rab27A in exosome secretion also showed similar cellular distribution to that seen with the GFP-Rab27A construct used here. The dissimilarity between endogenous Rab27A distribution detected by immunofluorescence and GFP-Rab27A localisation requires further investigation to determine the efficacy of both detection methods. For example, SKMEL28 cells transiently transfected with GFP-Rab27A may be fixed and stained with the anti-Rab27A antibody to determine the level of co-localisation. The specificity of the antibody was not further explored here due to time constraints as well as the non-specificity of Rab27A to melanosomes rendering the protein less useful than other candidates. In further investigations, immunofluorescence experiments to observe the co-localisation between endogenous Rab27A and HMB45, as well as between mNG-Pmel17 (MaC) and Rab27A, would be a valuable supplement to the experiments presented here.

4.1.1 GFP-Rab27A live imaging with reflectance

The GFP-Rab27A construct was also imaged in conjunction with reflectance imaging for detection of melanosomes (Figure 3.5). It was expected that there would be some co-localisation of Rab27A with melanosomes as Rab27A captures the stage IV mature subset for transfer along microtubules and actin filaments. Reflectance signal alone (Figure 3.5 B)

shows a number of granules of approximately equal size, marginally smaller in diameter than the reported value for melanosome size. However, none of these granules appear to co-localise with or be surrounded by strong GFP signal in GFP-Rab27A-transfected cells. Furthermore, the granules appear to move very little during time-course imaging over a period of just over 2 minutes, mostly shaking in place. Previously successful studies (Lai and Xu, 2011; Yamashita, Kuwahara, González and Takahashi, 2005) have used an 830nm diode laser for the detection of melanin in tissues. Another group (Majdzadeh *et al*., 2015) used a combination of multiphoton microscopy (MPM) and reflectance confocal microscopy (RCM) at 760 nm to detect melanin pigment in skin sections. As previous studies have shown successful detection of melanin at higher wavelengths, it is possible that 633 nm reflectance is highlighting a different cellular structure. It is also a possibility that the melanosomes of SKMEL28 cells are not darkly pigmented enough to produce the reflectance signal, as these cells are lightly pigmented. An examination of the reflectance signal at 633 nm in an MNT1 melanocyte may help to elucidate this, as MNT1 cells are highly pigmented with visible melanocytes in bright field images. Alternatively, SKMEL28 cells stained with anti-HMB45 antibody could be examined with reflectance microscopy to observe any co-localisation of reflectance with Pmel17 protein, reflecting melanosomes.

4.2 Investigating the TRP2 protein for melanosome tracking

After investigating Rab27A, the second protein candidate examined for tracking melanosomes was TRP2. TRP2 protein was tagged with tdTomato, a bright orange/red fluorescent protein, at the N-terminus, adjacent to the signal sequence. A two-amino acid linker sequence was included at the start and end of the tdTomato sequence to link it to the TRP2 sequence. When the tdTomato-TRP2 construct was transfected into SKMEL28 cells, the localisation of the tagged protein appeared diffuse throughout the cell (Figure 3.8). There are no distinct structures highlighted which may correspond to melanosomes. TRP2 is an enzyme involved in the biosynthesis of melanin, and would thus be expected to be detected on the surface of melanosomes. The diffuse appearance of the construct may indicate that it does not remain intact in SKMEL28 cells. Even though the tdTomato tag was placed downstream of the signal sequence in order to avoid disrupting protein localisation, the tag's placement my still have had an effect on the protein's function, or caused it to be targeted for degradation. An additional experiment required here is a western blot examination of

SKMEL28 lysate transfected with the construct. This would help to resolve whether the tagged protein is being degraded. Additionally, staining transfected SKMEL28 cells with TRP2 protein with a secondary antibody of a different emission wavelength would help to elucidate whether the tdTomato tag remains attached to TRP2. This was not investigated due to time constraints, and a more suitable tag was preferred for use in subsequent experiments.

A study by Patwardhan *et al*. (2017) used a GFP-TRP2 construct to co-localise TRP2 with MART-1, a protein involved in Pmel17 processing, and Rab6, which was implicated in the transport of the two aforementioned proteins to melanosomes. The researchers were able to show that GFP-tagged TRP2 co-localises with melanosomes in MNT1 cells, and both GFP-TRP2 and GFP-Rab6 co-localise with MART-1 staining in immunogold labelling of MNT1 cells. The construct shows a punctate appearance in the MNT1 cells, as would be expected for TRP2 protein, and does not show signs of degradation. The construct used in this study was created by fusing GFP to the transmembrane and cytosolic domains of TRP2, whereas here the tdTomato marker was fused to the lumenal domain of TRP2. For the TRP2 protein, this may be an inappropriate position for addition of a tag, which may be triggering its degradation or mislocalisation.

4.3 Primary evaluation of the mNG-Pmel17 constructs

As the Pmel17 protein is present in melanosomes from their earliest developmental stage to the latest stage in maturation, this protein was identified as the most suitable candidate for tracking melanosome movement. Two different constructs were designed, corresponding to two different structures that emerge from the Pmel17 protein to form the amyloid fibrils in melanosomes. The CAF forms the core of the fibrils and the MaC fragments increase the surface area of the fibrils. The constitutively active forms of the constructs were both examined first by collecting lysates of transfected cells and resolving these by non-reducing SDS PAGE. Examination of the gel using a Typhoon fluorescent gel reader (Figure 3.11 A) showed an mNG band in the lysate containing mNG-Pmel17 (MαC), with a substantially lower signal in the lysate containing mNG-Pmel17 (CAF). Transfer of the protein to a PVDF membrane and subsequent staining of the membrane with anti-HMB45 antibody showed a signal in all three SKMEL28 lysates, reflecting both endogenous and mNG-tagged Pmel17 expression (Figure 3.11 B). The band in transfected lysates is darker, reflecting higher

expression due to transfection with the constitutive constructs. The band visible in the lysate containing mNG-Pmel17 (MαC) is in the same position as the mNG signal detected in the same lane on the gel. Stripping and re-staining the membrane with anti-mNG antibody (Figure 3.11 C) revealed a strong band in lysate containing mNG-Pmel17 (MαC) in the same position as the HMB45 band in figure 3.11 B, and a band in the positive control. A very faint band can be discerned in the mNG-Pmel17 (MAC)-containing lysate, but it is almost imperceptible. The non-reducing gel and subsequent western blotting indicate that the mNG-Pmel17 (MαC) construct remains intact in transfected cells, whereas the CAF-tagged form is largely cleaved, separating the Pmel17 protein from the mNG. Although two repeats are already present on the same gel, this experiment should be repeated in order to increase the reliability of the results. Furthermore, it would be prudent to generate additional lysates from different cell lines expressing the two mNG-Pmel17 constructs, such as MNT1 melanocytes, HT1080 fibroblasts and HaCaT keratinocytes. The examination of these additional lysates on a non-reducing gel would provide further information on how the constructs are processed in non-melanocyte cell lines, which may not be equipped to process Pmel17.

4.3.1 mNG-Pmel17 (CAF) live imaging

When transfected into SKMEL28 cells, the CAF-tagged form of the construct did not appear to localise to melanosomes, but instead the mNG signal was diffuse and appeared to highlight a network towards the periphery of the cell (Figure 3.12). The appearance of the construct is consistent with the results obtained from the non-reducing gel discussed above, suggesting that the mNG-Pmel17 (CAF) fusion protein is degraded in the cell. A fusion protein of this nature has not been attempted previously, likely due to the extensive processing the Pmel17 protein undergoes. The processing steps and cleavage sites are shown in figure 1.3, detailed in the following papers: Ho *et al.* (2015), Watt *et al.* (2009), Berson *et al.* (2003), Rochin *et al*. (2013), Kummer *et al.,* 2008; Hoashi *et al*., 2006; Harper *et al.*, 2007; McGlinchey *et al*., 2009; Hee *et al*, 2017). This processing makes placing a fluorescent tag while also retaining the function of the protein challenging. It is possible that placement of mNG within the region of the protein which is cleaved to produce CAF renders the fragment too large to be incorporated into the tightly packed core fibrils in melanosomes. This might cause the re-routing of the mNG-tagged CAF for degradation. Furthermore, the structure of the N-terminal region has been shown to be vital for the correct formation of the

CAF (Leonhardt *et al.*, 2013). It is possible that, although the mNG-tagged CAF fusion protein is not a deletion mutant, the addition of the fluorescent tag was enough to disrupt the protein's normal function. Alternatively, there may be a thus far unreported cleavage site which separated the mNG tag from the CAF, leading to mNG being observed more diffusely throughout the cell. In conclusion, this construct was deemed unsuitable for melanosome tracking and was not used in any subsequent experiments.

The majority of the experiments in which amyloidogenic proteins, of which Pmel17 is an example, have been tagged involve the addition of a polyhistidine tag. This tag permits the purification of the protein it is fused with. Due to its small size, it is also less likely to exert any effects on the protein's function. One such study was able to add a C-terminal hexa-histidine (His) tag to a number of different fragments of Pmel17 (Watt *et al.*, 2009). The researchers used this tag to purify the Pmel17 fragments and observe their ability to form amyloid fibrils in vitro. The His tag did not impact the processing of Pmel17, likely due to its small size. A number of different tagged fragments was generated, and all exhibited fibrillogenic behaviour in vitro except for the RPT domain tag, which largely remained soluble. The variety of the constructs generated illustrates the ability of Pmel17 to be tagged with a small protein in a variety of positions, without functional consequences for the formation of fibrils. In a separate study (Dean and Lee, 2021) researchers tagged the RPT domain of Pmel17 with a His tag and placed a tobacco etch virus protease recognition sequence upstream of a native glycine residue in the RPT domain. This allowed them to both purify the fragment of the protein using the His tag, and separate the His tag from the RPT domain by cleavage with a tobacco etch virus protease. Apart from a small His tag, no other attempts have been made to fuse Pmel17 with different proteins such as fluorescent proteins. The behaviour of a fluorescently-tagged Pmel17 protein was thus not able to be predicted. Given that here mNG, a fluorescent protein significantly larger (26.6 kDa) than a hexahistidine tag (0.8 kDa), is being inserted into the Pmel17 sequence, it is not entirely unexpected that it might produce the results seen with the CAF-tagged construct.

A further example of the use of the His tag for amyloidogenic protein isolation without impacting physiological protein behaviour and function was also demonstrated by Jia *et al*. (2018), who used a His tag to purify amyloid-β peptide ($A\beta_{1\text{-}42}$). This protein fragment is derived from amyloid-β precursor protein and is involved in the formation of extracellular amyloid plaques seen in Alzheimer's disease. The group showed that isolation and

purification of the protein using a His tag did not impact the $A\beta_{1-42}$ fragment's ability to form the β-sheet-rich plaques seen in the disease phenotype. This example, and the aforementioned examples of Pmel17 His-tagging, illustrate that it is possible to tag fibrillogenic proteins with at least small markers.

4.3.2 mNG-Pmel17 (MαC) live imaging

In contrast to the CAF-tagged Pmel17 construct, the MαC-tagged construct formed vesicles of a roughly consistent size when transfected into SKMEL28 cells (Figure 3.13 A). In this case, the mNG is attached to the fragments of Pmel17 which increase the surface area of the fibrils before melanin deposition. The fusion protein would thus be expected to localise to vesicles transported to the plasma membrane and subsequent internalised in order to reach melanosomes. The mNG signal would be expected to be contained within vesicles, as was seen in transfections in the SKMEL28 cells. These vesicles were found to be approximately the same size as melanosomes (Figure 3.14; Sturm, Box and Ramsay, 1998), indicating that the fusion protein is correctly trafficked, despite being fused to mNG. The movement of the vesicles seen in live imaging is both away from and towards the centre of the cell. As there is no differentiation between unprocessed and processed mNG-Pmel17, the vesicles can be taken to represent both full-length protein being trafficking from the Golgi to the plasma membrane, as well as processed forms of the protein in early endosomes and melanosomes. The speed of movement of the vesicles was variable, with the example shown in figure 3.15 B travelling at approximately 1.44 μm/s. This is more rapid than might be expected for a maturing or mature melanosome. Maturing melanosomes moving along microtubules also move more rapidly than mature melanosomes tracking along the actin cytoskeleton (Hume *et al*., 2011). Hume *et al*. studied the movement of melanosomes co-localising with either EGFP-Rab27A, reflecting mature melanosomes, or EGFP-Rab32/38, reflecting maturing melanosomes. They found that Rab32/38-bound melanosomes moved faster than the Rab27A-bound population. The median speed melanosomes bound to either of the Rab proteins was found to be considerably lower than 1.44 μm/s seen here, however this is only one isolated melanosome and a more detailed analysis of a number of cells would be required to establish a mean mNG-Pmel17 vesicle speed. One limitation which has made this analysis challenging is the movement of vesicles between z-planes. Imaging this construct on a confocal microscope has allowed its observation in great detail at a high magnification,

however the narrow z-plane field of view allows some vesicles to go out of view. This can prevent tracking over a sufficient number of frames to establish the path and velocity of vesicles. The example vesicle shown here moving at a high speed may represent unprocessed Pmel17 not contained within a melanosome, being trafficked to the plasma membrane. Fast deconvolution using a Lattice LightSheet (Zeiss) could be used here in order to view the entire volume of the cell while maintaining a sufficient frame rate. In conclusion, these initial findings provided encouraging indications that mNG tag was inserted in the correct position to be retained post-processing, while also not impacting protein function.

Although no previous attempts have been made to fluorescently tag Pmel17, a group of researchers (Solovyov *et al*., 2011) were able to tag two fibrillogenic proteins, transthyretin and β2-microglobulin, with superfolder green fluorescent protein (sfGFP). This variant of GFP shows improved folding ability, even when attached to misfolded proteins, and is more resistant to denaturation (Pédelacq *et al*., 2005). They also used an additional His tag on the C-terminus of sfGFP in order to purify the fusion proteins. Solovyov *et al*. showed that the proteins retained their ability to form fibrils with the fluorescent tag attached, demonstrating that it is possible to fluorescently tag a fibrillogenic protein and retain its function. However, examples such as this one are rare in the literature. The mNG-Pmel17 (MαC) construct is therefore another rare example of a successful fluorescently-tagged fibrillogenic fusion protein.

The tetracycline-inducible version of the construct was then examined in SKMEL28 cells, and produced mNG-Pmel17-containing vesicles like those seen with the constitutive construct (Figure 3.13 B). However, the fusion protein was expressed even before treatment of the transfected cells with tetracycline. This rendered the construct unusable as its primary benefit was to observe melanosomes as they begin to form, and their journey in the cell as they mature. Tetracycline-inducible constructs are known to sometimes be "leaky," depending on the insertion site of the construct in the cell's DNA and the experimental conditions, causing enhancer sequences to trigger expression of the protein before tetracycline induction (Dong *et al*., 2007). Unfortunately, this cannot be counteracted without creating a new construct with a more tightly controlled induction system. The "leaky" expression may also have been due to tetracycline present in the growth medium, despite this being at a low concentration. In order to investigate this, the experiment should

be repeated with cells sub-cultured in tetracycline-free medium, for a time period long enough to allow all traces of the antibiotic to leave the cells. This avenue was not investigated further due to time constraints.

4.4 mNG-Pmel17 (MαC) validation

After initial encouraging results from the mNG-Pmel17 (MαC) construct, it was further validated by examination of co-localisation and endogenous protein. As shown in figure 3.16, endogenous protein distribution in SKMEL28 cells appears almost identical to the distribution of mNG-Pmel17 vesicles in transfected cells. In order to take this experiment one step further, cells transfected with the construct were fixed and stained with anti-HMB45 antibody in order to co-localise mNG with Pmel17. Unfortunately, fixation caused the mNG signal to become diffuse instead of punctate and the experiment was unsuccessful. Although not examined in this study, different fixation or permeabilisation methods could be tested in order to clarify this. Furthermore, mNG-Pmel17 (MαC) co-localisation with lysosomes was examined, using LysoTracker probe (Figure 3.17 A and B). Very limited co-localisation was observed, reflected in an experiment examining endogenous Pmel17 co-localisation with lysosomes (Figure 3.17 C). Lysosomes are acidic compartments responsible for the degradation of biomolecules that derive from secretory, endocytic, autophagic and phagocytic pathways. Significant co-localisation of the mNG-Pmel17 construct with lysosomes would suggest that the fusion protein is being targeted for degradation and is not localising to melanosomes. The LysoTracker probe targets acidic vesicles specifically, and the pH of lysosomes is measured at 4.5-5 (Mindell, 2012). The pH of melanosomes has also been shown to vary; the higher the pigment content, the higher the pH. The acidity of melanosomes regulates the activity of Tyrosinase, the main enzyme responsible for melanin synthesis. As SKMEL28 cells are lightly pigmented, their melanosomal pH would be below neutral, but the majority would be less acidic than lysosomes (Ancans *et al*., 2001). The LysoTracker probe may thus be expected to target to a small population of mNG-Pmel17 vesicles, as was seen in live imaging, denoted by orange/yellow-coloured vesicles. In order to examine endogenous Pmel17 localisation relative to lysosomes, anti-LAMP1 antibody was used to stain lysosomal compartments. Very few instances of co-localisation were observed, shown by orange/yellow vesicles, illustrating that mature Pmel17 does not co-localise with lysosomal compartments. The same observations have been made by Raposo

et al. (2001), who examined both Pmel17 and TRP1 in relation to lysosomal compartment markers LAMP1 and cathepsin D. Overall, these results lend further credibility to the mNG-Pmel17 (MαC) construct, showing that it is not broken down.

The mNG-Pmel17 (MαC) construct was then examined in relation to the actin cytoskeleton. Melanosome trafficking is characterised first by movement along microtubules, before capture and transport along the local actin network at the cell periphery, mediated by the three proteins Rab27A, Mlph and MyoVA. This final step in intracellular trafficking precedes transport to neighbouring keratinocytes via the melanocyte's dendrites. This was demonstrated with endogenous Pmel17 protein by immunofluorescence (Figure 3.20), with highlighted areas of substantial co-localisation. Having established that endogenous Pmel17 in SKMEL28 cells accumulates peripherally, mNG-Pmel17 (MαC) vesicle localisation was then observed in relation to two different actin probes. The first, SiR actin, selectively binds to endogenous filamentous actin in live cells. This probe was shown to be very effective, with actin filaments being seen in great detail (Figure 3.18 A). SiR actin has been widely used (Müller *et al*., 2019; D'Este *et al*., 2015; Klementieva *et al*., 2016), owing to the ease with which the cell-permeable probe selectively stains F-actin in live cells within 30 minutes. However, it should be noted that the probe is based on Jasplakinolide, a toxin derived from *Jaspis johnstoni* which binds strongly to F-actin. The strong similarity of SiR actin to Jasplakinolide may cause it to have similar effects, as the probe has been reported to trigger filament formation and stabilisation (Bubb *et al*., 1994). However, for the purposes of establishing mNG-Pmel17 co-location with actin at the cell periphery, these potential side-effects do not impact the results. The main benefit of the SiR actin probe is that it does not require transfection, and can be more easily used to co-localise with a second protein in transfected cells. Melanosome capture by the actin cytoskeleton was imaged at high resolution by Alzahofi *et al*. (2020) using immuno-electron microscopy. The mNG-Pmel17 (MαC) construct provides the unique opportunity to observe that capture dynamically and in real time.

The second probe used to observe actin in live cells was a tdTomato-LifeAct construct. LifeAct is a short peptide 17 amino acids in length which specifically binds to F-actin in live and fixed cells (Riedl *et al*., 2008). It is non-toxic and does not compete with other actin-binding proteins, meaning that it has no effect on actin polymerisation or depolymerisation at optimised concentrations. It also does not interfere with cellular processes, and a

homologous sequence has not been observed in eukaryotes, meaning that competition with endogenous protein is unlikely. The tdTomato-LifeAct fusion protein was selected to allow co-transfection with the green mNG. tdTomato also exhibits higher photostability and brightness than other red/orange fluorescent proteins. When transfected into SKMEL28 cells, the actin cytoskeleton was visualised in great detail, enhanced by Airyscan detection and processing. The transfection efficiency was very high, likely aided by the non-toxicity of the protein. In successfully co-transfected cells, the mNG-Pmel17 vesicles co-localised well with prominent actin networks at the cell periphery (Figure 3.19 D and E). This confirms the result obtained with the SiR actin probe, confirming that it was not specific to the probe or any potential effects it may have had on the cell or the actin cytoskeleton. This experiment also demonstrates the ability of both the mNG-Pmel17 (MαC) and tdTomato-LifeAct to be viably co-transfectable. Although fluorescently-tagged LifeAct has been used extensively in research (Galeano Niño *et al*., 2020; Vidali, Rounds, Hepler and Bezanilla, 2009), research has shown that at high concentrations, it can have a negative effect on actin dynamic remodelling (Belyy, Merino, Sitsel and Raunser, 2020). The group found that LifeAct interacted with a binding pocket on filamentous actin which stabilised the bound subunit along with two adjacent subunits, and may have competed with actin-binding proteins such as cofilin for that binding site. However, when used at low to normal levels these interactions should not occur. As the tdTomato-LifeAct construct was highly effective in staining the actin cytoskeleton in live cells and showed a very high transfection efficiency, an SKMEL28 cell line with stable expression was established (Figure 3.27). This cell line is an invaluable tool for melanosomal research as cell morphology and cytoskeletal health play a vital role in functional melanosome transfer to keratinocytes. It can also be more readily used with a second construct, such as mNG-Pmel17 (MαC) or other melanosome-related protein constructs, improving the co-transfection rate. As the stable cell line is of a mixed population, the protein expression between cells varies. This may be relevant if expression in a proportion of cells is particularly high, with the potential to trigger effects seen by Belyy, Merino, Sitsel and Raunser (2020). SKMEL28 cells stop proliferating at low confluency, rendering a single-clone population more challenging, and was not possible within the time limit of this study.

In addition to the validation experiments presented here, two supplementary experiments to show definitively that the mNG-Pmel17 (MαC) construct maps onto the melanosome development pathway and exists in mature melanosomes would have been valuable further

proof of the construct's efficacy. Firstly, the construct could be co-imaged with reflectance, discussed in section 4.1 in relation to Rab27A. After confirming that the reflectance signal is truly highlighting melanosomes, it may be used in live imaging with transfected cells to establish co-localisation. Only a fraction of the mNG-Pmel17 vesicles corresponding to mature melanosomes would be expected to co-localise with the reflectance signal, but any degree of co-localisation would provide strong evidence that mNG-Pmel17 (MαC) localises to melanosomes. The second validation experiment would complement the co-localisation experiments with actin. A SiR tubulin probe could be used in order to track the movement of mNG-Pmel17 particles along microtubules in live cells, while endogenous tubulin could be examined in relation to Pmel17 in fixed cells to establish the extent of endogenous protein co-localisation. Overall, although these two described experiments would provide even stronger evidence of the construct's functionality, the set of validation experiments detailed above represents robust verification that the construct truly exhibits the same activity as endogenous Pmel17.

4.5 Examination of a second melanocyte cell line: MNT1

Having established that mNG-Pmel17 (MαC) functions well in SKMEL28 cells, a second melanocyte cell line was obtained in order to confirm that the fusion protein observations are not restricted to one cell line. As SKMEL28 cells are lightly pigmented, the darkly pigmented MNT1 melanoma cell line was selected. These cells are generally smaller than SKMEL28 cells and do not develop dendrites. They contain a large number of dark melanosomes throughout their cytoplasm which are visible by bright field microscopy (Figure 3.21 B). The mNG-Pmel17 fusion protein transfection appears analogous to the respective SKMEL28 transfections, with fluorescent vesicles measuring at approximately the same diameter (~0.4-0.5μm). Overall, these experiments confirm the observations made in SKMEL28 cells, demonstrating that the construct's functionality is not restricted to one melanocyte cell line. However, the transfection efficiency in MNT1 cells was considerably lower than in SKMEL28 cells. This was confirmed with the tdTomato-LifeAct construct, which showed a very high transfection efficiency in SKMEL28 cells. This may be a result of an incompatibility of MNT1 cells with the transfection method used. For all MNT1 transfections, JetPei reagent was used, which is composed of a linear polyethylenimine to condense plasmid DNA. It has been reported that nucleofection is more effective than other

methods in melanoma cell transfection (Han et al., 2008). They used specific solutions and nucleofection parameters to directly insert plasmids into the nucleus of a number of SKMEL melanoma cell lines. They showed this method to be more effective than lipid-based transfection methods, including lipofectamine 2000 (Invitrogen). Although MNT1 cell transfection were not examined in this study, it illustrates how alternative methods may be more appropriate for melanoma cell line transfection. A high transfection efficiency was not necessary for the purposes of validating the mNG-Pmel17 (MαC) construct, however the evaluation of alternative transfection methods would be useful for more extensive research in these cells.

4.6 Examining the effects of bioactive compounds using the mNG-Pmel17 (MαC) probe

Having validated the mNG-Pmel17 (MαC) construct, it was used to examine what effects bioactive compounds have on melanogenesis. These particular compounds were selected as they are of interest to the industrial partner. The first compound tested was Undecylenoyl Phenylalanine (Sepiwhite), thought to reduce pigmentation by acting as a beta-adrenergic receptor antagonist (Katoulis et al., 2014). Beta-adrenergic receptor 1 (ADRB1) has been implicated as a propigmentation receptor (Osborne, Hakozaki, Laughlin and Finlay, 2012) similar to the MC1R. Skin treatment formulations containing Sepiwhite have also been shown to reduce hyperpigmentation in vivo (Bissett et al., 2009; Katoulis et al., 2014; Gold and Biron, 2011). Following 48-hour treatment at 0.001% w/v (6 μM), transfected SKMEL28 cells contained fewer mNG-Pmel17 vesicles on average than untreated cells, standardised by cell surface area (Figure 3.23). In fixed untransfected cells, endogenous Pmel17 was reduced after the same treatment, detected by immunofluorescence (Figure 3.24). The observed decrease of endogenous Pmel17 illustrates that the compound is producing an effect in SKMEL28 cells independent of transfection. This is consistent with the purported mode of action of Sepiwhite, as a reduction in MC1R activation would reduce the expression of downstream products, including Pmel17. In the transfected cells, a reduction in the number of mNG-Pmel17-containing vesicles was observed in Sepiwhite-treated cells compared to control cells, even though the construct is constitutively expressed irrespective of ADRB1 or MC1R activation. One explanation for this reduction could be that an attenuation in the amount of endogenous Pmel17 resulted in fewer early endosomes

differentiating into melanosomes, meaning that the number of melanosomes overall was reduced, and these mostly contained mNG-Pmel17. By contrast, untreated cells would produce normal amounts of Pmel17 and melanosomes would contain a mixture of endogenous and mNG-tagged Pmel17. Additionally, there may be unknown Sepiwhite-induced effects involving other proteins, and a more in depth examination at the molecular level is required. An analogous experiment using MNT1 melanocytes would also be valuable, as the effects of the compound would be directly observable due to their high melanin content.

The second bioactive compound tested was sucrose dilaurate. This compound acts as a surfactant and has been used in skin products owing to its emulsifying properties. A 48-hour treatment of transfected SKMEL28 cells with 0.004% w/v (56 μM) sucrose dilaurate produced a statistically significant reduction in mNG-Pmel17 vesicles compared to control untreated cells (Figure 3.25). However, the same treatment in untransfected cells only produced a minor decrease in endogenous Pmel17, detected by immunofluorescence, which was not significant (Figure 3.26). As sucrose dilaurate did not decrease endogenous Pmel17, the observed effect on mNG-Pmel17 vesicles may be an effect of the transfection itself, or of an unknown effect of sucrose dilaurate not directly on Pmel17 itself. Again, a more thorough examination of the molecular mechanisms involved would clarify these observations. Sucrose dilaurate has been shown to reduce the accumulation of an advanced glycation end product (AGE) in skin cells by activation of autophagy (Laughlin et al., 2020). Autophagy activation may thus be involved in the reduction of mNG-Pmel17. When SKMEL28 cells stably expressing tdTomato-LifeAct were treated with 0.001% w/v (14 μM) sucrose dilaurate, a dramatic alteration in actin network dynamics was observed within 10 minutes (Figure 3.28). This extensive change was not seen in control cells treated with DMSO alone (Figure 3.29). Research has shown that surfactants can have a detrimental effect on skin cell integrity (Seweryn, 2018), which may be affecting intracellular calcium levels, causing the cytoskeletal changes seen here. The retraction of dendrites in the treated cells might in turn affect the cells' ability to transfer melanosomes, as dendrites are vital for this process. Further work could examine the effect of sucrose dilaurate on MNT1 cells transfected with mNG-Pmel17 (MαC), where effect on the fluorescent probe can be correlated with direct observable effects on the cells' pigmentation. Furthermore, it would be of interest to observe the effect of sucrose dilaurate on SKMEL28 cells co-transfected with mNG-Pmel17 (MαC) and tdTomato-LifeAct, made easier by the already-established

LifeAct stable cell line. Overall, the mNG-Pmel17 (MαC) construct has proven to be an invaluable tool for the examination of the activity of bioactive compounds of interest.

4.7 Future directions

The experiments laid out in this study demonstrate the efficacy of the mNG-Pmel17 (MαC) construct in tracking melanosomes, thus far within melanocytes. Future work could use this tool in order to observe melanosome transfer to keratinocytes in a co-culture system. As the majority of the existing knowledge on melanosome transfer has been obtained through static imaging techniques such as electron microscopy, the direct observation of melanosome transfer in real time would provide vital clarification, allowing either the confirmation of existing models or the creation of new models of transfer. As SKMEL28 cells are more dendritic, these may be used in an initial co-culture system, before expanding to more darkly pigmented cells such as MNT1 cells. These co-culture systems would also be invaluable for the evaluation of the effects of bioactive compounds on melanosome transfer. Furthermore, the use of the mNG-Pmel17 probe in primary melanocyte cell lines of variable pigment content would provide a more biologically relevant view of melanosomal behaviour, in normal conditions and in response to bioactive compounds. Such a system could then be used to identify compounds with the potential to treat skin conditions such as melasma, characterised by an abnormal production of melanin.

5 References

Alzahofi, N., Welz, T., Robinson, C., Page, E., Briggs, D., Stainthorp, A., Reekes, J., Elbe, D., Straub, F., Kallemeijn, W., Tate, E., Goff, P., Sviderskaya, E., Cantero, M., Montoliu, L., Nedelec, F., Miles, A., Bailly, M., Kerkhoff, E. and Hume, A., 2020. Rab27a co-ordinates actin-dependent transport by controlling organelle-associated motors and track assembly proteins. *Nature Communications*, 11(1), p.3495.

Amatya, B., Jha, A., & Shrestha, S., 2020. Frequency of different types of facial melanoses referring to the Department of Dermatology and Venereology, Nepal Medical College and Teaching Hospital in 2019, and assessment of their effect on health-related quality of life. BMC Dermatology, 20(1), p.4.

Ambrosio, A., Boyle, J., Aradi, A., Christian, K. and Di Pietro, S., 2016. TPC2 controls pigmentation by regulating melanosome pH and size. *Proceedings of the National Academy of Sciences*, 113(20), pp.5622-5627.

Ancans, J., Tobin, D., Hoogduijn, M., Smit, N., Wakamatsu, K. and Thody, A., 2001. Melanosomal pH Controls Rate of Melanogenesis, Eumelanin/Phaeomelanin Ratio and Melanosome Maturation in Melanocytes and Melanoma Cells. *Experimental Cell Research*, 268(1), pp.26-35.

Belyy, A., Merino, F., Sitsel, O. and Raunser, S., 2020. Structure of the Lifeact–F-actin complex. *PLOS Biology*, 18(11), p.e3000925.

Berson, J., Harper, D., Tenza, D., Raposo, G. and Marks, M., 2001. Pmel17 Initiates Premelanosome Morphogenesis within Multivesicular Bodies. *Molecular Biology of the Cell*, 12(11), pp.3451-3464.

Berson, J., Theos, A., Harper, D., Tenza, D., Raposo, G. and Marks, M., 2003. Proprotein convertase cleavage liberates a fibrillogenic fragment of a resident glycoprotein to initiate melanosome biogenesis. *Journal of Cell Biology*, 161(3), pp.521-533.

Bissett, D., Robinson, L., Raleigh, P., Miyamoto, K., Hakozaki, T., Li, J. and Kelm, G., 2009. Reduction in the appearance of facial hyperpigmentation by topicalN-undecyl-10-enoyl-l-phenylalanine and its combination with niacinamide. *Journal of Cosmetic Dermatology*, 8(4), pp.260-266.

Booth, A., Tarafder, A., Hume, A., Recchi, C. and Seabra, M., 2014. A Role for Na+,K+-ATPase α1 in Regulating Rab27a Localisation on Melanosomes. *PLoS ONE*, 9(7), p.e102851.

Bubb, M. R., Senderowicz, A. M., Sausville, E. A., Duncan, K. L., & Korn, E. D., 1994. Jasplakinolide, a cytotoxic natural product, induces actin polymerization and competitively inhibits the binding of phalloidin to F-actin. *The Journal of biological chemistry*, 269(21), pp.14869–14871.

Bultema, J., Boyle, J., Malenke, P., Martin, F., Dell'Angelica, E., Cheney, R. and Di Pietro, S., 2014. Myosin Vc Interacts with Rab32 and Rab38 Proteins and Works in the

Biogenesis and Secretion of Melanosomes. *Journal of Biological Chemistry*, 289(48), pp.33513-33528.

Dean, D. and Lee, J., 2021. Purification and characterization of an amyloidogenic repeat domain from the functional amyloid Pmel17. *Protein Expression and Purification*, 187.

D'Este, E., Kamin, D., Göttfert, F., El-Hady, A. and Hell, S., 2015. STED Nanoscopy Reveals the Ubiquity of Subcortical Cytoskeleton Periodicity in Living Neurons. *Cell Reports*, 10(8), pp.1246-1251.

D'Mello, S., Finlay, G., Baguley, B. and Askarian-Amiri, M., 2016. Signaling Pathways in Melanogenesis. *International Journal of Molecular Sciences*, 17(7), p.1144.

Dong, X., Yan, S., Weiwang, G. and Xigu, C., 2007. Tetracycline- controlled transcriptional regulation systems: countermeasures to eliminate basal transgene leaks in Tet-based systems. *Progress in Natural Science*, 17(1), pp.11-19.

Falcon, K., Fors, M., Palacios Alvarez, S., Veintimilla, K., Lasso, N. and Navas, C., 2019. Assessment of Predictors of Sun Sensitivity as Defined by Fitzpatrick Skin Phototype in an Ecuadorian Population and Its Correlation with Skin Damage. *Dermatology*, 235(5), pp.400-406.

Figueiredo, A., Wasmeier, C., Tarafder, A., Ramalho, J., Baron, R. and Seabra, M., 2008. Rab3GEP Is the Non-redundant Guanine Nucleotide Exchange Factor for Rab27a in Melanocytes. *Journal of Biological Chemistry*, 283(34), pp.23209-23216.

Fowler, D., Koulov, A., Alory-Jost, C., Marks, M., Balch, W. and Kelly, J., 2005. Functional Amyloid Formation within Mammalian Tissue. *PLoS Biology*, 4(1), p.e6.

Galeano Niño, J., Tay, S., Tearle, J., Xie, J., Govendir, M., Kempe, D., Mazalo, J., Drew, A., Colakoglu, F., Kummerfeld, S., Proud, C. and Biro, M., 2020. The Lifeact-EGFP mouse is a translationally controlled fluorescent reporter of T cell activation. *Journal of Cell Science*, 133(5).

Gold, M. and Biron, J., 2011. Efficacy of a novel hydroquinone-free skin-brightening cream in patients with melasma. *Journal of Cosmetic Dermatology*, 10(3), pp.189-196.

Graham, M., Tzika, A., Mitchell, S., Liu, X. and Leonhardt, R., 2019. Repeat domain-associated O-glycans govern PMEL fibrillar sheet architecture. *Scientific Reports*, 9(1), p.6101.

Grimes, P., 1995. Melasma. *Archives of Dermatology*, 131(12), p.1453.

Grimes, P., 1995. Melasma. Etiologic and therapeutic considerations. *Archives of Dermatology*, 131(12), pp.1453-1457.

Han, S., Gai, W., Yancovitz, M., Osman, I., Di Como, C. and Polsky, D., 2008. Nucleofection is a highly effective gene transfer technique for human melanoma cell lines. *Experimental Dermatology*, 17(5), pp.405-411.

Harper, D., Theos, A., Herman, K., Tenza, D., Raposo, G. and Marks, M., 2007. Premelanosome Amyloid-like Fibrils Are Composed of Only Golgi-processed Forms of Pmel17 That Have Been Proteolytically Processed in Endosomes. *Journal of Biological Chemistry*, 283(4), pp.2307-2322.

Hee, J., Mitchell, S., Liu, X. and Leonhardt, R., 2017. Melanosomal formation of PMEL core amyloid is driven by aromatic residues. *Scientific Reports*, 7, p.44064.

Hellström, A., Watt, B., Fard, S., Tenza, D., Mannström, P., Narfström, K., Ekesten, B., Ito, S., Wakamatsu, K., Larsson, J., Ulfendahl, M., Kullander, K., Raposo, G., Kerje, S., Hallböök, F., Marks, M. and Andersson, L., 2011. Inactivation of Pmel Alters Melanosome Shape But Has Only a Subtle Effect on Visible Pigmentation. *PLoS Genetics*, 7(9), p.e1002285.

Hexsel, D., Lacerda, D., Cavalcante, A., Filho, C., Kalil, C., Ayres, E., Azulay-Abulafia, L., Weber, M., Serra, M., Lopes, N. and Cestari, T., 2013. Epidemiology of melasma in Brazilian patients: a multicenter study. *International Journal of Dermatology*, 53(4), pp.440-444.

Hirobe, T. and Abe, H., 2006. The slaty mutation affects the morphology and maturation of melanosomes in the mouse melanocytes. *Pigment Cell Research*, 19(5), pp.454-459.

Hirobe, T., Wakamatsu, K., Ito, S., Kawa, Y., Soma, Y. and Mizoguchi, M., 2006. The slaty mutation affects eumelanin and pheomelanin synthesis in mouse melanocytes. *European Journal of Cell Biology*, 85(6), pp.537-549.

Ho, T., Watt, B., Spruce, L., Seeholzer, S. and Marks, M., 2015. The Kringle-like Domain Facilitates Post-endoplasmic Reticulum Changes to Premelanosome Protein (PMEL) Oligomerization and Disulfide Bond Configuration and Promotes Amyloid Formation. *Journal of Biological Chemistry*, 291(7), pp.3595-3612.

Hoashi, T., Muller, J., Vieira, W., Rouzaud, F., Kikuchi, K., Tamaki, K. and Hearing, V., 2006. The Repeat Domain of the Melanosomal Matrix Protein PMEL17/GP100 Is Required for the Formation of Organellar Fibers. *Journal of Biological Chemistry*, 281(30), pp.21198-21208.

Hoashi, T., Watabe, H., Muller, J., Yamaguchi, Y., Vieira, W. and Hearing, V., 2005. MART-1 Is Required for the Function of the Melanosomal Matrix Protein PMEL17/GP100 and the Maturation of Melanosomes. *Journal of Biological Chemistry*, 280(14), pp.14006-14016.

Hume, A., Collinson, L., Hopkins, C., Strom, M., Barral, D., Bossi, G., Griffiths, G. and Seabra, M., 2002. The leaden Gene Product Is Required with Rab27a to Recruit Myosin Va to Melanosomes in Melanocytes. *Traffic*, 3(3), pp.193-202.

Hume, A., Wilson, M., Ushakov, D., Ferenczi, M. and Seabra, M., 2011. Semi-Automated Analysis of Organelle Movement and Membrane Content: Understanding Rab-Motor Complex Transport Function. *Traffic*, 12(12), pp.1686-1701.

Jackson, I., Chambers, D., Tsukamoto, K., Copeland, N., Gilbert, D., Jenkins, N. and Hearing, V., 1992. A second tyrosinase-related protein, TRP-2, maps to and is mutated at the mouse slaty locus. *The EMBO Journal*, 11(2), pp.527-535.

Jia, L., Wang, W., Sang, J., Wei, W., Zhao, W., Lu, F. and Liu, F., 2018. Amyloidogenicity and Cytotoxicity of a Recombinant C-Terminal His6-Tagged Aβ1–42. *ACS Chemical Neuroscience*, 10(3), pp.1251-1262.

Katoulis, A., Alevizou, A., Soura, E., Mantas, N., Bozi, E., Gregoriou, S., Makris, M. and Rigopoulos, D., 2014. A double-blind vehicle-controlled study of a preparation containing undecylenoyl phenylalanine 2% in the treatment of melasma in females. Journal of Cosmetic Dermatology, 13(2), pp.86-90.

Klementieva, N., Snopova, L., Prodanets, N., Furman, O., Dudenkova, V., Zagaynova, E., Lukyanov, K. and Mishin, A., 2016. Fluorescence Imaging of Actin Fine Structure in Tumor Tissues Using SiR–Actin Staining. *Anticancer Research*, 36(10), pp.5287-5294.

Kummer, M., Maruyama, H., Huelsmann, C., Baches, S., Weggen, S. and Koo, E., 2008. Formation of Pmel17 Amyloid Is Regulated by Juxtamembrane Metalloproteinase Cleavage, and the Resulting C-terminal Fragment Is a Substrate for γ-Secretase. *Journal of Biological Chemistry*, 284(4), pp.2296-2306.

Kuroda, T., Ariga, H. and Fukuda, M., 2003. The Actin-Binding Domain of Slac2-a/Melanophilin Is Required for Melanosome Distribution in Melanocytes. *Molecular and Cellular Biology*, 23(15), pp.5245-5255.

Kushimoto, T., Basrur, V., Valencia, J., Matsunaga, J., Vieira, W., Ferrans, V., Muller, J., Appella, E. and Hearing, V., 2001. A model for melanosome biogenesis based on the purification and analysis of early melanosomes. *Proceedings of the National Academy of Sciences*, 98(19), pp.10698-10703.

Lai, L. and Xu, A., 2011. In vivo reflectance confocal microscopy imaging of vitiligo, nevus depigmentosus and nevus anemicus. *Skin Research and Technology*, 17(4), pp.404-410.

Laughlin, T., Tan, Y., Jarrold, B., Chen, J., Li, L., Fang, B., Zhao, W., Tamura, M., Matsubara, A., Deng, G., Wang, X. and Hakozaki, T., 2020. Autophagy activators stimulate the removal of advanced glycation end products in human keratinocytes. *Journal of the European Academy of Dermatology and Venereology*, 34(S3), pp.12-18.

Leonhardt, R., Vigneron, N., Hee, J., Graham, M. and Cresswell, P., 2013. Critical residues in the PMEL/Pmel17 N-terminus direct the hierarchical assembly of melanosomal fibrils. *Molecular Biology of the Cell*, 24(7), pp.964-981.

Lim, H., Jin, S. and Yun, S., 2016. Modulation of Melanogenesis by Heme Oxygenase-1 via p53 in Normal Human Melanocytes. *Chonnam Medical Journal*, 52(1), pp.45-52.

Lin, J. and Fisher, D., 2007. Melanocyte biology and skin pigmentation. *Nature*, 445(7130), pp.843-850.

Lopes, V., Ramalho, J., Owen, D., Karl, M., Strauss, O., Futter, C. and Seabra, M., 2007. The Ternary Rab27a-Myrip-Myosin VIIa Complex Regulates Melanosome Motility in the Retinal Pigment Epithelium. *Traffic*, 8(5), pp.486-499.

Lukinavičius, G., Reymond, L., D'Este, E., Masharina, A., Göttfert, F., Ta, H., Güther, A., Fournier, M., Rizzo, S., Waldmann, H., Blaukopf, C., Sommer, C., Gerlich, D., Arndt, H., Hell, S. and Johnsson, K., 2014. Fluorogenic probes for live-cell imaging of the cytoskeleton. *Nature Methods*, 11(7), pp.731-733.

Luzio, J., Pryor, P. and Bright, N., 2007. Lysosomes: fusion and function. *Nature Reviews Molecular Cell Biology*, 8(8), pp.622-632.

Majdzadeh, A., Lee, A., Wang, H., Lui, H., McLean, D., Crawford, R., Zloty, D. and Zeng, H., 2015. Real-time visualization of melanin granules in normal human skin using combined multiphoton and reflectance confocal microscopy. *Photodermatology, Photoimmunology & Photomedicine*, 31(3), pp.141-148.

Maymone, M., Neamah, H., Wirya, S., Patzelt, N., Secemsky, E., Zancanaro, P., & Vashi, N., 2017. The impact of skin hyperpigmentation and hyperchromia on quality of life: A cross-sectional study. *Journal Of The American Academy Of Dermatology*, 77(4), pp.775-778.

McGlinchey, R., Shewmaker, F., McPhie, P., Monterroso, B., Thurber, K. and Wickner, R., 2009. The repeat domain of the melanosome fibril protein Pmel17 forms the amyloid core promoting melanin synthesis. *Proceedings of the National Academy of Sciences*, 106(33), pp.13731-13736.

Mindell, J., 2012. Lysosomal Acidification Mechanisms. *Annual Review of Physiology*, 74(1), pp.69-86.

Müller, A., Müller, S., Nasufovic, V., Arndt, H. and Pompe, T., 2019. Actin stress fiber dynamics in laterally confined cells. *Integrative Biology*, 11(5), pp.175-185.

National Center for Biotechnology Information. PubChem Compound Summary for CID 91864488, Sucrose 1,6'-dilaurate. https://pubchem.ncbi.nlm.nih.gov/compound/91864488. Accessed Nov. 16, 2021.

Olivares, C., Jimenez-Cervantes, C., Lozano, J., Solano, F. and Garcia-Borron, J., 2001. The 5,6-dihydroxyindole-2-carboxylic acid (DHICA) oxidase activity of human tyrosinase. *Biochemical Journal*, 354(1), pp.131-139.

Osborne, R., Hakozaki, T., Laughlin, T. and Finlay, D., 2012. Application of genomics to breakthroughs in the cosmetic treatment of skin ageing and discoloration. *British Journal of Dermatology*, 166(S2), pp.16-19.

Ostrowski, M., Carmo, N., Krumeich, S., Fanget, I., Raposo, G., Savina, A., Moita, C., Schauer, K., Hume, A., Freitas, R., Goud, B., Benaroch, P., Hacohen, N., Fukuda,

M., Desnos, C., Seabra, M., Darchen, F., Amigorena, S., Moita, L. and Thery, C., 2009. Rab27a and Rab27b control different steps of the exosome secretion pathway. *Nature Cell Biology*, 12(1), pp.19-30.

Pandya, A. and Guevara, I., 2000. DISORDERS OF HYPERPIGMENTATION. *Dermatologic Clinics*, 18(1), pp.91-98.

Patwardhan, A., Bardin, S., Miserey-Lenkei, S., Larue, L., Goud, B., Raposo, G. and Delevoye, C., 2017. Routing of the RAB6 secretory pathway towards the lysosome related organelle of melanocytes. *Nature Communications*, 8(1).

Pédelacq, J., Cabantous, S., Tran, T., Terwilliger, T. and Waldo, G., 2005. Engineering and characterization of a superfolder green fluorescent protein. *Nature Biotechnology*, 24(1), pp.79-88.

Plensdorf, S., and Martinez, J., 2009. Common pigmentation disorders. *American family physician*, 79(2), pp.109–116.

Plensdorf, S., Livieratos, M., and Dada, N., 2017. Pigmentation Disorders: Diagnosis and Management. *American family physician*, 96(12), pp.797–804.

Premi, S., Wallisch, S., Mano, C., Weiner, A., Bacchiocchi, A., Wakamatsu, K., Bechara, E., Halaban, R., Douki, T. and Brash, D., 2015. Chemiexcitation of melanin derivatives induces DNA photoproducts long after UV exposure. *Science*, 347(6224), pp.842-847.

Provance, D., James, T. and Mercer, J., 2002. Melanophilin, the Product of the Leaden Locus, is Required for Targeting of Myosin-Va to Melanosomes. *Traffic*, 3(2), pp.124-132.

Raposo, G., Tenza, D., Murphy, D., Berson, J. and Marks, M., 2001. Distinct Protein Sorting and Localization to Premelanosomes, Melanosomes, and Lysosomes in Pigmented Melanocytic Cells. *Journal of Cell Biology*, 152(4), pp.809-824.

Riedl, J., Crevenna, A., Kessenbrock, K., Yu, J., Neukirchen, D., Bista, M., Bradke, F., Jenne, D., Holak, T., Werb, Z., Sixt, M. and Wedlich-Soldner, R., 2008. Lifeact: a versatile marker to visualize F-actin. *Nature Methods*, 5(7), pp.605-607.

Rochin, L., Hurbain, I., Serneels, L., Fort, C., Watt, B., Leblanc, P., Marks, M., De Strooper, B., Raposo, G. and van Niel, G., 2013. BACE2 processes PMEL to form the melanosome amyloid matrix in pigment cells. *Proceedings of the National Academy of Sciences*, 110(26), pp.10658-10663.

Scott, G., Leopardi, S., Parker, L., Babiarz, L., Seiberg, M. and Han, R., 2003. The Proteinase-Activated Receptor-2 Mediates Phagocytosis in a Rho-Dependent Manner in Human Keratinocytes. *Journal of Investigative Dermatology*, 121(3), pp.529-541.

Serre, C., Busuttil, V. and Botto, J., 2018. Intrinsic and extrinsic regulation of human skin melanogenesis and pigmentation. *International Journal of Cosmetic Science*, 40(4), pp.328-347.

Seweryn, A., 2018. Interactions between surfactants and the skin – Theory and practice. *Advances in Colloid and Interface Science*, 256, pp.242-255.

Singh, S., Nizard, C., Kurfurst, R., Bonte, F., Schnebert, S. and Tobin, D., 2008. The silver locus product (Silv/gp100/Pmel17) as a new tool for the analysis of melanosome transfer in human melanocyte-keratinocyte co-culture. *Experimental Dermatology*, 17(5), pp.418-426.

Solovyov, K., Polyakov, D., Grudinina, N., Egorov, V., Morozova, I., Aleynikova, T. and Shavlovsky, M., 2011. EXPRESSION INE. coliAND PURIFICATION OF THE FIBRILLOGENIC FUSION PROTEINS TTR-sfGFP AND β2M-sfGFP. *Preparative Biochemistry and Biotechnology*, 41(4), pp.337-349.

Sturm, R., Box, N. and Ramsay, M., 1998. Human pigmentation genetics: the difference is only skin deep. *BioEssays*, 20(9), pp.712-721.

Tarafder, A., Wasmeier, C., Figueiredo, A., Booth, A., Orihara, A., Ramalho, J., Hume, A. and Seabra, M., 2011. Rab27a Targeting to Melanosomes Requires Nucleotide Exchange but Not Effector Binding. *Traffic*, 12(8), pp.1056-1066.

Thompson, M.J., 2019. *An Investigation of Hair and its Keratin Associated Proteins using Advanced Light Microscopy.* Doctoral thesis, Durham University, Durham.

Tsukamoto, K., Jackson, I. J., Urabe, K., Montague, P. M., and Hearing, V. J., 1992. A second tyrosinase-related protein, TRP-2, is a melanogenic enzyme termed DOPAchrome tautomerase. *The EMBO journal*, 11(2), pp.519–526.

Van Den Bossche, K., Naeyaert, J. and Lambert, J., 2006. The Quest for the Mechanism of Melanin Transfer. *Traffic*, 7(7), pp.769-778.

Vidali, L., Rounds, C., Hepler, P. and Bezanilla, M., 2009. Lifeact-mEGFP Reveals a Dynamic Apical F-Actin Network in Tip Growing Plant Cells. *PLoS ONE*, 4(5), p.e5744.

Watt, B., van Niel, G., Fowler, D., Hurbain, I., Luk, K., Stayrook, S., Lemmon, M., Raposo, G., Shorter, J., Kelly, J. and Marks, M., 2009. N-terminal Domains Elicit Formation of Functional Pmel17 Amyloid Fibrils. *Journal of Biological Chemistry*, 284(51), pp.35543-35555.

Watt, B., van Niel, G., Raposo, G. and Marks, M., 2013. PMEL: a pigment cell-specific model for functional amyloid formation. *Pigment Cell & Melanoma Research*, 26(3), pp.300-315.

Westbroek, W., Tuchman, M., Tinloy, B., De Wever, O., Vilboux, T., Hertz, J., Hasle, H., Heilmann, C., Helip-Wooley, A., Kleta, R. and Gahl, W., 2008. A novel missense

mutation (G43S) in the switch I region of Rab27A causing Griscelli syndrome. *Molecular Genetics and Metabolism*, 94(2), pp.248-254.

Wu, X., Rao, K., Bowers, M., Copeland, N., Jenkins, N. and Hammer, J., 2001. Rab27a enables myosin Va-dependent melanosome capture by recruiting the myosin to the organelle. *Journal of Cell Science*, 114(Pt 6), pp.1091-1100.

Wu, X., Tsan, G. and Hammer, J., 2005. Melanophilin and myosin Va track the microtubule plus end on EB1. *Journal of Cell Biology*, 171(2), pp.201-207.

Yamashita, T., Kuwahara, T., González, S. and Takahashi, M., 2005. Non-Invasive Visualization of Melanin and Melanocytes by Reflectance-Mode Confocal Microscopy. *Journal of Investigative Dermatology*, 124(1), pp.235-240.

Zubair, R., Lyons, A., Vellaichamy, G., Peacock, A. and Hamzavi, I., 2019. What's New in Pigmentary Disorders. *Dermatologic Clinics*, 37(2), pp.175-181.